Three-Dimensional Fabrication of Hepatic Lobule Model Using Electrodeposition Technology

Zeyang LIU

献给我敬爱的祖国

To my parents and my friends

Acknowledgments

I would like to thank one of my advisors, Prof. Toshio Fukuda, for his kind guidance, expertise, understanding, patience, encouragement and great help to fulfilling this research in these 3 years. He has been a great mentor, developing in me the ability to think both critically and creatively. This work would not have been possible without his guidance and support, and I am truly grateful. The other advisor, Prof. Yasuhisa Hasegawa, gave me valuable suggestions and huge support during my PhD period. He is a nice and gentle person who gives his all heart and passions to his students.

I greatly thank to the following professors who guided me so much and gave me many useful comments during my research life. Assoc. Prof. Kosuke Sekiyama guided me a lot on how to make an innovative research proposal, how to design the research roadmap and how to make a clear presentation. I studied with him for half year for the research topic of autonomous distribution system at the beginning of my study life in Japan. He taught me how to read the journal papers and find the advantages and disadvantages in them although some authors didn't mention those things. He also gave me the available suggestion and permission for my later transfer to the bio-fabrication team. I thank him. Prof. Fumihito Arai taught me that the important thing about research life is to feel the satisfaction of the achievement for example the moment you get your paper accepted. Thanks Prof. Shimizu to give me the available comments on my thesis to make it more convincing and easy to be read.

I also had the privilege to work with Asst. Prof. Masahiro Nakajima and Asst. Prof. Masaru Takeuchi who were always willing to discuss experimental results and suggest rational explanations. Technical assistant, Mr. Hideo Matsuura gave a wonderful support whenever I need mechanical design support for the experiments. Many of my experimental setup would be difficult to realize without his help.

I would like to thank the past members of the micro-nano bio-fabrication research group: Dr. Yue Tao taught me a lot of things about how to do a research in micro/nano field, helped me in microscope observation and cell culture protocols. He also gave me many suggestions on how to plan my research career. Dr. Chengzhi Hu taught me how to do experiment independently, and helped me a lot in writing papers. Dr. Huaping Wang taught me the important of being an honest person. Dr. Sun Tao taught me the never-give-up spirits not only for research but also for the life.

My mother Lixia Zhang, thank you for making the sacrifices that companied with me in Japan, 2014; for supporting me through the bulk of my graduate work; for making me remember the important things in life; for encouraging me when I was down; and most of all, for your unconditional love. I am grateful beyond expression. My father Xiaohua Liu, thank you for supporting me to study abroad and giving me the insight guidance of the life journey.

I have to say there are so many people who have been involved in the creation of this work (Dr. Yajing Shen, Dr. Pei Di, Dr. Fei Chen, Dr. Ning Yu, Dr. Xiaoming Liu, Dr. Mengze Li, etc.). Some have been intricately involved in the technical details, while others have enriched my life in other ways. If I neglect to mention your name, you know who you are and how you have helped me through this process, and I thank you.

Finally, I suddenly remember a proverb to perfectly conclude my PhD life: “A good beginning makes a good ending.”

Nagoya, Dec. 2017

Zeyang Liu

Contents

List of Figures

List of Tables

Chapter 1
Introduction

1.1 Regenerative Medicine

The loss or failure of an organ or tissue is one of the most frequent, devastating, and costly problems in human health care. The typical therapy is to get an artificial organ or a transplant. Unfortunately, artificial organs and other implanted abiotic devices often fail over time. Transplantation of organs to replace the incurable ones, such as heart, liver, or kidney, is a highly successful therapy [3]. A successful transplant requires a compatible and willing donor. However, the need for donor organs far exceeds the supply. Each year, millions of patients die while waiting for the organ transplantations. This donor scarcity problem has resulted in new technique which is to build artificial organs by cells and organic materials, which is defined as tissue engineering [4]. Langer and Vacanti defined this tissue engineering as “A new field, tissue engineering, applies the principles of biology and engineering to the development of functional substitutes for damaged tissue [3]."

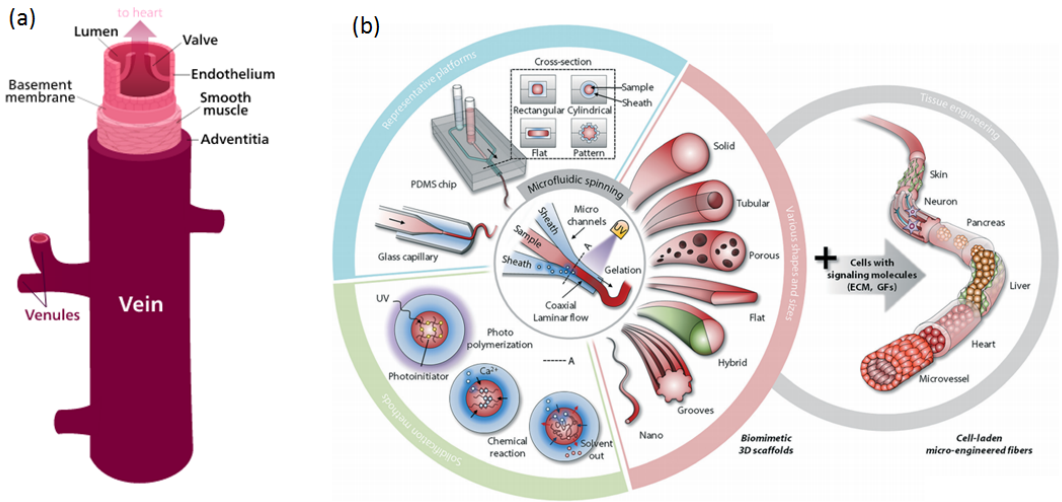

Figure 1.1 (a) Typical real tissues such as blood vessel. (b) Major approaches to build 3D artificial tissue[5].

The regenerative medicine is mainly carried out on the following aspects: cell therapy for tissue and organs; activation of endogenous cells as an approach to regenerative medicine; regeneration of tissue using biocompatible materials and cells. The latter aspect is usually referred as tissue engineering, and is believed to be highly promising for tissue regeneration. Generally, tissue engineering is considered as a sub-discipline of regenerative medicine that intends to use cell-constructs to achieve tissue repair and is aimed at delivering safe, effective and consistent therapies. However, scientists are still in the early stages of understanding how this works [6]. Like in our bodies, the tissues and organs are with complex three-dimensional (3D) shapes and structures, as shown in Figure 1.1(a). Therefore, how to control the positions of cells and form certain shapes by cells as the real tissues is a promised way to generate artificial cell tissues [7].

Assembly of cells to form 3D shapes and structures offers a practical alternative to natural tissue models. These systems provide an environment in which one or more cell types can be encouraged to form tissues-like constructs. If an artificial organ is to assemble and work properly, specific cells must be directed to specific locations at a specific time, forming patterns of cells with a defined function [8]. This is a fundamental feature of tissue and organ assembly in all living organisms. A specific 3D multi-cellular structure is often critical for proper cellular function. The ability to build such a structure would be useful for tissue engineering [9]. A common method to build 3D tissues from 2D cell structures as basic building blocks as shown in Figure 1.1(b). One useful application would be for organ repair. Another useful purpose would be the study of diseases whose progress is impacted by multi-cellular topology [10].

1.2 Tissue engineering

Generally, tissue engineering is considered as a sub-discipline of regenerative medicine that intends to use cell-constructs to achieve tissue repair and is aimed at delivering safe, effective and consistent therapies. Tissue engineering (TE) combines biological and engineering expertise to provide artificially developed substitutes for tissues and organs, hence studying the tissue formation process for generating implantable artificial tissues and organs. [3, 4, 11, 12].

1.2.1 Background and current issues

Tissue engineering completely avoids the risks of immunological responses such as rejections, as well as viral infections, by using autologous cells, as shown in Figure 1.2. Traditionally, the basic concept of tissue engineering includes a scaffold that provides an architecture on which seeded cells can organize and develop into the desired organ or tissue prior to implantation [11]. Building an organ model using tissue engineering

approaches relies on the fabrication of 3D polymeric scaffolds upon which cells can proliferate and differentiate into a structurally and functionally appropriate target tissue or organ. Cells within engineered tissues may be those that are stimulated to grow into an implanted scaffold or cells that are pre-seeded within the scaffold [13].

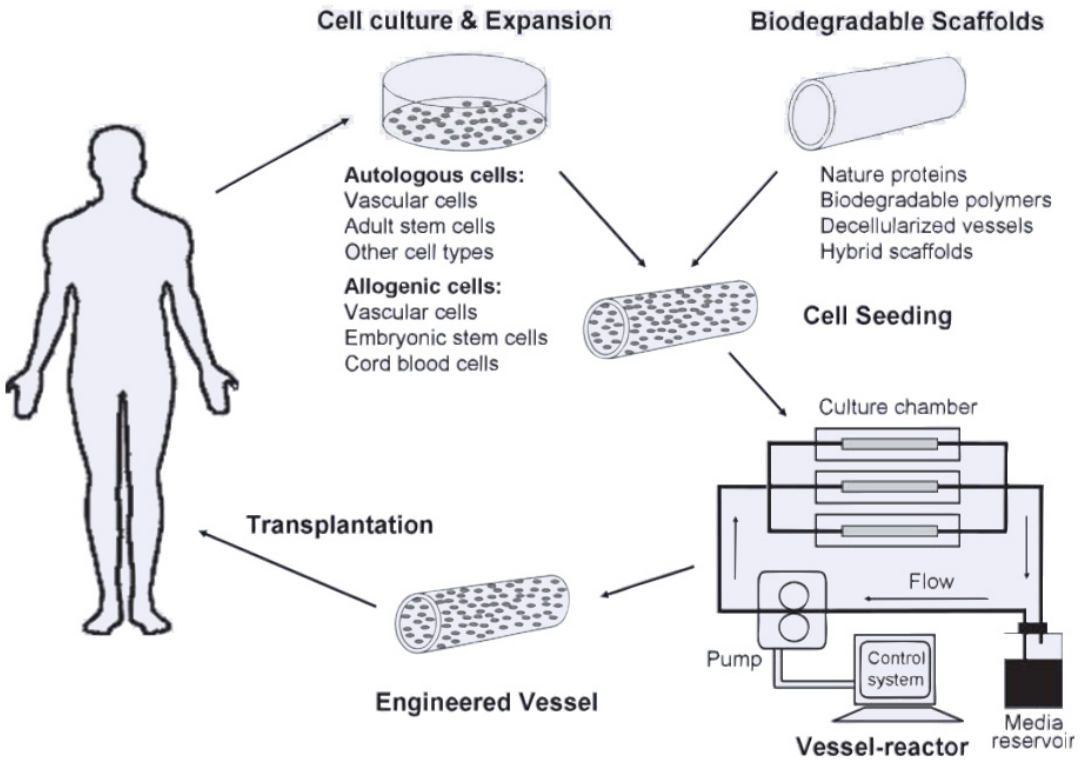

Figure 1.2 Concept of tissue engineering[14].

1.2.2 Extracellular Environment

What's more, tissues are not made up solely of cells. A substantial part of their volume is extracellular space, which is largely filled by an intricate network of macromolecules constituting the ECM. This matrix is composed of a variety of fibrous proteins and polysaccharides that are secreted locally and assembled into an organized meshwork in close association with the surface of the cell that produced them. Therefore, the specific composition and distribution of the ECM constituents will vary depending on the tissue source. Table 1.1 shows the major components of ECM and their function, and location.

The ECM is more than an inert packing material or a nonspecific glue that holds cells together; it often plays a key regulatory role in determining the shape and activities of the cell. For example, enzymatic digestion of the ECM that surrounds cultured cartilage cells or mammary gland epithelial cells causes a marked decrease in the synthetic and secretory activities of the cells. Addition of extracellular matrix materials back to the culture dish can restore the differentiated state of the cells and their ability

to manufacture their usual cell products [15].

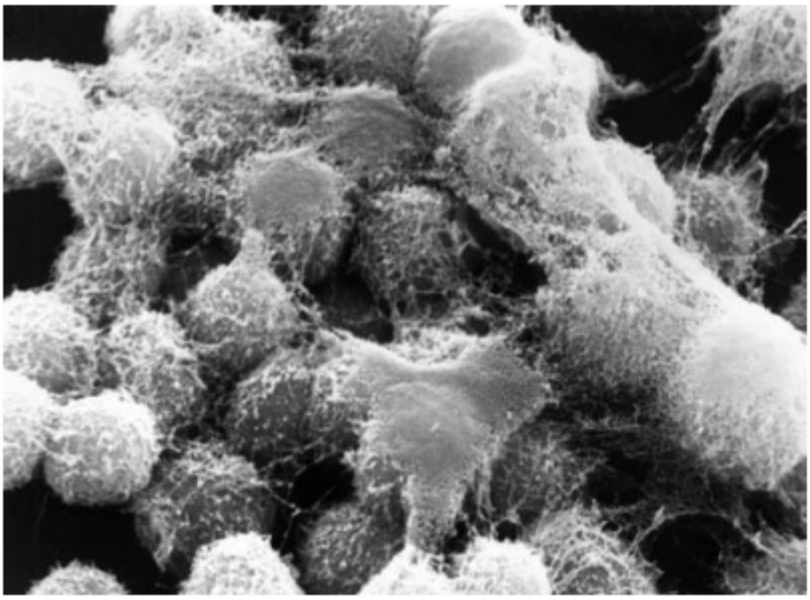

(a)

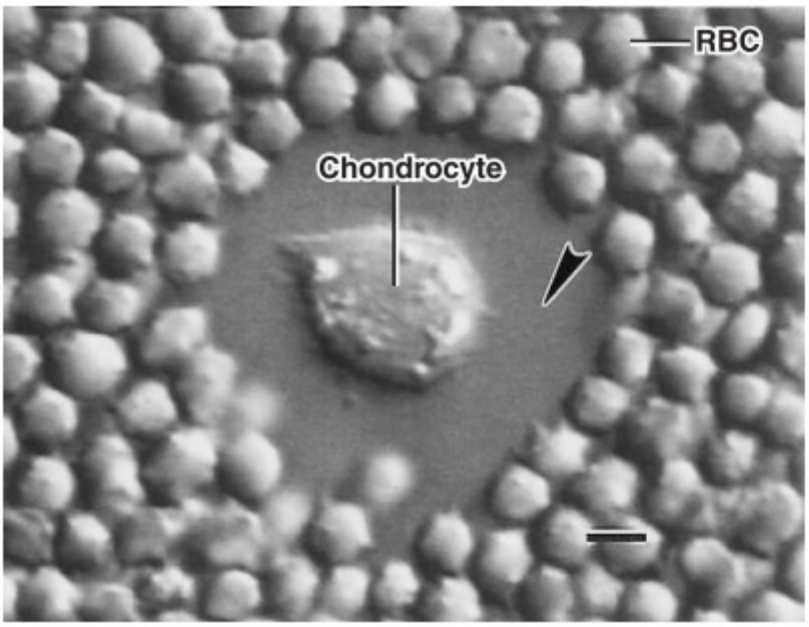

(b)

Figure 1.3 The extracellular matrix (ECM) of cartilage cells. (a) Scanning electron micrograph of a portion of a colony of cartilage cells (chondrocytes) showing the extracellular materials secreted by the cells. (b) The ECM of a single chondrocyte has been made visible by adding a suspension of red blood cells (RBCs). The thickness of the ECM is evident by the clear space (arrowhead) that is not penetrated by the RBCs[15]. The bar represents 10 um.

Table 1.1 The major components of ECM and their function, and location [16].

Component	Function	Location
Collagen	Tissue architecture, tensile strength, cell–matrix interaction, matrix–matrix interaction	Widely distributed
Elastin	Tissue architecture, elasticity	Tissues requiring elasticity (lung, blood vessel, skin)
Proteoglycans	Cell–matrix interaction, matrix–matrix interaction, cell proliferation, cell migration	Widely distributed
Hyaluronan	Cell–matrix interaction, matrix–matrix interaction, cell proliferation, cell migration	Widely distributed
Laminin	Basement membrane component, cell migration	Basement membranes
Fibronectin	Tissue architecture, cell–matrix interaction, matrix–matrix interaction, cell proliferation, cell migration	Widely distributed
Fibrinogen	Cell proliferation, cell migration, hemostasis	Blood, wound healing

1.2.3 Construction methods for artificial tissues

Currently, there are mainly two fundamental construction methods in tissue engineering, which are Top-down approaches and Bottom-up approaches, as shown in Figure 1.4. In top-down approaches, cells are seeded on a biodegradable polymeric scaffold and grow according the shape of the scaffold to be a tissue. The cells are expected to populate the scaffold and create the appropriate microarchitecture often with the aid of perfusion, growth factors or mechanical stimulation [17]. However, even the surface patterning or more biomimetic scaffolding are used, top-down approaches often have difficulty recreating the intricate microstructural features of tissues [18], because the current biomaterials and micro fabrication methods are with certain limitation for creating intricate 3D biomimetic structures.

So far, many achievements have been obtained by conventional top-down approaches. In 1997, Dr. Joseph Vacanti in US grew a human ear from cartilage cells on the back of a mouse, which demonstrated the scaffold based 3D cell structures and tissues [19]. This study evaluated the feasibility of growing tissue-engineered cartilage in the shape of a human ear using chondrocytes seeded onto a synthetic biodegradable polymer fashioned in the shape of a 3-year-old child's auricle. A polymer template was formed in the shape of a human auricle using a nonwoven mesh of polyglycolic acid. Each polyglycolic acid-polylactic acid template was seeded with chondrocytes isolated from bovine articular cartilage and then implanted into subcutaneous pockets on the dorsa of 10 athymic mice. The 3D structure was well maintained after removal of an

external stent that had been applied for 4 weeks. Specimens harvested 12 weeks after implantation and subjected to gross morphologic and histologic analysis demonstrated new cartilage formation. The overall geometry of the experimental specimens closely resembled the complex structure of the child's auricle. These findings demonstrated that polyglycolic acid-polylactic acid constructs can be fabricated in a very intricate configuration and seeded with chondrocytes to generate new cartilage that would be useful in plastic and reconstructive surgery, as an artificial part used in tissue engineering. However, the auricle is a simple structure and this method is difficult to be used for building complex tissues.

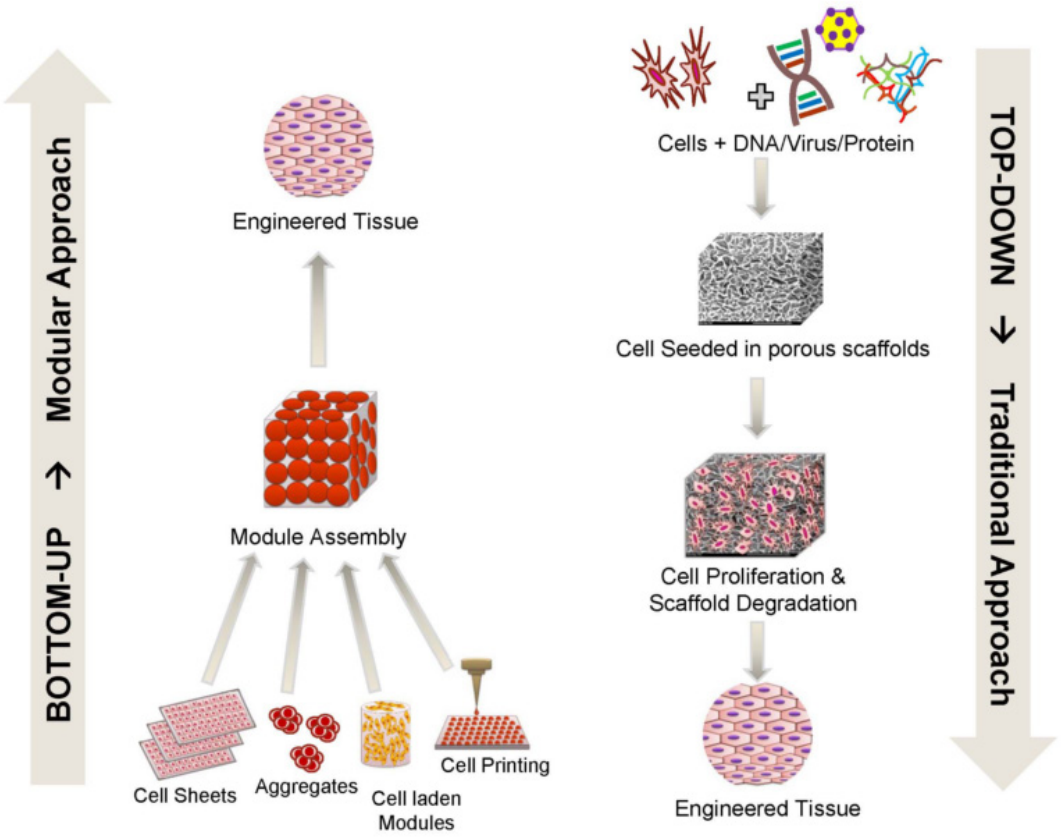

Figure 1.4 The traditional, top-down approach (right) involves seeding cells into full sized porous scaffolds to form tissue constructs. This approach poses many limitations such as slow vascularization, diffusion limitations, low cell density and non-uniform cell distribution. In contrast, the modular or bottom-up approach (left) involves assembling small, non-diffusion limited, cell-laden modules to form larger structures and has the potential to eliminate the shortcomings of the traditional approach[20].

In contrast to the traditional scaffold-based “top-down” approaches, “bottom-up” tissue fabrication methods using micro scale units as building blocks, including cell sheets and cell aggregates, are potentially powerful tools to reconstruct organomimetic and uniformly dense microstructures [21, 22]. Bottom-up approaches aim to address the challenge of recreating 3D biomimetic structures by designing structural features on the microscale to build modular tissues that can be used as building blocks to create larger tissues. These "building block" can be created in many ways, such as cell

aggregation, cell embedded bio-scaffold, creation of cell sheets [7, 23, 24]. These "building block" can be assembled into larger 3D tissues through microtechnology such as fluidic system, rapid prototyping or electrical manipulation [25-27]. Therefore, the bottom-up approaches are recommended for 3D cell structure assembly in tissues engineering field.

One method for building artificial macroscopic three-dimensional (3D) tissue architectures has been presented as shown in Figure 1.5. This is for rapid construction of collagen gel-based micro-tissue units seeded complex "tissue-like" microstructure. Seeded cell beads immediately stick to each other to assemble uniform and arbitrary shaped macroscopic 3D tissues within a PDMS mold.

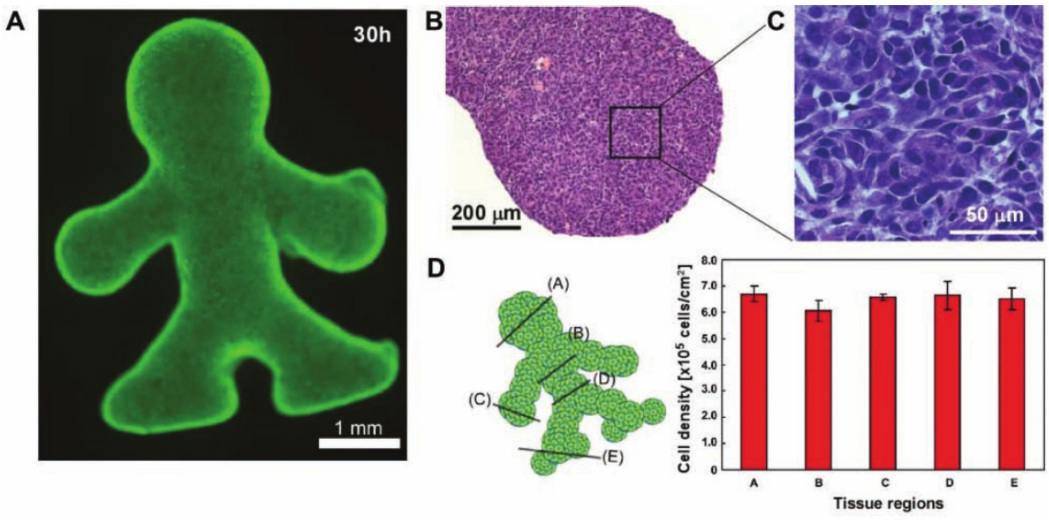

Figure 1.5 Analyses of the reconstructed 3D tissue architectures. A) Cell viability of 30 h cultured 3D tissue assessed using the live/dead assay kit. B–C) Microscopic views of the tissue section after reconstruction for 24 h. The cell densities are uniform and tissue necrosis is not observed. D) Cell density of the 3D tissue architecture at various regions measured from the tissue section. The cell density was broadly comparable in all regions of the tissues after 24 h of reconstruction ($6.5 \times 10^5 \pm 0.1$ cells cm^{-2}).[21]

Based on cell aggregation, large-scale cell pattern can be formed using PDMS mold as shown in Figure 1.5. The monodisperse cell beads were molded into a 3D tissue architecture. Size-controlled cell beads were prepared by culturing cells over the surface of monodisperse collagen gel beads or collagen gel beads encapsulating another cell type. Cell beads were stacked into the designed silicone mold to form 3D tissues. During tissue formation, the medium diffused into the cavities between the cell beads, supplying nutrients into the 3D constructs. The cells located on the surface of the beads form cell–cell connections, then migrated and grew within the collagen gel beads and finally formed the 3D tissues [21]. However, the low design flexibility of current mold limited this method to form complex "tissue-like" structure in three-dimension. Another limitation is that the multi-cellular tissue is difficult to build since it is impossible to

address different type of cell beads at the proper position or layer in mold so far.

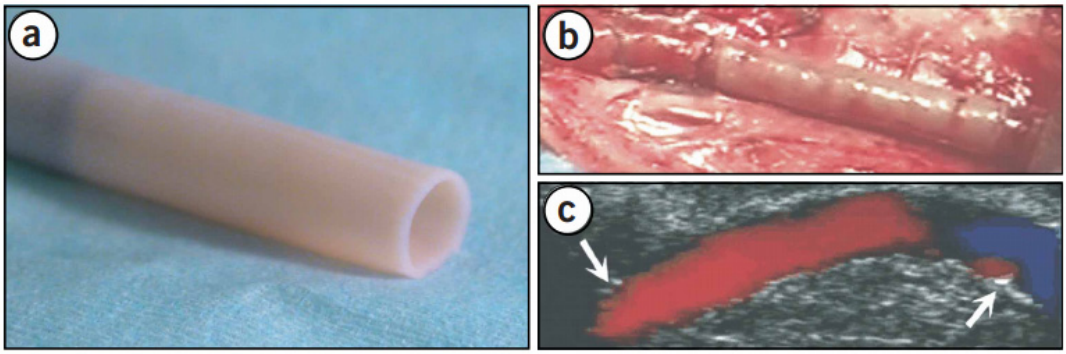

Figure 1.6 Cell sheet engineering for constructing 3D cell tissues. (a) Age- and risk-matched tissue-engineered blood vessels (TEBVs) TEBV before implantation (4.2 mm internal diameter) being removed from its temporary tubular support. (b)TEBV, anastomosed as end-to-end interpositional femoral graft, immediately after removal of the cross-clamps [28].

Stacking of cell layers, also referred to "Cell sheet engineering", has been developed for regenerate many tissues. Cell sheet engineering allows for tissue regeneration by either direct transplantation into host tissues or the creation of three-dimensional structures such as tissue-engineered blood vessels (TEBVs) that serve as arterial bypass grafts in long-term animal models via wrapping sheet around a Teflon-coated stainless-steel temporary support tube. as shown in Figure 1.6 [28]. By avoiding the use of any additional materials such as carrier substrates or permanent synthetic scaffolds, the complications associated with traditional tissue engineering approaches such as host inflammatory responses to implanted polymer materials, can be avoided. However, the cell sheet engineering method is suitable to construct functional small-diameter conduits, but not flexible enough for building complex 3D shape of tissues.

A new manufacturing technology called rapid prototyping (RP) was developed at the Freiburg Materials Research Center to meet the demands for desktop fabrication of scaffolds useful in tissue engineering [29, 30]. A key feature of this RP technology is using a deposition system to lay down a material in a layer by layer manner in RP three motorized axis. In spite of the increasing interest of tissue engineers in the use of RP, there are several challenges that need to be addressed, namely the limited range of materials, the optimal scaffold design, the bioactivity of the scaffold, as well as the issues of cell seeding and vascularization [31].

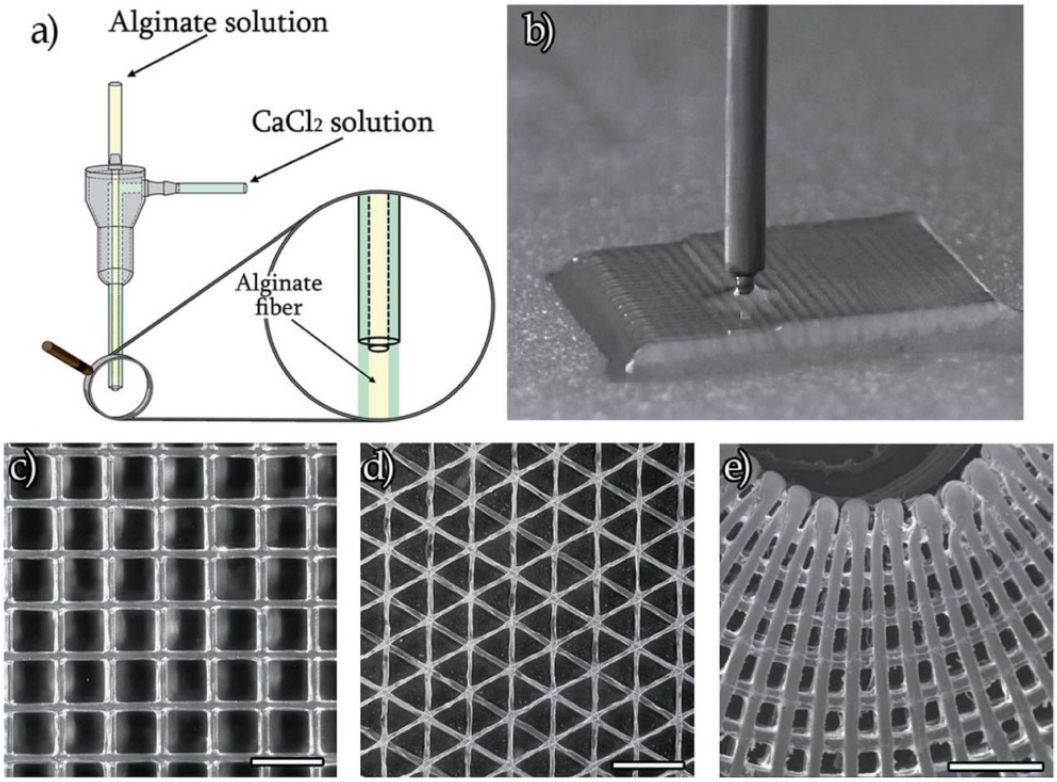

Figure 1.7 (a) Schematic representation of the coaxial needle system for the extrusion of alginate fibers. (b) Photograph of the 3D fiber deposition system during scaffold production. (c–e) Optical micrographs of printed structures with (c) squared, (d) hexagonal and (e) radial patterns of fibers. Scale bars: 500 mm.[27].

In Figure 1.7, hydrogel scaffolds with a designed physical model from Computer-Aided-Design (CAD) data were generated by this RP process. Surface coating were achieved by the deposition of a chitosan on the scaffold fiber and its subsequent cross-linking with EDC and genipin, assured their structural stability in the culture medium for a prolonged period of time. Preliminary culture tests and high level of albumin and urea secretion prove the feasibility of this system as an attractive tool for testing the toxicity of new drugs.

Direct printing of cell embedded microstructures and assembly them to large tissues provides an alternative to scaffold-based tissue engineering, as shown in Figure 1.8. Organ-printing technology using self-assembled tissue spheroids has been visualized by building an intraorgan vascular tree based on using three basic types of tissue spheroids: solid (non-lumenized) vascular tissue spheroids; mono-lumenized ascular spheroids (cyst-like spheroids with one big lumen); and histotypical microvascularized tissue spheroids [32].

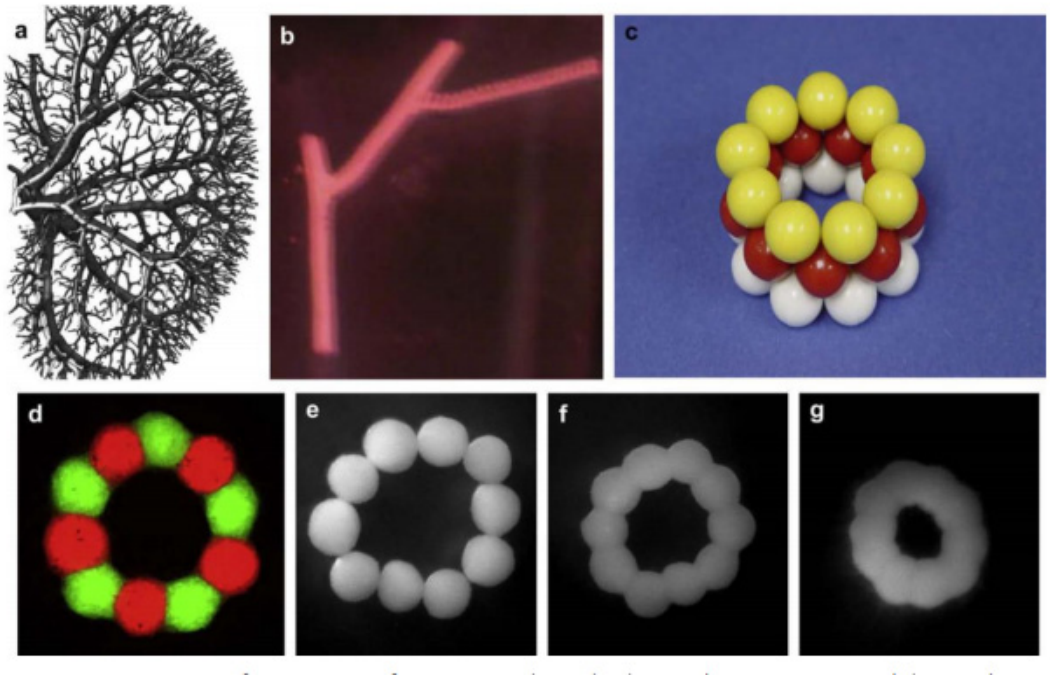

Figure 1.8 Bioprinting of segments of intraorgan branched vascular tree using solid vascular tissue spheroids: (a) Kidney intraorgan vascular tree. (b) Bioprinted segment of vascular tree. (c) Physical model of bio-assembly of tube-like vascular tissue construct using solid tissue spheroids. (d) Bio-assembled ring-like vascular tissue constructs of tissue spheroids fabricated from human smooth muscle cells. Tissue spheroids are labeled with green and red fluorescent stains in order to demonstrate absence of cell mixing during tissue fusion process. (e-g) Sequential steps of morphological evolution of ring-like vascular tissue construct during tissue fusion process [32].

Compared to 2D cell culture, three-dimensional (3D) cell culture has drawn much attention in various applications, including tissue engineering, drug discovery, cancer biology, regenerative medicine and basic life science research. There are a variety of platforms used to facilitate the growth of three-dimensional (3D) cellular structures such as nanoparticle facilitated magnetic levitation and gel matrices microwell. The microwell array has been widely used for 3D cell aggregates such as spheroids[33]. By immobilizing cells on micropatterned surfaces, cell shape, size and homogeneity can be controlled. Also, the cell aggregates can be retrieved to generate nearly homogenous cell aggregates for various research purposes. However, how to choose an optimal material for fabricating microwell is one of the challenges that we faced.

In general, hydrogel materials that are employed for 3D cell culture present natural binding sites cells can interact with, and that these interactions generate signaling cascades which in turn promotes cell migration, differentiation and remodeling of the gel matrix[34]. A. Khademhosseini introduced a novel microwell to culture hES cells with controlled cluster sizes for maintenance and subsequent differentiation [35]. Jeffrey used soft lithography to fabricate microwells without the use of complicated chemicals or expensive clean rooms [36], As shown in Figure 1.9 the cells can be aggregated using hydrogel microwells. PDMS molds were fabricated by curing

prepolymer on silicon masters patterned with SU-8 photoresist. To fabricate PEG microwells, a PDMS mold containing protruding features was pressed onto a thick PEG polymer layer followed by crosslinking with UV and removal of the mold. Acrylate groups were used to anchor the photocrosslinkable PEG to the substrate. To generate EBs, a high-density cell suspension was placed on the microwell arrays and allowed to settle within the wells.

These papers proved that PEG microwells are possible to template ES cell aggregates to generate large numbers of isolated EBs within an array. However, this approach has drawbacks in that the mold will easily damage the gel structure during the cell retrieve process due to the fragile property of gel.

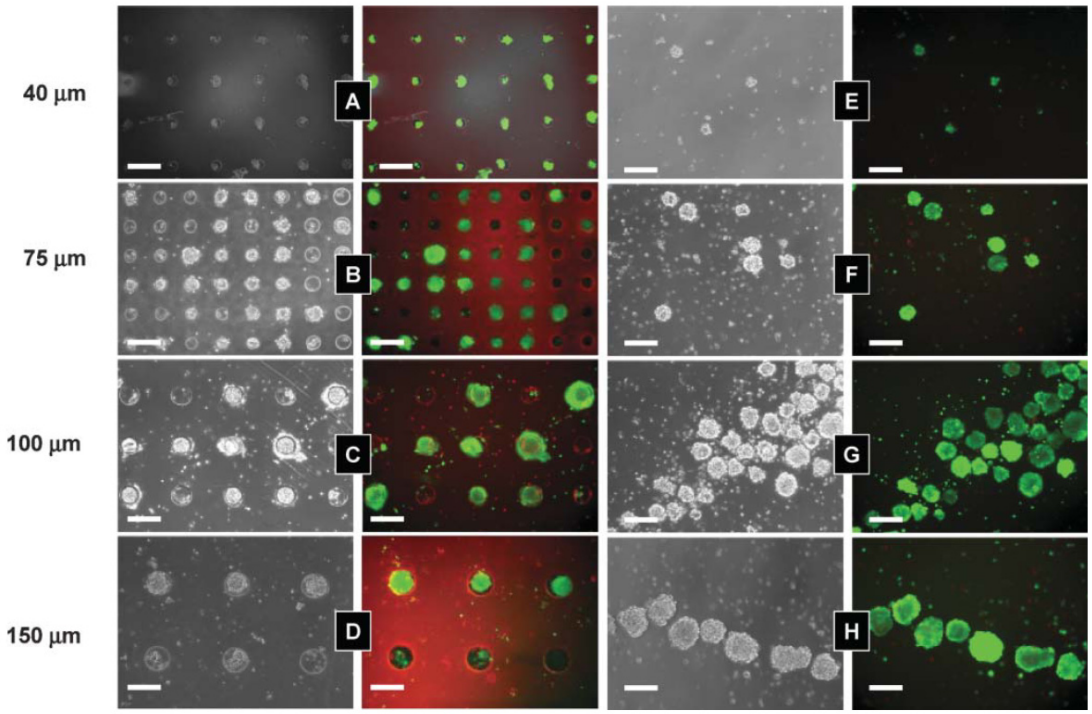

Figure 1.9 Cells seeded in PEG microwells of different sizes: 40 mm (A), 75 mm (B), 100 mm (C), and 150 mm (D) were stained for viability after 10 d both within microwells and after cell aggregates were harvested from the microwells (E, F, G, and H, respectively). Viability was measured using Molecular Probes' live-dead stain, where live cells metabolize calcein AM and fluoresce green while dead cells uptake ethidium homodimer and fluoresce red. Columns 1 and 3 show light microscope images of cell aggregates whereas columns 2 and 4 show fluorescent images. Scale bars correspond to 200 mm[36].

Multi-functional microfluidic devices show high potential to be used in tissue engineering filed with many advantages, such as easy handling, closed environment and high efficiency [37]. These devices are not only for testing regeneration process, but also used to construct cell structures. One dielectrophoretic microfluidic device was demonstrated for generating sphere shaped cell structures [38].

Table 1.2 Summary of the construction methods for artificial tissues

Approach	Material and method	Advantages	Disadvantages	Ref.
Scaffold	Biodegradable polymer	Directly 3D shape formation	Difficult for complex multi-cellular tissues and cell differentiation	[19, 39-41]
Cell aggregation	Cell beads, cell stimulation	Scaffold-free, multi-cellular structure	Low design flexibility and shape controllability	[21, 42]
Micro fabrication	Hydrogel, photolithography	Arbitrary shape, microscale resolution	2D shaped cell units needs further 3D assembly	[43-46]
Cell sheets and stacking	Cell layers	Scaffold-free, direct transplantation, mass products	Low design flexibility, difficult for complex shapes	[47-49]
Cell printing	Printing, position support	High design flexibility, directly 3D shape formation	Difficult for thick structures, limited resolution	[50-53]
Random assembly	Cell encapsulated units	Microscale resolution, complex structures	Low shape controllability	[54]
Directed assembly	cell plates	Microscale resolution, self-assembly	Special designed cell plates	[55, 56]

The summary of these methods is shown in Table 1.2. These undergoing issues, such as fabrication of cell blocks, control of cell aggregation and assembly of engineered tissue building blocks, involve many techniques in terms of observation, micro manipulation, micro fabrication and microfluidic system. Therefore, those techniques provide the promising ways to realize the bottom-up approach (3D cell structure assembly) of tissue engineering.

1.3 Bio-assembly for tissue engineering

In order to greatly raise the level of basic technology for regenerative medicine by

constructing 3D cellular systems in *in vitro* environments, creating 3D tissues suitable for medical applications, and elucidating the functions that make these cell systems act as tissues, manipulation and immobilization of the cells are needed as shown in Figure 1.10.

Microtechnology is the technology with features near one micrometer (one millionth of a meter, μm). For the naked eye, an object larger than 100 μm is visible. Cells can vary between 1μm and hundreds of micrometers in diameter. As the main research object is the cells in tissue engineering, microscale technologies are needed in this research field because this small scale is already beyond the limitation of our naked eye and hands. Therefore, microtechnologies, such as micro fabrication, micromanipulation and microfluidic devices, are used as promising means for constructing 3D cellular structures in tissue engineering.

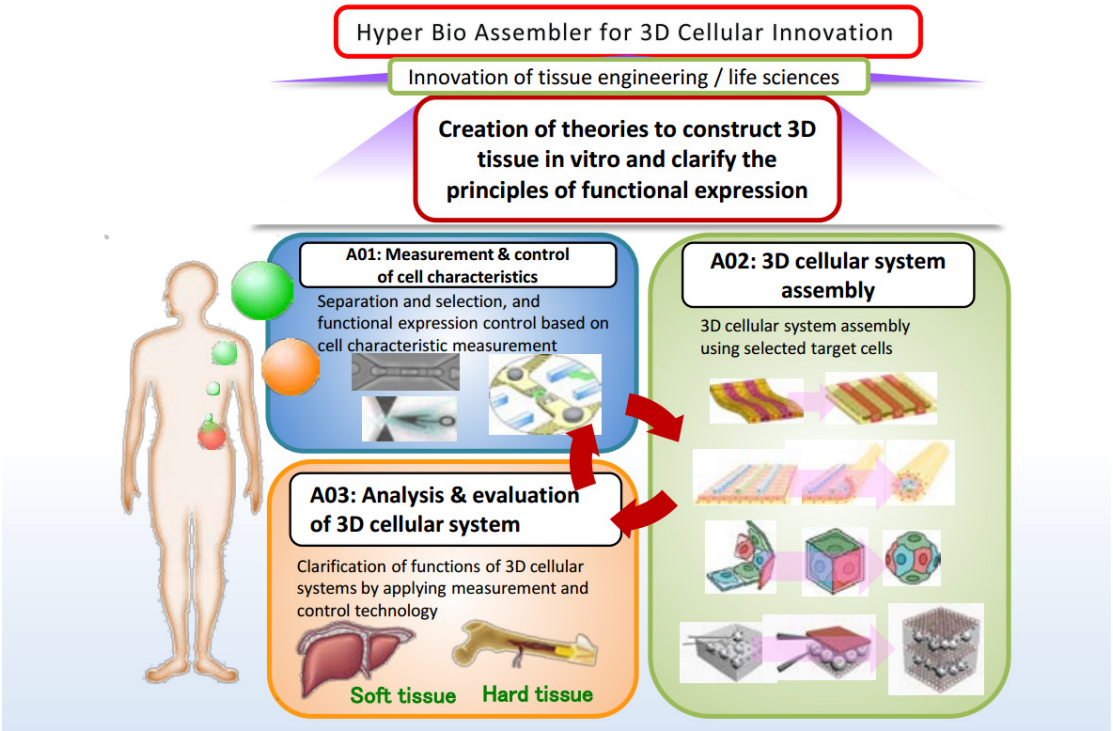

Figure 1.10 Research in a new field, the hyper bio assembler for 3D cellular innovation (Copyright (C) Arai Laboratory, Osaka University, All Right Reserved.)

In order to construct 3D cell structures for tissue engineering, manipulation and immobilization of the cells are needed. Most of the cell embedded components are also fabricated in microscale. Besides, for controlling the growth of assembled cell structures, devices with microscale features are also needed [57]. The fabrication, manipulation and assembly process need a suitable micro scale environment. The microfluidic system is one of the proper tools for example. However, for doing such tasks under microscale, the fundamental observation equipment is needed, which is an optical microscope (often referred to as the "light microscope"). Besides, a lot of technologies developed with optical microscope are used in cell manipulation and 3D

assembly.

1.3.1 Optical microscope system

The optical microscope is a type of microscope which uses visible light and a system of lenses to magnify images of small samples. Since the first development of the compound microscope by Zaccharias Janssen in the end of 16th century, the design was further improved by Anton Leeuwenhoek and Robert Hooke (Figure 1.11), scientists have done huge jobs to improve the performance of the OM [58, 59]. Nowadays, the image from an optical microscope can be captured by cameras to generate a micrograph rather than directly observed by eye. There are many variants of the basic compound optical microscope design for specialized purposes up to now, such as comparison microscope, confocal microscope, USB microscope, and digital microscope, etc.

Figure 1.11 18th century microscopes from the Musée des Arts et Métiers, Paris.

These powerful equipment and tools under optical microscopes provide many approaches which are able to be involved in the cell manipulation and 3D assembly for tissue engineering.

1.3.2 Micromanipulation system

In microscale, the control of objects by our hands is impossible. Micromanipulation system which based on microtechnology is developed to enhance the manipulation ability for handling cells and small objects. For micromanipulation, special requirements are added compared to macroscale manipulation such as gentle handling to prevent damages to cells during manipulation, low complexity of the device because of the limited space, and mechanisms to prevent adhesion of handled objects because of surface forces [60]. Many micromanipulation systems are developed such as direct manipulation, magnetic driven manipulation, and optical / electrical based manipulation [61-64].

Recently, micro-robotic techniques aiming at the observation, measurement and immobilization of micro-/nano-scale objects have been developed. Amicro-assembly technique with a micro-robotic system has been applied in manufacturing and biomedical research [65]. In particular, mechanical micro-gel assembly techniques with optical or magnetic micro-robotic systems provide novel methods for bottom-up assembly with higher controllability [66]. As one method of bottom-up assembly in generating complex biological tissues, through direct contact between the mechanical end-effector and the microstructure without the restriction of the operational environment interfering (electrically or optically), micro-robotics can provide more stable and flexible manipulation with a greater force [65]. For most micro-robotic systems to be able to assemble a cellular 3D structure, the main issue is how to achieve precise control and direct contact of the assembly units during manipulation. Due to the uncertainties in the micro-world, with a confined working space under the microscope, unpredictable dynamic effects strongly influence manipulation [66].

The 2D donuts (PEGDA by UV exposure) were prepared in the dish and monitored by the vision feedback system. The outer diameter, inner diameter and thickness of the fabricated donuts were 200 μm, 100 μm and 70 μm, respectively. As shown in Figure 1.12(a) and Figure 1.12(b), the up-down micro-assembly with the mainmanipulator was performed once the system finished the initialization. Figure 1.12(c) to Figure 1.12(f) show the frequent switching of different coordinated manipulation strategies during micro-assembly to adjust or compact the assembled donuts. As a result, the postures of the assembled donuts were optimized and aligned as an array. After regulating the expected 2D components on the main-manipulator, the secondary UV cross-linking was utilized to connect the donuts as a whole microchannel.

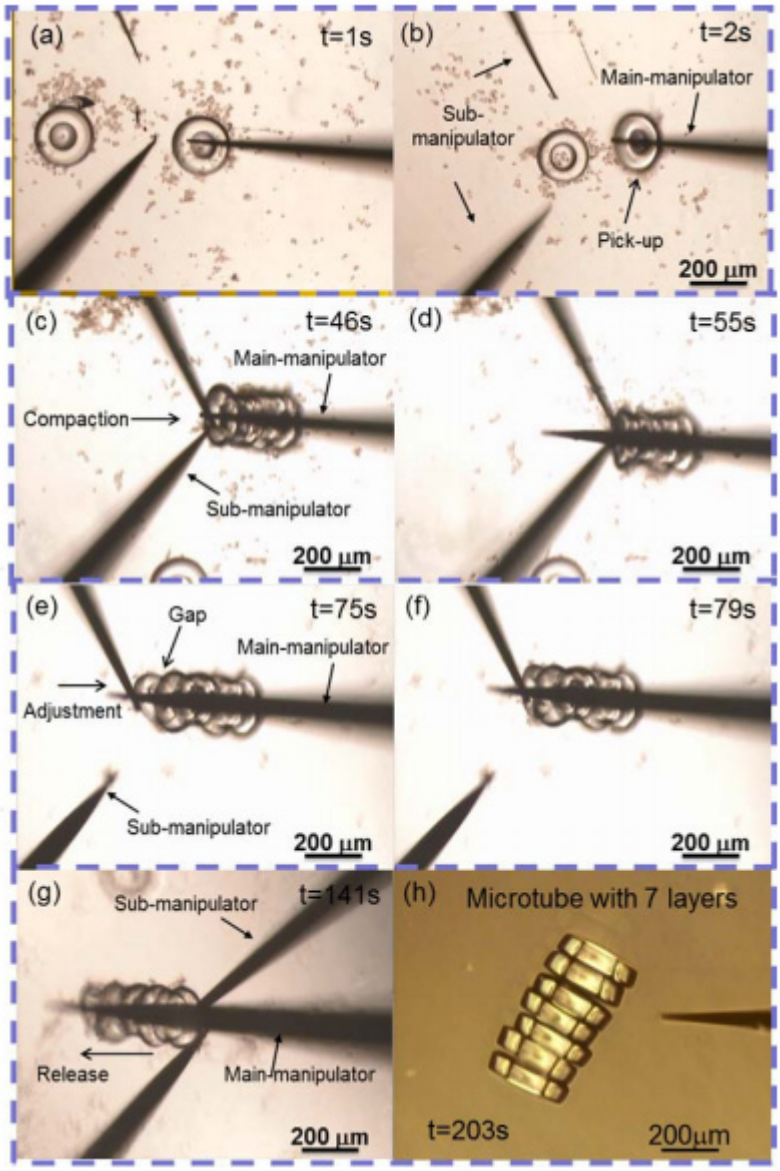

Figure 1.12 Micro-robot-team assembly of the vascular-like microchannel[67].

Soft lithography is a set of techniques for creating microstructures and nanostructures based on printing, embossing and molding using elastomeric stamps with the patterns of interest, which is a robust, reproducible, biocompatible and inexpensive fabrication approach that enables patterning of both planar and non-planar substrates [68]. The central component for soft lithography is a layer of PDMS, or another polymer with similar characteristics, with embossed structures or bas-relief structures on the surface.

As shown in Figure 1.13, the soft lithographic techniques that have been widely explored include the microcontact printing, replica molding, microtransfer molding, micromolding in capillaries, and the microfluidics [127]. Among them, microcontact printing refers to the transformation of patterns from the surface of a topographically patterned PDMS stamp to the surface of a substrate; the replica molding refers to

duplicating the shape, size and pattern of features on a master; micromolding in capillaries refers to using a typographically patterned layer of PDMS in contact with a surface to form a network of microchannels; microtransfer molding refers to patterning materials in which a thin layer of a liquid prepolymer is applied to the patterned surface of a PDMS stamp; microfluidics refers to a set of channels that have micron-scale dimensions (typically between 5–500 μm), and are used to manipulate fluids. And it involves the techniques using the elastomeric polymers such as PDMS to fabricate microfluidic channels and networks which are formed by placing a layer of PDMS with channels embossed on the surface in contact with a glass (or polymer) surface that forms the roof or floor of the channel [69].

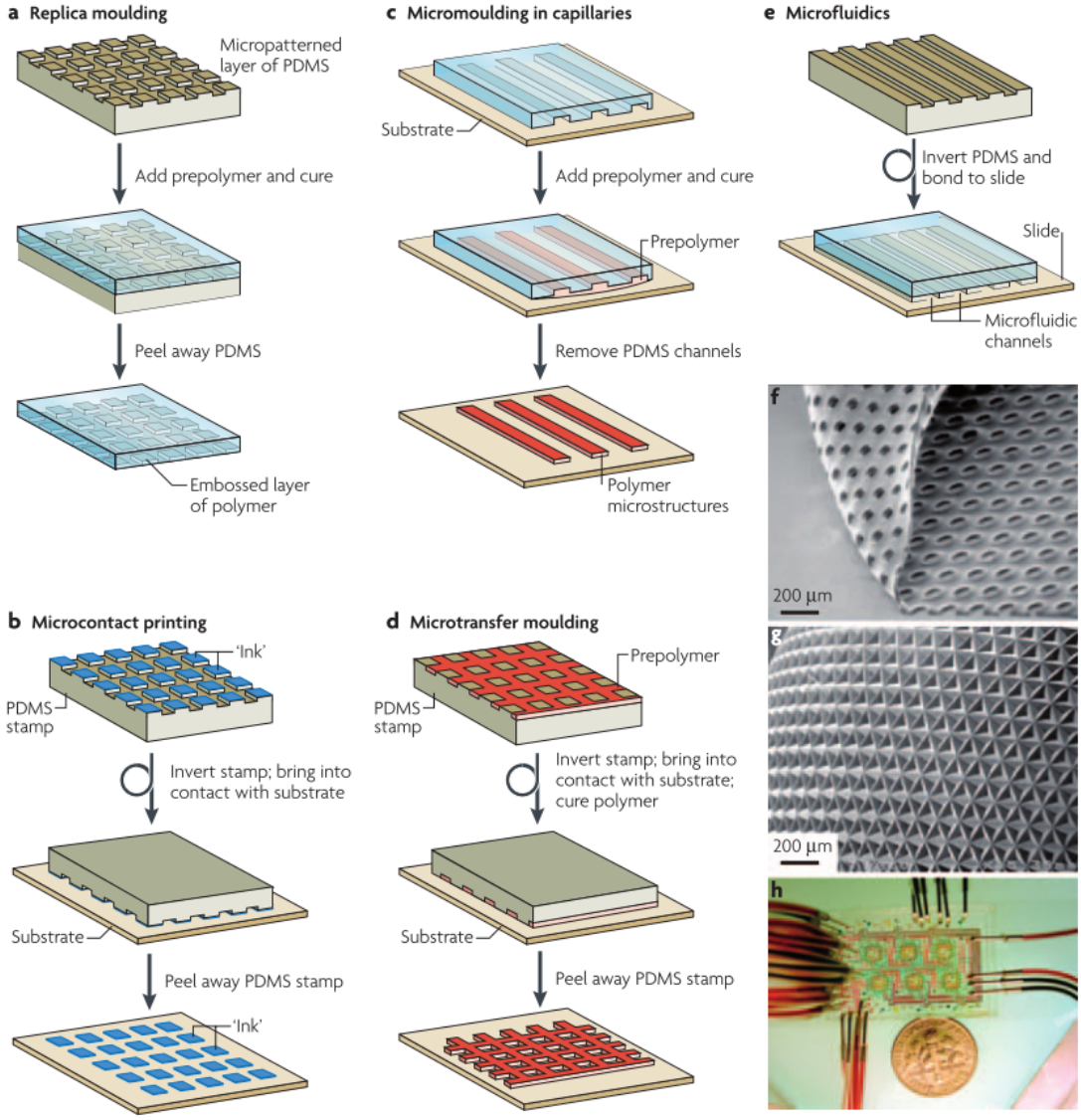

Figure 1.13 The core techniques of soft lithography. The key stages of each of the following techniques are shown: (a) replica moulding; (b) microcontact printing; (c) micromoulding in capillaries; (d) microtransfer moulding; and (e) microfluidics. (f) A PDMS membrane with microfabricated holes created by replica moulding from a master with circular posts. (g) A curved layer of micropatterned

polyurethane created by bending a micropatterned layer of PDMS and then replica moulding against it; (h) A microfluidic chemostat for the growth and culture of microbial cultures. The device incorporates six reactors with an intricate network of plumbing, in a footprint that is approximately 5 cm^2[69].

The contact between objects and manipulator is needed in the direct assembly and the mentioned magnetic driven manipulation, which caused certain damage to the biological objects. Non-contact manipulation overcomes this problem by applying optical electrical based forces for the manipulation. The optical manipulation is often referred to as the "optical tweezers". The detection of optical scattering and gradient forces on microscale particles was first reported by Arthur Ashkin in 1970 [70]. Years later, Ashkin and colleagues first reported that a tightly focused beam of light is capable of holding microscopic particles stable in three dimensions [71]. Today, Optical tweezers has been a comment scientific instrument in studying a variety of biological problems [72-74], such as trapping cells and the moving cells to particular positions. During the manipulation, there is no outer object contacting cells which reduces the damage to low lever.

As shown in Figure 1.15. Yue Tao presented the fabrication and assembly of microstructures inside a microfluidic device based on a photocrosslinkable resin and optical tweezers. Microstructures of arbitrary shapes were fabricated by photocrosslinkable resin inside a microfluidic channel. A novel cell cage was fabricated and the long-term cultivation of a single yeast cell (w303) was demonstrated in the cage, inside the microfluidic device[75].

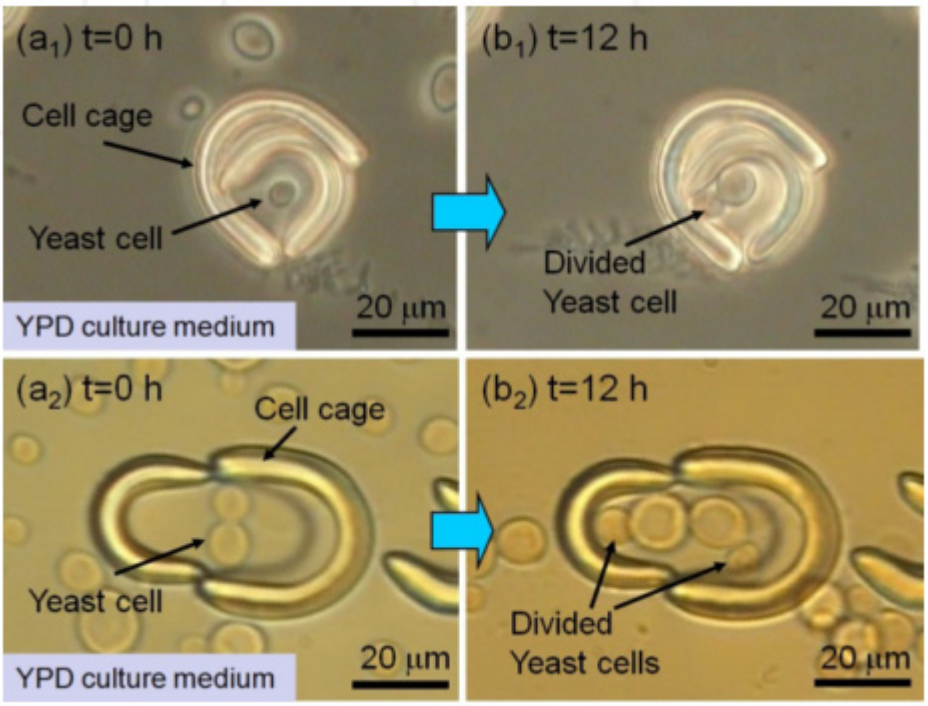

Figure 1.14 . Images of the division of yeast cells during 12 hours culturing inside the cell cages[75].

Dielectrophoresis (DEP) is a phenomenon in which a force is exerted on a dielectric

particle when it is subjected to a non-uniform electric field [76-78]. This force does not require the particle to be charged. It was also wildly used for the cell trapping, movement or sorting, especially inside liquid environment which is also necessary for cells. The drawback of DEP is that the strength of the force depends strongly on the electrical properties of the medium and particles, the shape of particles and the frequency of the electric field. Another problem is that it is difficult to change the shape of electrodes after fabrication of the whole devices.

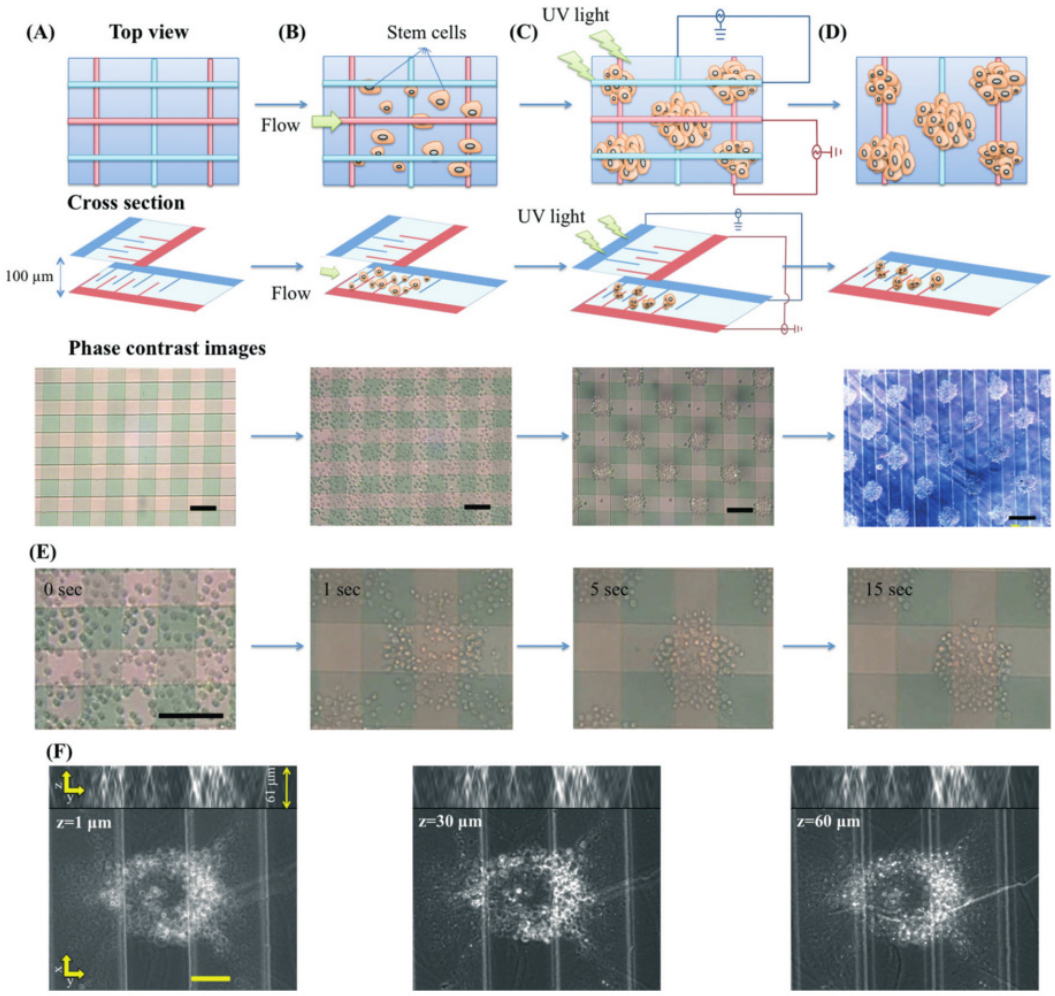

Figure 1.15 Formation of 3D ESC aggregates in the GelMA hydrogel using DEP. (A) ITO-IDA electrodes were arranged face-to-face and a microfluidic chamber was maintained between them using a polyester film of 100 µm thickness. (B) The stem cells in the GelMA prepolymer were introduced into the 100 µm height chamber and (C) localized by n-DEP forces to the low electric field regions within the ITO-IDA electrodes. The GelMA prepolymer was then exposed to UV light, embedding the cells in a stable microscale organization. (D) Aggregated ESCs within the GelMA hydrogel were removed from the top IDA electrode and cultured. (E) Phase-contrast images of the ESC patterning over time. The ESCs were dielectrophoretically patterned within 15 s. (F) Phase-contrast images of ESC aggregates at different z-axis stacks indicating the 3D structure of stem cells. Projection of stem cells along the z- and y-axes is shown at the top of images. Scale bars: 50 µm [79].

To overcome these drawbacks, a new concept called optoelectronic tweezers (OETs)

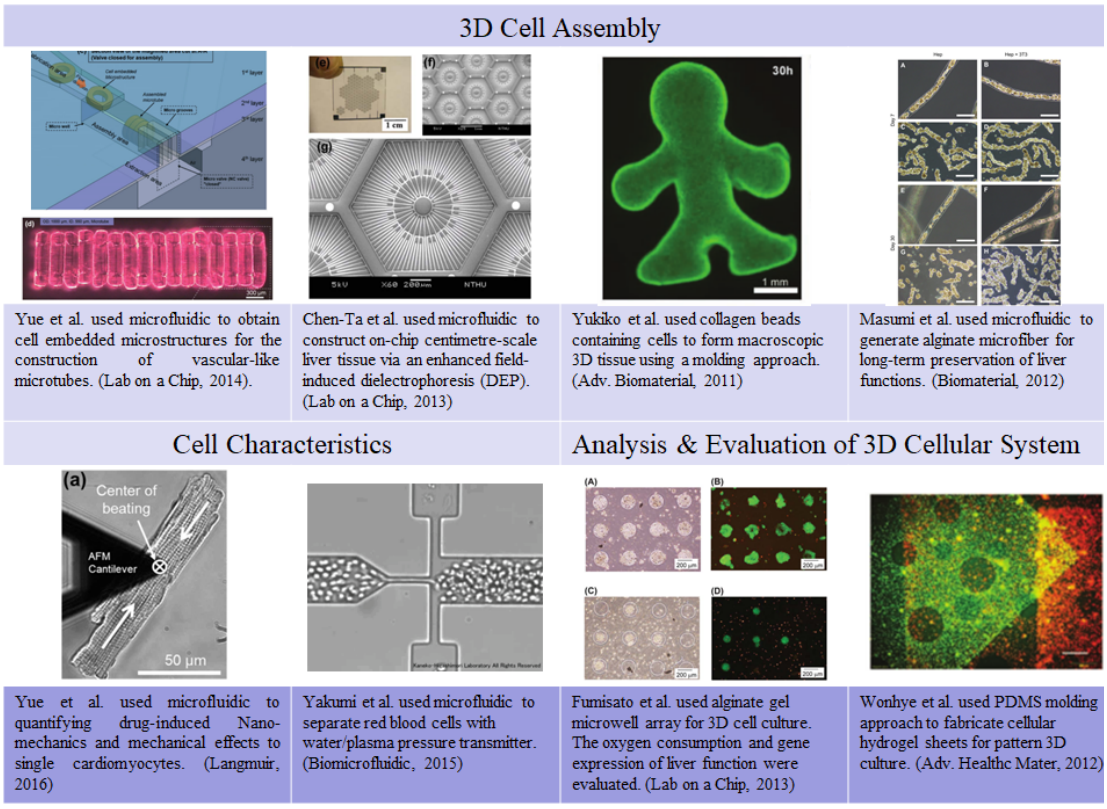

Figure 1.16 Summarize of the conventional works on tissue engineering

[80] is proposed [81]. OETs use projected optical images to grab and corral tiny particles, Light first creates 'virtual electrodes' on the substrate. Secondly, the image in conjunction with an externally applied electrical bias creates the localized DEP traps in the illuminated areas. It combines the advantages of optical tweezers and electrode-based DEP and contributes to building cell structures for tissue engineering.

In summary, lots of applications related to new techniques for tissue engineering has been well established recently as shown in Figure 1.16. In this figure, we divided these researches into three categories: 3D bio-assembly, cell characteristics and analysis & Evaluation of 3D cellular system. In this chapter, we have briefly introduced the typical methods of 3D bio-assembly for artificial tissue or organ fabrication. From next chapter, we will focus on the specific method we used and how we improve the method for the new applications of in vitro 3D tissue formation.

1.4 Organization of the thesis

In chapter 1, we present the motivation and requirements of cell-laden structures assembly for tissue engineering. 3D in vitro tissue models have been used in tissue research as a compromise between 2D cultures of isolated cells and the artificial 3D

tissue architecture. Constructing 3D cell models provide a potential alternative to in vivo approaches for whole-organism, and 2D culture with its spatial limitations. Recent advances in tissue engineering have relied upon development of methods to place spatially selective biological components at specific three-dimensional (3D) locations. There is similar interest in developing methods to assemble cells within bio-scaffolds for fabrication of 3D cell structures. Current methods to assemble cells into two-dimensional (2D) or 3D structures include non-spherical polymeric microparticle in situ photo-polymerization, cell patterning on 2D surfaces by using dielectrophoresis technique, 3D bio-printing, cell sheet engineering, and cell encapsulation units. Thus, many fabrication methods have been developed to immobilize and culture cells in 3D formats. However, the challenges for better mimicking the native tissue microenvironment are still remained.

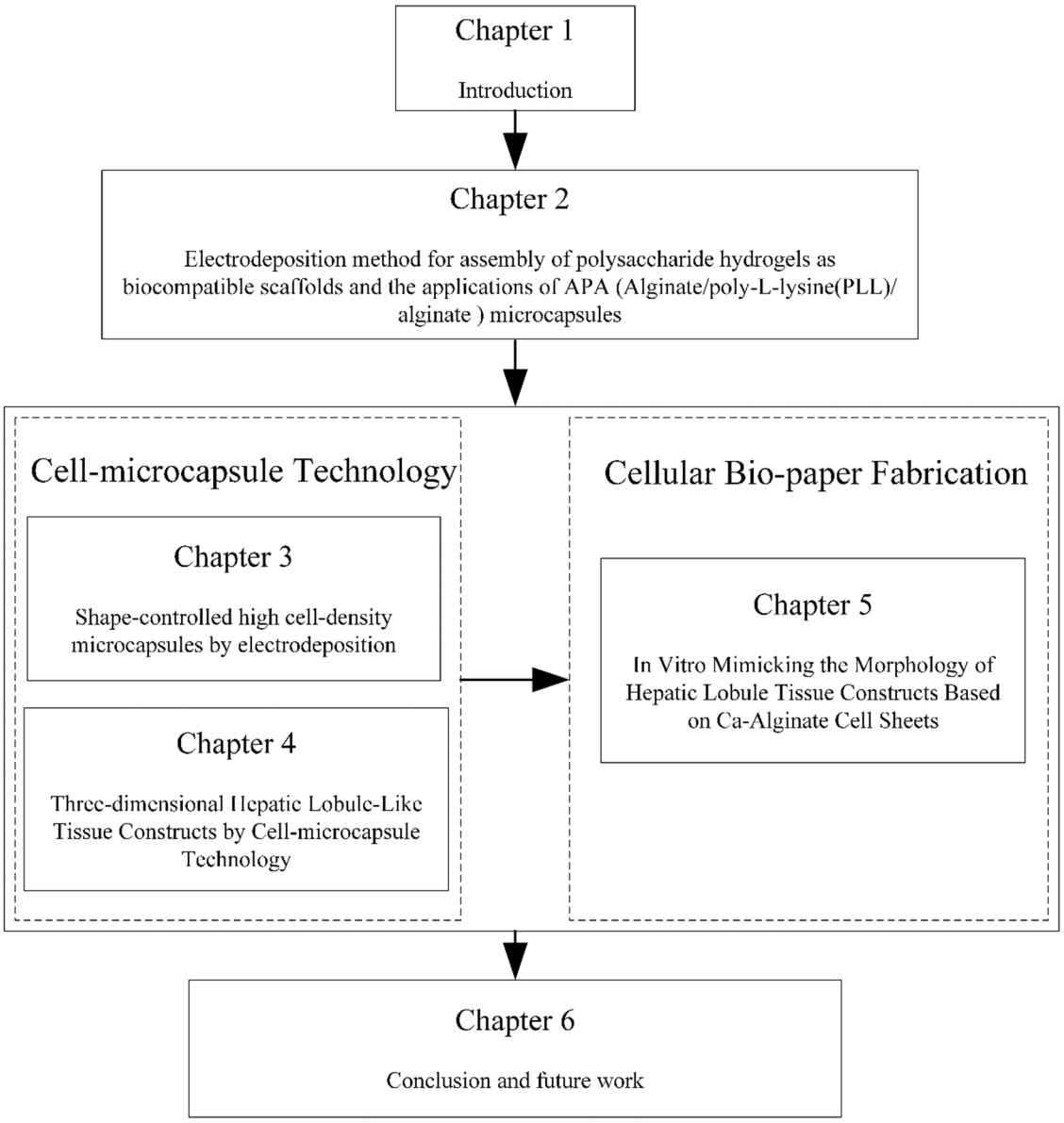

Figure 1.17 Organization of the thesis. This thesis can be divided into three sections.

In chapter 2, the background of electro-device basing on electrodeposition is briefly introduced. The current applications in cell manipulation and assembly are also reviewed. We introduce the basic fabrication methods for building micro-pattern electrode devices. Various function integrated electro-devices are referred. Some of our fabricated functional parts on electro-device are presented. The management of used cell lines is introduced.

In chapter 3, a novel method for fabricating shape-controlled alginate-PLL microcapsules to construct 3D cell structures based on electrodeposition method is provided. Two-dimensional Ca-alginate cell-laden gel membranes were electrodeposited onto a micro-patterned electrode and further detached from the electrode. The PLL was coated onto the gel structures to form alginate-PLL complex as an outer shell and sodium citric solution was utilized to melt the internal alginate to achieve miniaturized 3D microcapsules (sphere, cuboid, and rod shape). By this proposed method, rat liver cells (RLC-18) formed multi-cellular aggregates with high cell-density after cultivation for 2 weeks.

In chapter 4, we present the fabrication of hepatic lobule-shaped microtissue (HLSM) containing rat liver (RLC-18) cells. By using cell-microcapsule technology, RLC-18 cells were encapsulated in the core region of poly-L-lysine-alginate microcapsules. After 14 days of long-term cultivation, RLC-18 cells self-assembled into HLSM, and the cells fully occupied the microcapsule. By monitoring the cell number and albumin secretion during culture and characterizing the dimensions of the fabricated tissue, we demonstrated that the HLSM showed higher hepatic function as compared with normal cell spheroids. We also showcased the assembly of these microtissues into a 3D four-layered hepatic lobule model by a facile micromanipulation method. Our technology for fabricating 3D multilayer hepatic lobule-like, biofunctional tissue enables the precise control of tissue shape in three dimensions. Furthermore, these constructs can serve as tissue-engineered building blocks for larger organs and cellular implants in clinical treatment.

In chapter 5, we propose a novel approach in the fabrication of cellular bio-paper made of Ca-alginate hydrogel, embedded with liver cells (RLC-18) in order to mimic liver lobule tissue. Ca-alginate sheets with hepatic lobule-shaped patterns were deposited onto a micro-electrode device using electrodeposition. Viability of embedded cells was ensured to exceed 80%. Cell morphology and bio-functionality were monitored during the one-week culture period and results compared with those of traditional 2D culture. In addition, we detached cell sheets from the electrode substrate and stacked them into a 3D multi-layered hepatic lobule-like tissue.

In chapter 6, the summary of this thesis is presented and future works are prospected.

Chapter 2
Electrodeposition method for assembly of polysaccharide hydrogels as biocompatible scaffolds and the applications for Alginate/poly-L-lysine(PLL)/alginate microcapsules

2.1 Electroaddressing of biological components at specific device addresses

As mentioned in chapter 1, current methods to assembly cells at specific addresses spatially include; selective adhesion of cells onto patterned 2D microwells, photolithographic polymerization to entrap cells within 3D hydrogel block (PEGDA or GelMA), rapid prototyping (RP) methods that fabricates 3D cell-laden scaffold layer by layer, and microfluidic technology that enable addressing or immobilization of cells within specific channel. Thus, a variety of novel methods have been developed to address and cultivate cells in array and microfluidic formats. Nevertheless, the search continues for simpler, generic, less expensive and more benign methods for cell addressing [82].

The electroaddressing technology plays a role as a powerful tool in the cell manipulation and assembly, because it provides a programmable method for the spatiotemporally controllable assembly of cell populations for 3D cell culture and for hyper bio assembler. To our knowledge, chitosan was the first hydrogel-forming polysaccharide to be electro-deposited [83]. An applied voltage was used to deposit a thin layer onto a negative electrode when the electrode is immersed in a chitosan solution. Additionally, the thickness of the deposited layer can be controlled by the deposition conditions. Finally, once the deposited layer is neutralized, it can be retained on the electrode surface even in the absence of an applied voltage

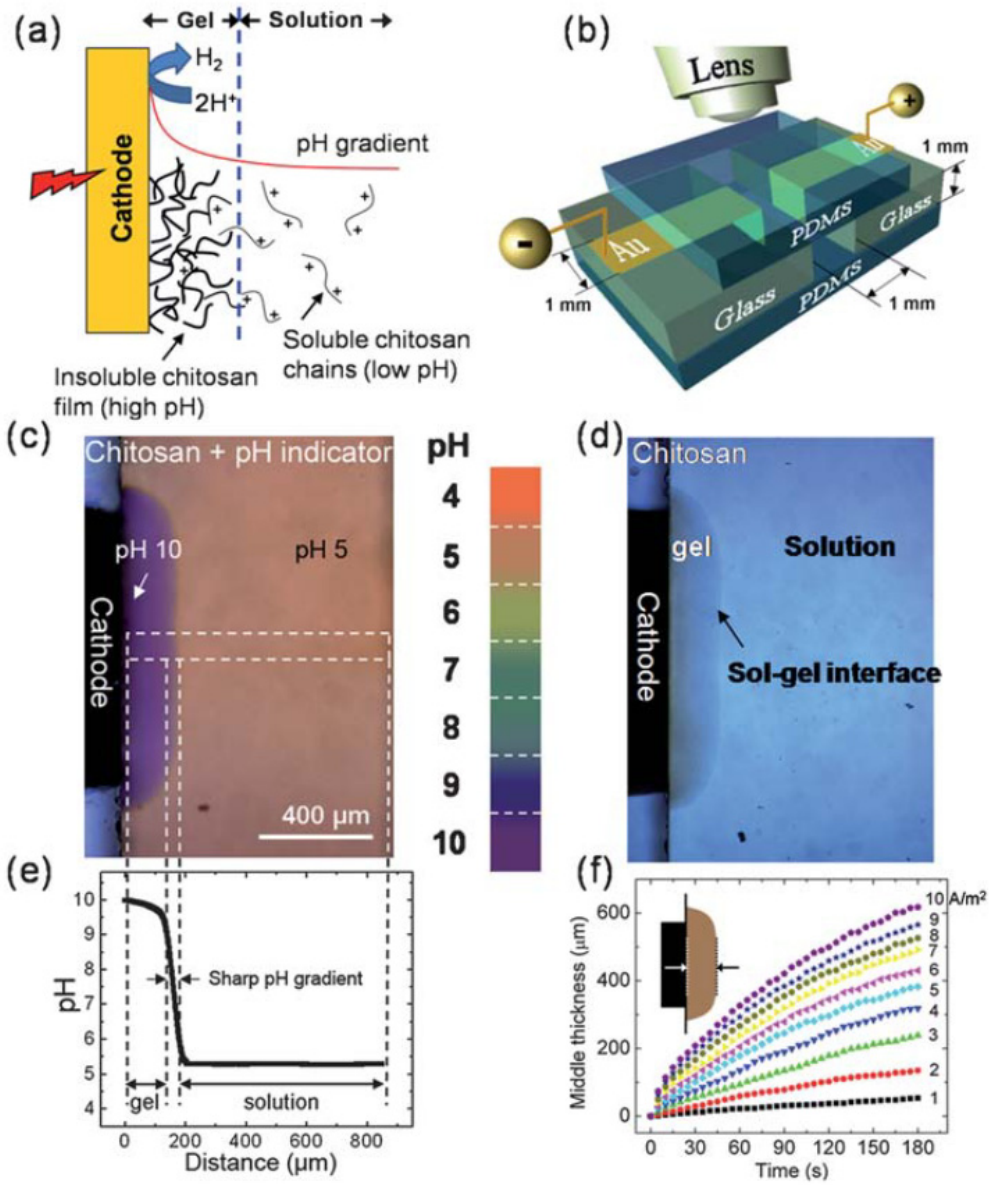

Figure 2.1 Visualization and quantification of chitosan electrodeposition. (a) Schematic diagram illustrating the mechanism of the electrodeposition of chitosan hydrogel. (b) Schematic diagram of a microfluidic device structure. Sidewall electrodes are defined by angled thermal evaporation by using a shadow mask. The glass slides are placed side by side and sandwiched between two thin layers of solid PDMS to form the microfluidic channel. Bright field microscopic images show the chitosan hydrogel growth at the cathode surface with a constant 4 A m^{-2} current density at 85 s during deposition using 0.5% (w/v) chitosan polyelectrolyte solution (c) with pH indicator solution and (d) withoutpHindicator solution. (e)pHprofile of the area highlighted by white dashed rectangle in (c). (f) Time-dependent gel thickness as a function of current density varied from 1 to 10A m^{-2} (from bottom to top). Inset, a schematic diagram illustrating the measured thickness in the middle of the gel[84].

Chitosan is produced from an N-deacetylation of chitin under alkaline conditions. Chitin occurs mainly in the cuticles of arthropods, the endoskeletons of cephalopods,

and fungi. With biodegradable and good biocompatibility, chitosan plays an important role in cell regulation and tissue regeneration. Chitosan, as chitin, belongs to the family of linear copolymers of (1→4)-2-amino-2-deoxy-β-D-glucan (GlcN) and (1→4)-2-acetamido-2-deoxy-β-D-glucan (GlcNAc) [85]. The primary amines on chitosan's glucosamine residues can be protonated at low pH, making chitosan a water-soluble cationic electrolyte. At pH higher than its pKa=6.3, the primary amines can be deprotonated and the chitosan undergoes a sol–gel transition to form a stable hydrogel network [84]. As shown in Figure 2.1, by creating a pH gradient, the pH-responsive solubility of chitosan hydrogel was fabricated on the cathode electrode.

Stimuli-responsive polysaccharides, not only chitosan but also alginate, can be induced by chemical reaction to undergo reversible sol–gel transition to generate soft material structures on conductive surfaces [82]. Alginate is a biopolymer isolated from brown seaweeds, which is composed of two monomers:β-D-mannuronate and R-L-guluronate. Generally, alginate forms a physical gel by cooperative binding with divalent cations such as Ca^{2+} or Ba^{2+}. Many methods have been developed to generate different alginate gel structures such as microfiber and matrixes using microfluidic devices. Studies of alginate hydrogels for programmable 3D cell assembly also indicated that it is appropriate for long-term culture and cell entrapment in vitro.

Unlike other techniques, the electrodeposition of alginate hydrogel provides a programmable and biocompatible method for spatially selective cell entrapment and 3D cell culture. During the electrodeposition process, instead of directly adding the Ca^{2+} ions into the solution, Ca^{2+} ions are released via $CaCO_3$ particles by reacting with H^+. Conventionally, an electro-device basing on electroaddressing technology is a set of two conductive electrodes as anode and cathode immersed inside the deposition solution (generally contain alginate and carbon dioxide particles). A DC voltage was then applied to the electrode to induce an electrolysis reaction. Thus, the alginate hydrogel membrane will be fabricated on the anode electrode. This approach is promising for electroaddressable biological component assembly for the Ca^{2+}-alginate deposition provides a mechanism that can limit significant pH excursions away from neutral condition [86].

However, fabrication of cell-laden hydrogel structures with arbitrary shape are in needed for constructing 3D cell structures in tissue engineering, because these structures can act as a basic unit to assembly complex 3D cell structures. In this chapter, the fabrication and various conventional functional electro-device systems, for cell-laden hydrogel structure fabrication system, will be described.

2.1.1 The mechanism of electrodeposition method.

The mechanism of the cation-crosslinked with alginate using electrodeposition method is depicted in Figure 2.2 The two electrodes were firstly immersed into deposition solution which normally contains alginate and $CaCO_3$ particles. A DC

voltage was then applied to the electrode to induce an electrolysis reaction. As we known, the electrolysis process splits water into its elements, namely hydrogen and oxygen. It will reduce the amount of hydrogen ions and oxygen ions of solution continuously, which just broke the balance system inside the deposition solution. Because of that, hydrogen ions move toward the anode surface losing its electronic to generate oxygen ($4OH^- - 4e^- \rightleftharpoons 2H_2O+O_2\uparrow$) and form an acidification environment at the anode surface. (Presence of H^+) Then, Ca^{2+} will be released due to the protons encounter and react with the suspended $CaCO_3$ particles at the anode. The alginate hydrogel will be formed on the anode surface in the presence of Ca^{2+}, because the cations act as ionic bridges between L-guluronic acid residues on adjacent chain segments [87].

$$(Ca^{2+} + 2Alg–COO^- = Alg–COO^- - Ca^{2+} –^-OOC–Alg)$$

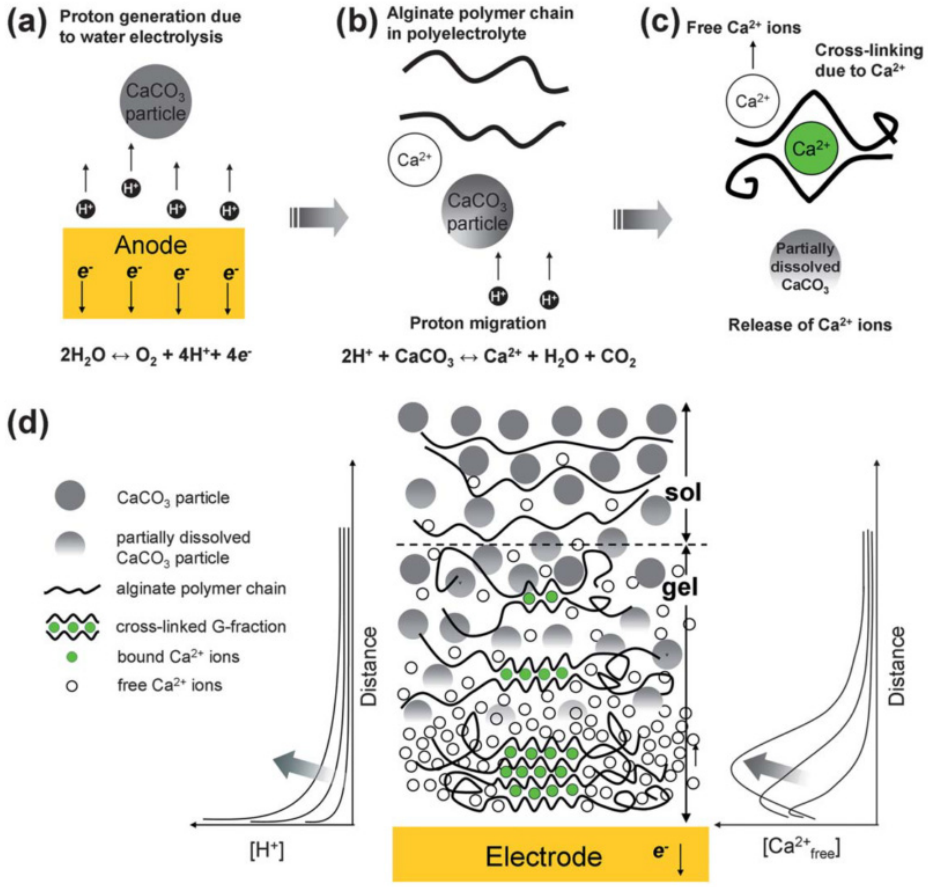

Figure 2.2 Schematic illustration of the mechanism for calcium alginate electrodeposition. (a) Water electrolysis generates excess protons (H^+ ions) at the anode surface. (b) The protons migrate away from anode and release Ca^{2+} ions from $CaCO_3$ particles suspended in solution. (c) The released Ca^{2+} ions crosslink alginate chains, forming a gel. (d) Overall picture of electrodeposition of calcium alginate. The proton concentration decreases with the distance away from the electrode surface. The highest concentration of free calcium ions is associated with the dissolution front of the $CaCO_3$ particles (the interface between dissolved and undissolved $CaCO_3$) during the deposition[86].

In addition to the required functionalities and the quality goals, electrodeposition

method highly improves the uncontrollability of cation-crosslinked alginate gels due to the conductive region that can be designed. Here we list the main advantages of electrodeposition method for bio-assembler.

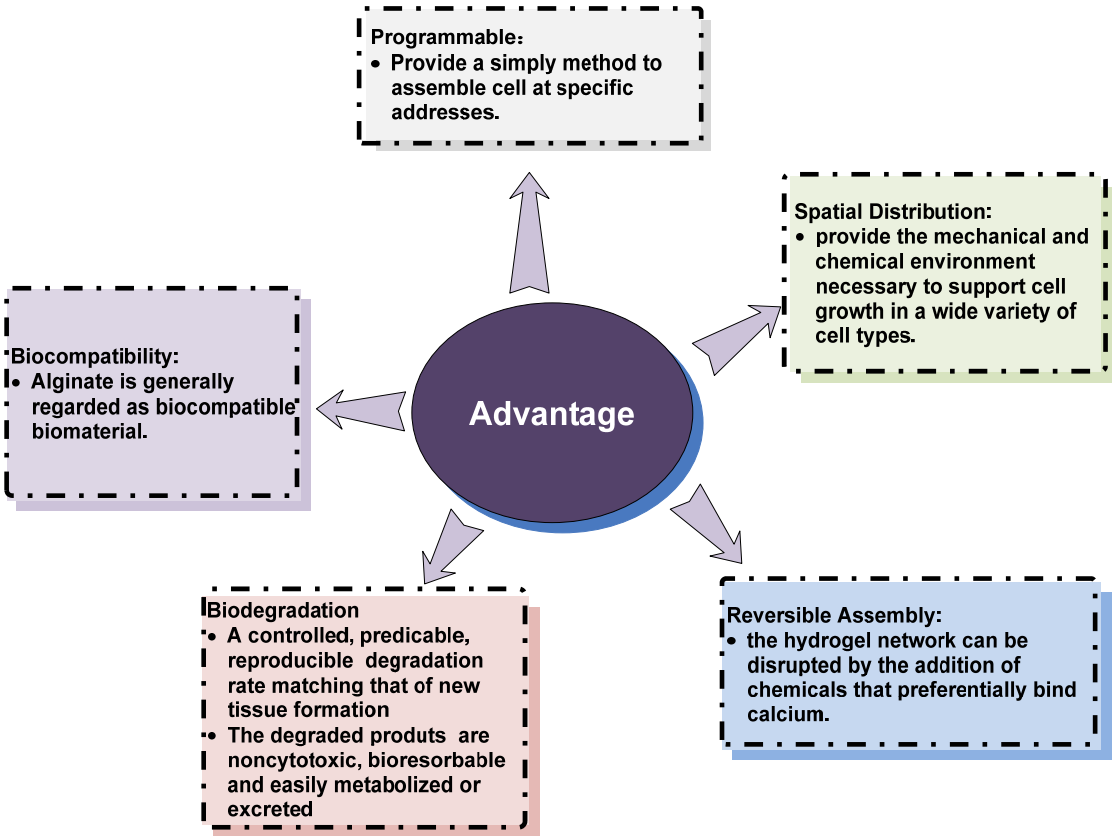

Figure 2.3 The characteristic of electrodeposition method for tissue engineering

It shows the high potential of the microfluidic system to be used in the complex tasks, such as fabrication, manipulation and assembly like a factory line in one chip. Besides, it has high potential to be pushed towards portability, more low-cost and high efficiency. Therefore, it is a promising way to perform the 3D cell structures assembly inside multi-functional devices.

The parameters of the scaffold can significantly affect cell differentiation, amount and rate of tissue formation, and intensity or duration of any transient or sustained inflammatory response in vivo [88]. The scaffold based on electrodeposition method can be arbitrary shapes, even highly complex structures. A number of general issues may need to be considered for the choice of biomaterial and the design of scaffolds as shown in Figure 2.3. The characteristic of electrodeposition method for tissue engineering

- Be 3D, highly porous, and biocompatible with a controlled degradation rate;
- Have cytocompatibility with an appropriate surface for cell adhesion, proliferation, migration, differentiation and axon outgrowth;

- Maintain proper mechanical properties (elasticity, strength, tenacity) that approach those of the host tissue to protect the seeded or recruited cells and maintain its structure under mechanical perturbations;
- Provide a three-dimensional environment to maintain chondrocyte phenotype and a surface chemistry and topography to which cells can anchor;
- Be cost effective and and possible to scale up in number.

2.1.2 Applications of electrodeposition method in entrapment of biological components

An integrated electro-device incorporates many of the necessary components and functionality of a typical room-sized laboratory on to a small chip. This device is not only with the scaling down of the size, but also reveals other significant advantages including: minimized consumption of reagents, increased automation, and reduced manufacturing costs. It integrates one or several laboratory functions on a single chip, which has the dimension of only millimeters to a few square centimeters in size. Actually, the integrated electro-device is a combined system rather than one independent kind of technique, which can be considered as a complex system. Many techniques mentioned above, not only the electrodeposition method but also like microfluidic, micro aspiration and DEP, are always employed in one chip at the same time. Figure 2.2 shows large integrated electro-systems. The electrodeposition method has many advantages, such as low cost, faster analysis and response times, and it has been used in biological field for manipulating cells and building cell structures [89].

As shown in Figure 2.2A calcium-alginate composite hydrogel biofilm entrapping bacterial cells was fabricated on the gold electrodes inside the microfluidic system, with 3D control using electrical signals. The reported multi-strain cell co-assembly and stratified cell assembly with controlled separation in pseudo-3D hydrogel structures expands our toolbox towards understanding the distance-dependent interactions and communication between the same or different species of cell colonies. The induced protein expression and quorum-sensing behavior of the bacterial cells entrapped in the pseudo-3D model bio-films, demonstrated in their microfluidic device [90]. It shows the high potential of the electrodeposition method to be used in the complex tasks, such as fabrication, manipulation and assembly like a factory line in one chip. Besides, it has high potential to be pushed towards programmable, more low-cost and high efficiency. Therefore, it is a promising way to perform the 3D cell structures assembly inside multi-functional devices.

With different functions, there are many applications of the electro-devices for cell structure construction and assembly. By controlling the PH gradient, the chitosan hydrogel can be manipulated according certain direction or position. Enzyme can be assembled to 2D microstructures inside the hydrogel.

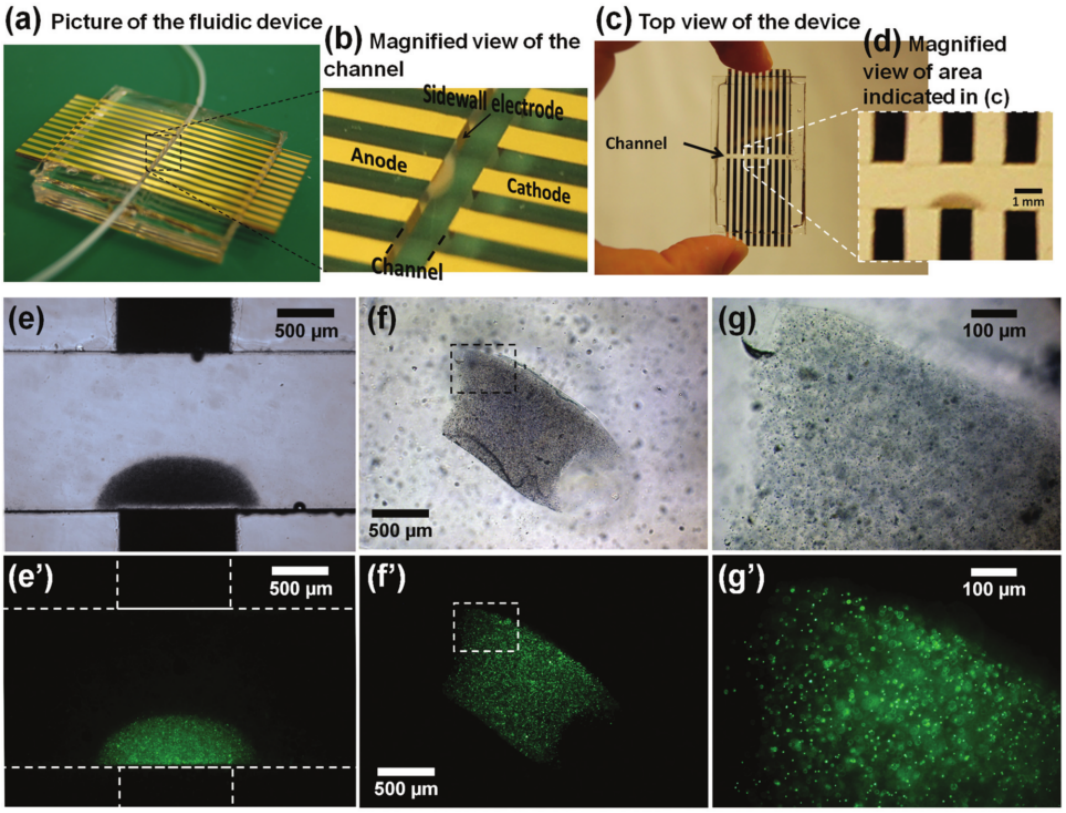

Figure 2.4 Pictures of the fluidic device and micrographs of the electrodeposited calcium alginate hydrogel. a) An overview of the fluidic device with built-in sidewall electrodes inside the channel and plastic tubes connected as an inlet and outlet. b) A magnified view of the fluidic device with a cloudy-white hydrogel deposited on one of the sidewall electrodes (anode). c) Top view of the fluidic device. d) A magnified top view of the fluidic channel with the electrodeposited hydrogel on one of the electrodes. e – e′) Optical (e) and fluorescence (e′) micrographs of a calcium alginate hydrogel (side view) deposited on an anodic electrode inside the fluidic channel. f – f ′) Optical (f) and fluorescence (f ′) micrographs of the calcium alginate hydrogel (top view) detached from the electrode and placed on a glass slide. g – g′) Magnified optical (g) and fluorescence (g′) micrographs of a part of the hydrogel [90].

A light-addressable electrolytic system used to perform an electrodeposition of calcium alginate hydrogels using a digital micromirror device, as shown in Figure 2.5. In this system, a patterned light illumination is projected onto a photoconductive substrate serving as a photo-anode to electrolytically produce protons, which can lead to a decreased pH gradient. The low pH generated at the anode can locally release calcium ions from insoluble calcium carbonate ($CaCO_3$) to cause gelation of calcium alginate through sol-gel transition. This device performed an electrodeposition of enzyme-entrapped chitosan membranes for multiplexed enzyme-based bioassay using a DMD. The DMD provides spatio-temporal illumination pattern switching, which is used to readily applicable to achieve flexible electrode patterning for the dynamical and multiplexed electrodeposition of chitosan membranes. [91]. However, this method is

not suitable for entrapment of biological cells for tissue engineering due to the low PH value.

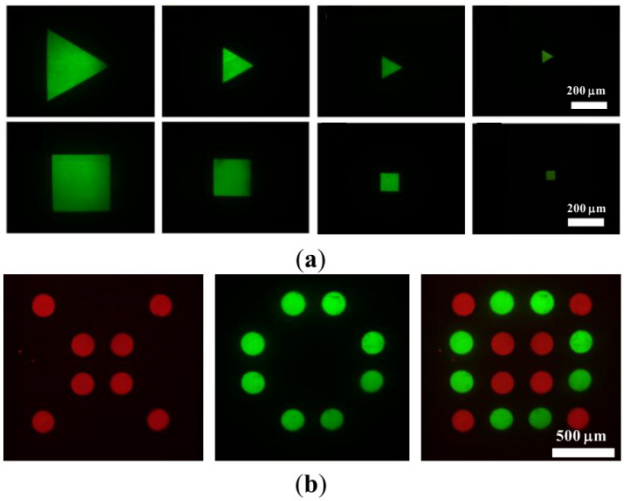

Figure 2.5 (a) Images of chitosan membranes with triangular and square shapes with different dimensions ranging from 50 m to 300 m. (b) The images of multiplexed micropatterning of chitosan membranes created by performing a light-addressed electrodeposition using two different illumination light patterns in sequence. The rightmost image shows the fluorescence micrograph of an assembled 4 × 4 microarray of chitosan membranes with a specific arrangement.[89].

In another method, the construction of multiple layers 3D cell-laden structures is demonstrated. The cell manipulation and assembly are performed in this simple method, as shown in Figure 2.6.

A tubular hydrogel structure consisting of two layers with different cell types was fabricated as shown Figure 2.6A 300 mm diameter Pt wire was immersed deposition solution containing HUVECs cells at 3.1 V vs. Pt for 30 s. Following the formation of a tubular layer of HUVECs around the Pt wire electrode, the electrode was transferred to alginate solution containing 3T3 cells (3×10^6 cells/mL). Then, a potential of 3.1 V vs. Pt was applied to the electrode to deposit a layer of 3T3 cells for 30 s. Thus, multi-layers tubular hydrogel structures were constructed via electrodeposition using alginate gels. This simple method is a promising approach for construction of multi-layer tubular hydrogel structures for tissue engineering.[92]

Both 2D and 3D biomaterial-based culture platforms that are capable of mimicking the *in vivo* microenvironment to recapitulate the physiological conditions are vital tools in a wide range of cellular and clinical research. The 3D spheroid culture of embryonic stem (ES) cells or hepatocellular carcinoma cells (HepG2) on micro-pattern electrode-device was demonstrated. This device offered new opportunities to achieve active control of 2D cellular patterns and 3D multi-cellular spheroids on demand, and may be amenable toward the further construction of more complex cell structures [93].

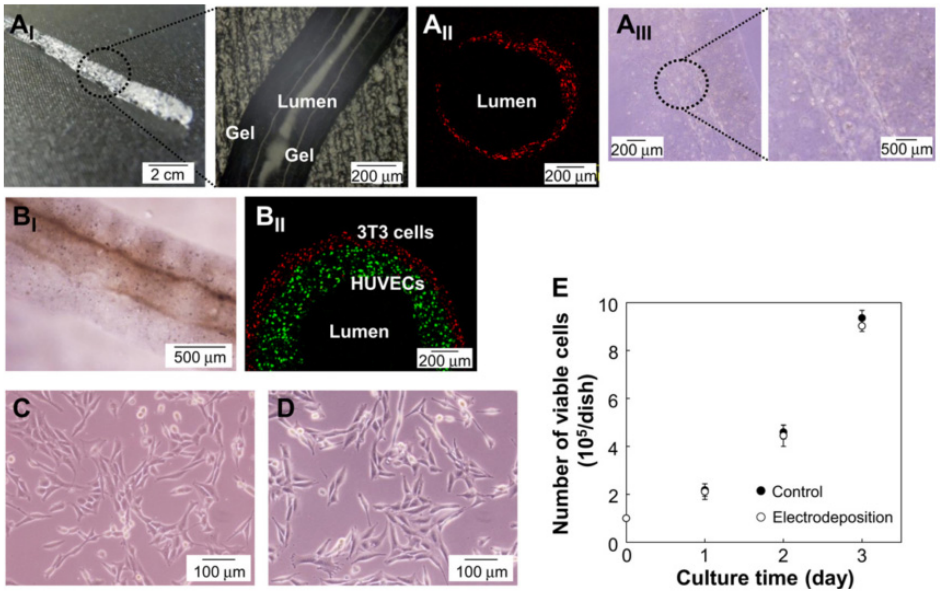

Figure 2.6 Tubular alginate gel containing cells. A single layer consisting of 3T3 cells or HUVECs (A), and a two-layer structure consisting of HUVECs and 3T3 cells (B) were fabricated. These tubular alginate gels were observed under an optical microscope (AI and BI). Cross-sections of the gels were observed under a fluorescence microscope (AII and BII). (AIII) Calcium alginate gel containing HUVECs was cultured for 1 day. After alginate gel containing cells, effects of anodic electrodeposition of calcium alginate on cell viability was investigated. Cells were harvested from calcium alginate gel after dissolution of the gel in citric acid. Collected 3T3 cells were seeded onto a conventional culture dishes (initial viable cell number, 1×10^5 cells). The cells with (C) or without (D) the electrodeposition were cultured for 3 days and observed by phase contrast microscope, and their cell growth was investigated using the trypan blue exclusion test (E) [92].

However, only spheroids can be constructed and the further assembly of these cell units is difficulty in the above methods. It means that the complex and large 3D cell structures are difficult to build in the current electro-device Therefore more functional parts such as microelectrodes, micro-pattern and new method are needed in our research. The device for constructing complex 3D cell structures should has the capabilities such as arbitrary shape structure fabrication, manipulation.

2.2 Micro fabrication for building micro-patterning electrode devices

2.2.1 Photolithography methods and equipment

This section describes the basic fabrication method for micro-patterning electrode

devices. The manufacture of a micro-patterning electrode device starts with the design of the pattern. Once this design is made, it is sent to a manufacturer of photomask to be transferred on a glass medium or a plastic film. The micro-patterning is printed with UV opaque ink (if the medium is a plastic film) or chromium (if the medium is a glass plate).

After fabricating the mask, the micro-pattern is the next target. The manufacture of micro-pattering mold is made by photolithography. This is the step when the drawings of the micro-pattering on the photomask are transformed into real micro-pattering. As shown in Figure 2.7, photoresist is spread on a flat surface (often a silicon wafer) with the desired thickness. The photoresist, protected by the mask on which micro-pattern are drawn, is partially exposed to UV light. Thus (in the case of a negative resin, SU-8 type) only the parts representing the non-pattern area are exposed to UV light and cured, the other parts of the micro-pattern being protected by the opaque areas of the mask. [94] Then, the photoresist is developed by a special solvent that etches the areas where were not exposed to UV light.

Thus, we have obtained the substrate with micro-pattern resin. generally, to fabricate the micro-pattern electrode device, there are several methods to achieve that. including: (a) Using ITO (Indium tin oxide) glass slide as the substrate. ITO glass slide is a kind of conductive and transparent material which is suitable for optical observation and experiment research. After coated the micrp-pattern resin on ITO slide by lithography, the slide will be immersed into etching solution to achieve the micro-pattern electro-device by removing the conductive area partially. However, the etch rate is hard to be controlled precisely. To achieve the micro-pattern as small as 10um is barely possible (b) With the spattering machine (such as Canon E-200), we can fabricate the micro-pattern as accurate as 1um with predefined shape. As shown in Figure 2.7. The patterned surface is fabricated by deposition 250 Å thick chromium and then 400 Å thick gold films on micro-pattern photoresiste as described above. Following of ultrasonic in ethanol for 10 min to obtain the electrode-device. However, this method can fabricate electro-pattern precisely, the fabrication process is too complex and the chromium layer is unstable during the electrolysis which leads to the corrosion of electrode (c) To simplify the fabrication process and increase the repeatability of electro-device, we choose FTO (Fluorine doped tin oxide) glass slide as the substrate which is a kind of conductive glass similar to ITO but can withstand higher apply voltage. Then micro-pattern photoresiste was fabricated on FTO slide. The accuracy of pattern is dependent on the type of photoresiste that we chose. Compared with the etching or spattering process, this method provides a simple and cheap approach for fabrication of micro-pattern electro-device

About the fabrication equipment, the spin coating, mask fabrication machine, UV or laser exposure machines and commonly used photoresist material are needed in the fabrication procedure.

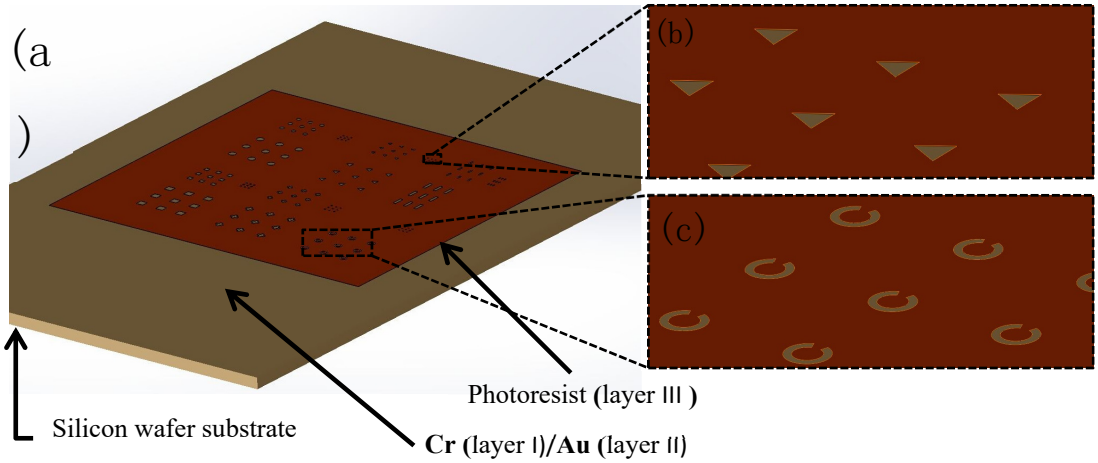

Figure 2.7 Common used fabrication method for our micro-pattern electro devices. (a) The patterned surface is fabricated by deposition 250 Å thick chromium and then 400 Å thick gold films on silicon wafer. Pattering is achieved using photolithography technique in which a primer and the photoresist (such as AZ5214E) is spin-coated onto the gold surface and is exposed to UV light (power: 19 mw/cm^2 time: 2s) through a specially designed mask. (b) A magnified top view of the pattern-electrode array at the center of the chip.

Many fabrication approaches are reported for different kind of requirements, such as high precision, repeatability, simple above. Based on their advantages and disadvantages, it's essential to choose a suitable methodology for the fabrication of the experimental device.

2.3 Applications of micro-pattern electro-devices

2.3.1 Microelectrode integrated devices

As mentioned in the last chapter, electrodeposition is suitable for using as a non-mold on-chip manipulation approach. In order to make electrolysis of water release proton, the microelectrodes are needed. These electrodes are made by the conventional photolithography techniques as described in the last section. The micro-pattern electro-device integrated chips for electrodeposition applications are called microelectrode integrated devices.

Figure 2.8 shows a typical microelectrode integrated device. This is a micro fabricated device that the pattern of the logo consisted of assembled E. coli cells expressing GFP, which were entrapped by the co-deposition with calcium alginate. With alginate serving as an electrotemplated coupling between the cells and the electrode, cell assembly onto specific locations in an arbitrary pattern could be easily achieved with micropatterning. Such a device has potential for cell assembly was highly

controllable and a lateral resolution down to tens of micrometers could be achieved.[90].

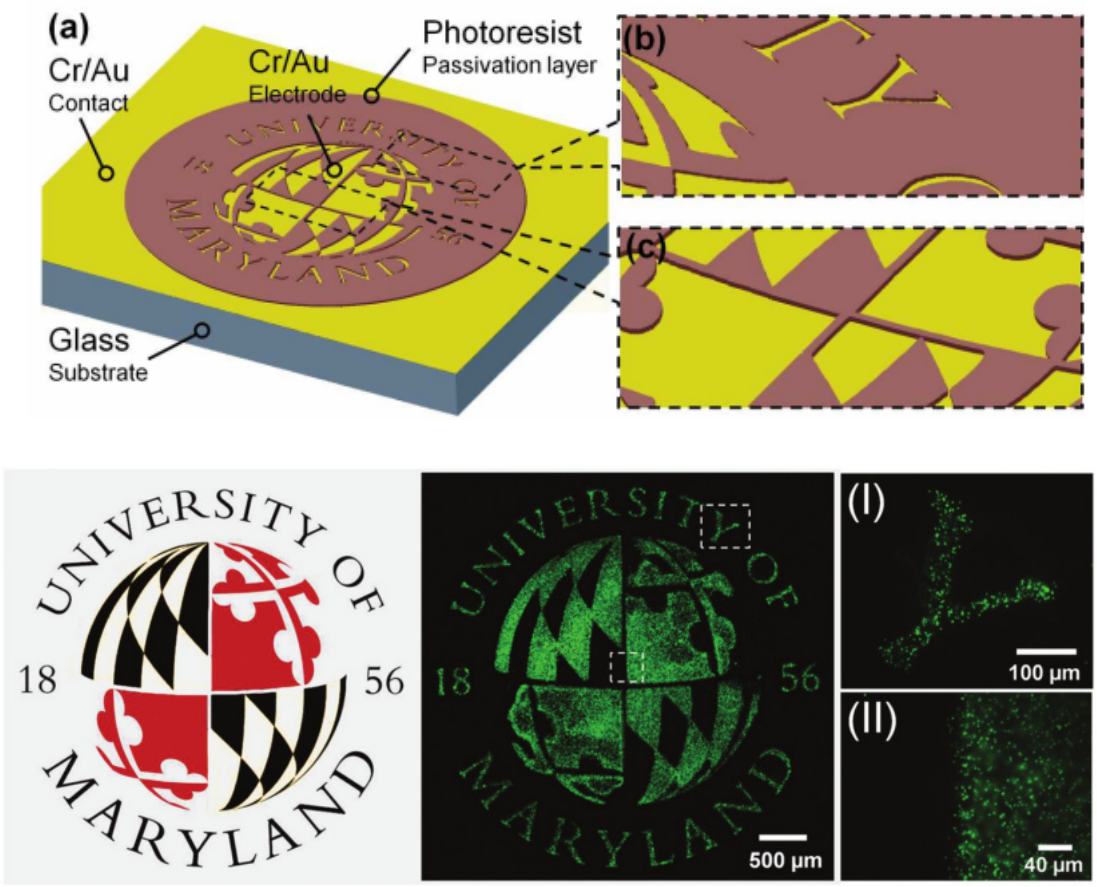

Figure 2.8 Schematic diagram of the planar device with the UMD logo pattern. (a) Schematic diagram of the planar device structure. The electrode and the photoresist passivation were defined by thermal evaporation of chromium and gold and photolithography. The deposition solution was only in contacts with the passivated circular region. The chromium and gold at the edge of the chip was used as an electrical contact. (b) and (c) Magnified regional views of the selective passivated regions, marked with black rectangles in (a) Fluorescence micrograph showing that the pattern of the logo consisted of assembled E. coli cells expressing GFP [90].

In the microelectrode integrated device, it not only can achieve the manipulation and patterning of cells by electrodeposition method or DEP technique, but also can run several exposure tests on living organisms such as Caenorhabditis elegans (C. elegans) simultaneously. Figure 2.9 shows a method to construct a microfluidic device with a multi-valve system. In this research, A pair of electrodes was installed in the device and the capacitance in-between the electrode was measured. When a C. elegans passed through the electrodes, the capacitance was changed. The capacitance change was proportional to the body volume of the worm, thus the body volume change by the heavy metal exposure was measured in the device. Thirty worms were divided into three groups and exposed to each solution. These results indicate that the microelectrode integrated device also gives a promising approach for simultaneously analyzing the effect of multiple stimuli on living organisms.

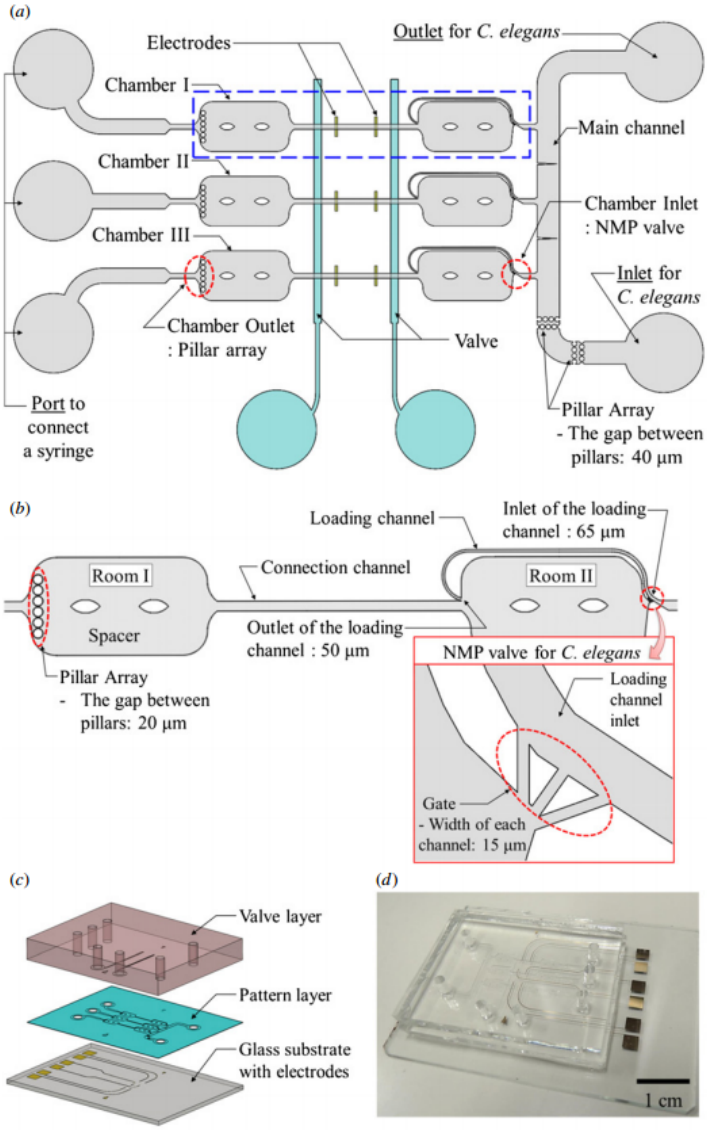

Figure 2.9 Schematic diagrams of the proposed microfluidic device. (a) A schematic diagram of the proposed microfluidic device, which has three chambers and a main channel. The chamber has two small rooms; a blue rectangle in figure1(a). (b) A schematic diagram of the chamber. It has two small rooms connected by the connection channel. The NMP valve comprises the gate and the loading channel. (c)The component of our proposed device; two PDMS layers and one glass substrate. (d) The fabrication of our proposed device; three layers are bonded by O2plasma treatment [95].

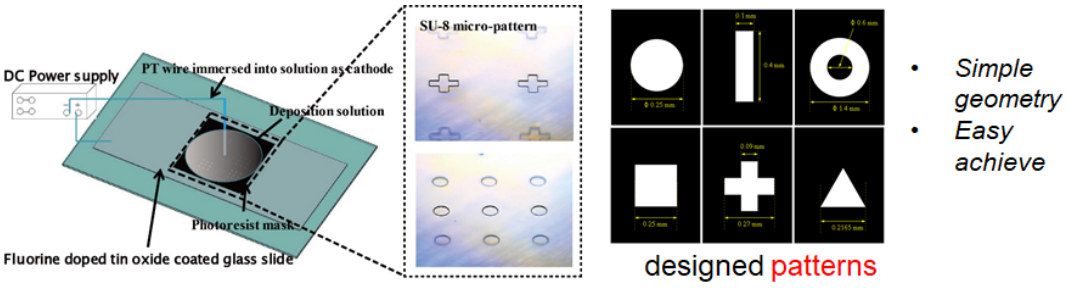

Figure 2.10 Fabrication of micro-electrode device for the deposition of Ca-alginate hydrogel structures

with varying shapes of micro-patterns in simple geometry for the demonstration.

The electrodeposition method is also called electroaddressing technique. Base on this technique, the microelectrode device integrated with programmable design and high throughput capability becomes a powerful tool for the 2D cell patterning applications. Figure 2.10 shows one of the fabricated micro-electrodes device in our research. we fabricated functional microelectrodes with different patterns in simple geometry for cell entrapment. Figure 2.11 showed the results of immobilization of RLC-18 liver cells onto the fabricated micro-patterns area based on the electrodeposition method. RlC-18 cells were successfully entrapped within alginate hydrogel structures which are transparent after electrodeposition for 30 seconds.

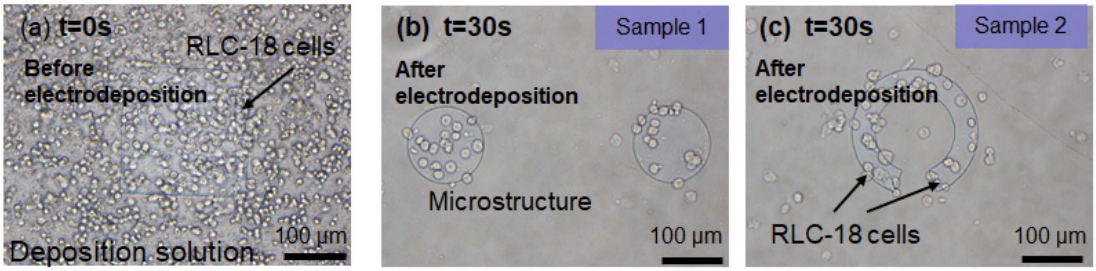

Figure 2.11 Fabrication of Ca-alginate gel structure embedded liver cells (RLC-18) based on electrodeposition method. (a) The deposition solution containing alginate, $CaCO_3$ particles and RLC-18 cells was dropped onto the micro-pattern area first. (b-c) A DC power was applied to the electrode to trigger the chemical reaction of electrodeposition. After 30 seconds, the non-cross-linked deposition solution was removed by washing process using HEPS buffer solution for several times.

2.4 Alginate/poly-L-lysine (PLL)/alginate (APA) microcapsules

The technique of Alginate /poly-L-lysine (PLL)/alginate (APA) microcapsules fabrication has been well established for several decades. It was firstly proposed by Franklin Lim and Anthony M. Sun in 1980 with the title of “Microencapsulated islets as bioartificial endocrine pancreas” [96]. In their work, the APA microcapsules encapsulated islets into rats with streptozotocin-induced diabetes corrected the diabetic for 2 and 3 weeks. The encapsulated islets remained morphologically and functionally intact throughout long-term culture studies lasting over 15 weeks. The results showed the possible potential of APA microcapsules for further implantation and drug release research. Later, since 1989, M.F.A. Goosen proposed several methods to study the mechanism of the formation of APA microcapsules. For example, he proposed a method to control the microcapsule membrane molecular weight cut-off to demonstrate how the APA microcapsules can protest transplanted cells from destruction by the recipient’s

immune system [97]. Since then, from 1990, the APA microcapsules technique has attracted lots of attentions of researchers for the varying applications, such as drug release, stem cells study and 3D cell culture system. The advantages of APA microcapsules include: 1) The alginate-PLL -alginate complex semi-membrane prevent the encapsulated islets from immune system. 2) The inner hollow structure of APA microcapsules provides a suitable “aqueous-like” microenvironment for the encapsulated cells after the transplantation. The PLL play an important role as extracellular matrix for better mimicking the in vivo state. In this chapter, we will briefly demonstrate the mechanism and typical proposed methods of APA microcapsules. Figure 2.12 has been the showcase of the fabricated APA microcapsules by our proposed method. The shape of the microcapsules can be controlled based on electroreception method by altering the design of the micro-electrode patterns.

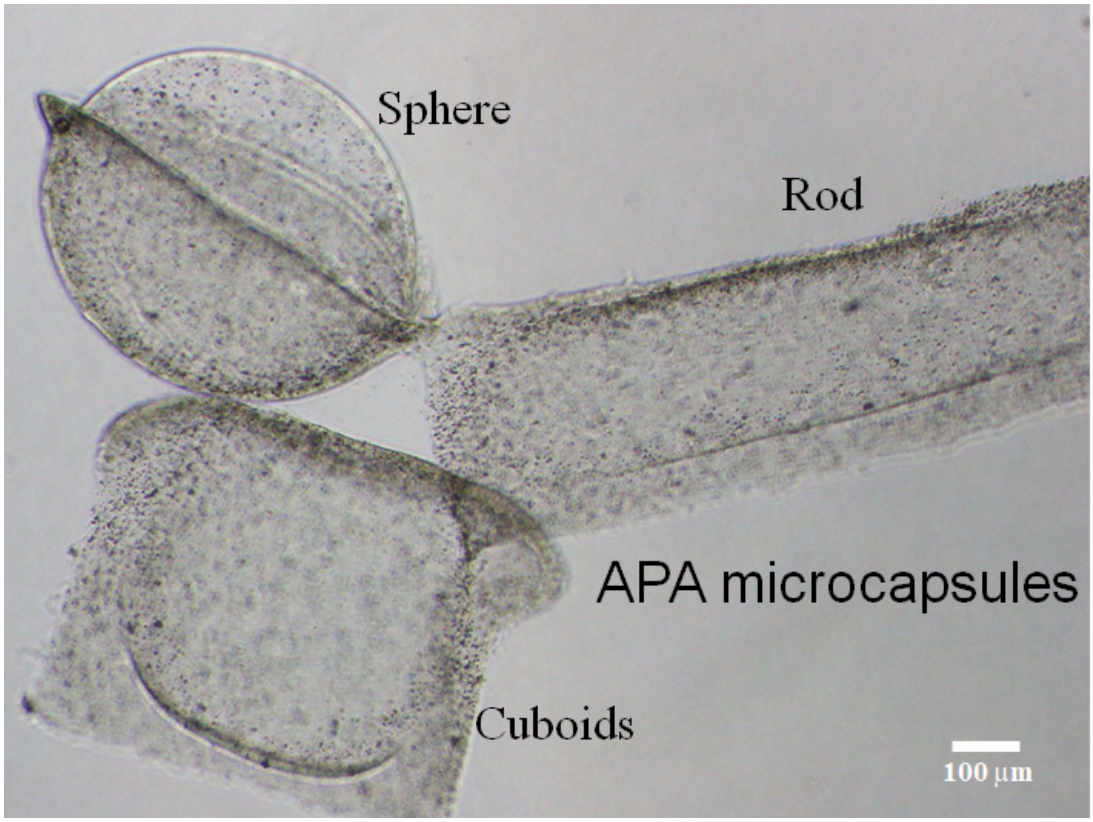

Figure 2.12 Shape-control production of APA microcapsules for tissue engineering based on electrodeposition [98].

2.4.1 Structure of alginate-poly-L-lysine capsules

The architecture of these APA microcapsules includes a central core of Ca^{2+}-cross-linked alginate gel that can provide an aqueous microenvironment and a two-layer shell consisting of a PLL inner layer and sodium alginate outer layer, as shown in Figure 2.13. The alginate-PLL semi-membrane permits passage of low molecular weight substances, such as nutrients and oxygen, to the core and passage of metabolic products from the core, while retaining the core material within the microcapsule. Sodium can be substituted by poly-L-lysine (PLL) to form a complex alginate-PLL-alginate (APA). The PLL-alginate layer can take three different structures by intramolecular hydrogen

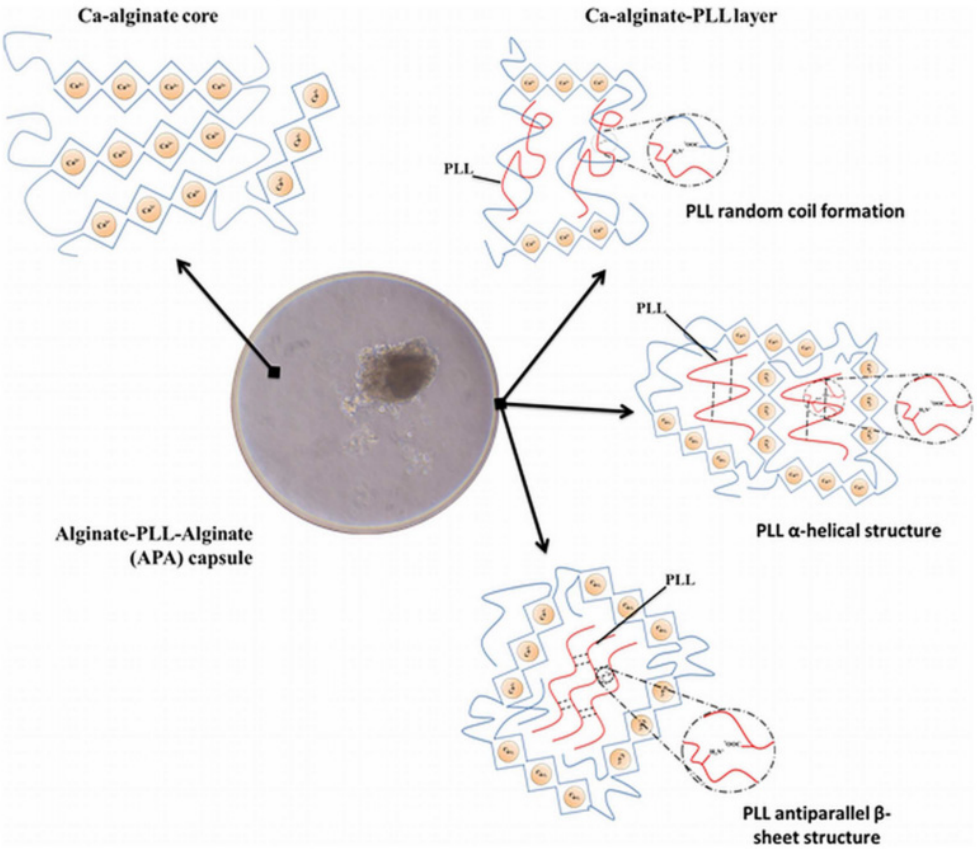

Figure 2.13 (A) The core of the capsule is composed of a matrix of alginate and calcium in which the islets are entrapped. The second layer is obtained after incubation of the calcium bead in sodium rich solutions to form a sodium-alginate complex at the surface. Sodium can be substituted by poly-L-lysine (PLL) to form a complex alginate-PLL-alginate (APA).The PLL-alginate layer can take three different structures by intramolecular hydrogen binding, (i) random coil formation between alginate and PLL, (ii) α-helicoidal structure between amide groups of PLL, and (iii) antiparallel β-sheet structure between amide groups of PLL [1].

binding, random coil formation between alginate and PLL, α-helicoidal structure between amide groups of PLL, and antiparallel β-sheet structure between amide groups of PLL.

2.4.2 Applications of APA microcapsules

By combining with micro-fabrication techniques (e. g., microfluidic and micro-nozzle device), the hundred-micrometer-size APA microcapsules can be fabricated. Therefore, the APA microcapsules proved a suitable platform for cell encapsulation since the microscale capsules can promote the cell activity and maintain highly differentiated functions [99]. The cell-encapsulated APA microcapsules have potentials to be applied to tissue engineering, drug release and 3D cell culture system. In this section, we will briefly showcase of the typical applications of APA microcapsules.

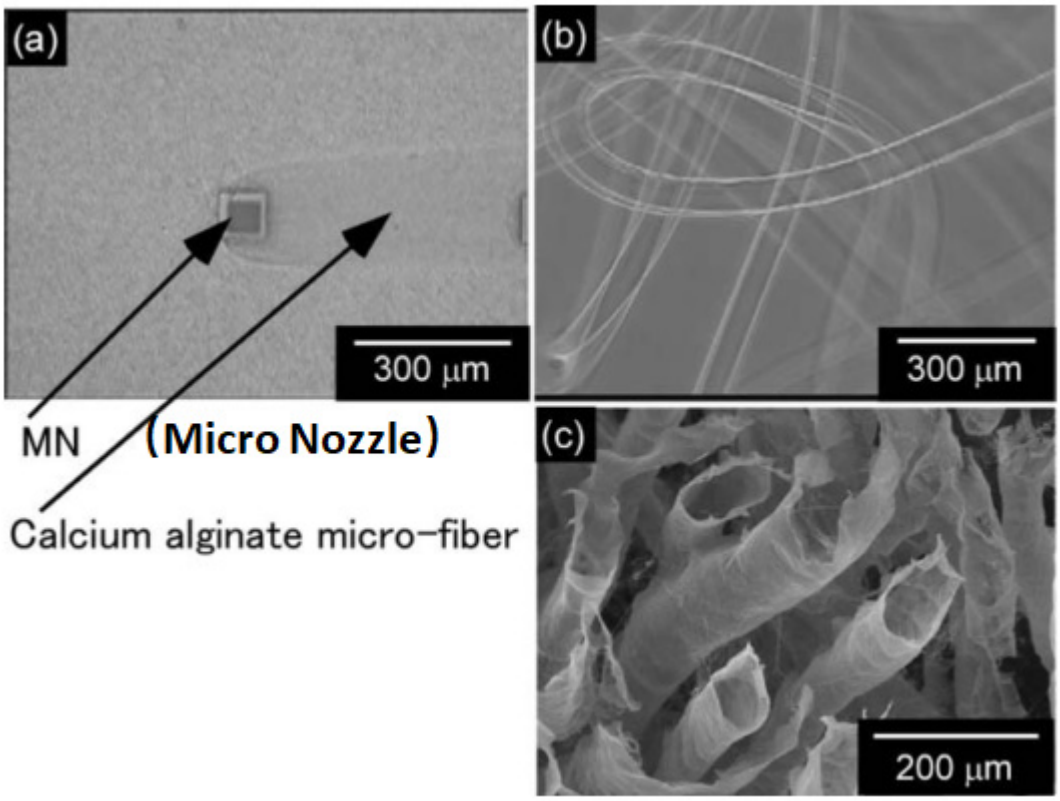

Figure 2.14 Formation of alginate micro-fibers and micro-tubes. (a) Formation process of calcium alginate micro-fibers. (b) The recovered calcium alginate micro-fibers. (c) SEM photograph of cross section of lyophilized alginate-PLL-alginate micro-tubes [99].

Shinji Sugiura's group proposed a promising technique to fabricate cell-laden APA micro-fibers by a micro-nozzle array as shown in Figure 2.14. The cells encapsulated within the APA micro-fibers formed a cylindrical multi-cellular aggregate after long-term culture. The proposed micro-nozzle array is capable of generating micro-fiber shape or droplet alginate hydrogel structures. It provides an alternative way for alginate gel formation compared with microfluidic technique. The cell-encapsulated tubular gels have potentials to be applied to vascular tissue engineering and drug delivery [99]. The fabrication details can be found in their report. The results showed that APA microfibers with 120 μm diameter were successfully fabricated by the nozzle device. Compared with simply encapsulated within alginate hydrogel, the cells encapsulated within APA

microcapsules showed higher cell activity and cell proliferation rate.

Unlike the demonstrated method above, Nurazhani Abdul Raof reported an easier technique to generated an array of one-dimensional alginate gel microstrands and aqueous microstrands through an SU-8 filter device by means of capillary action [100].

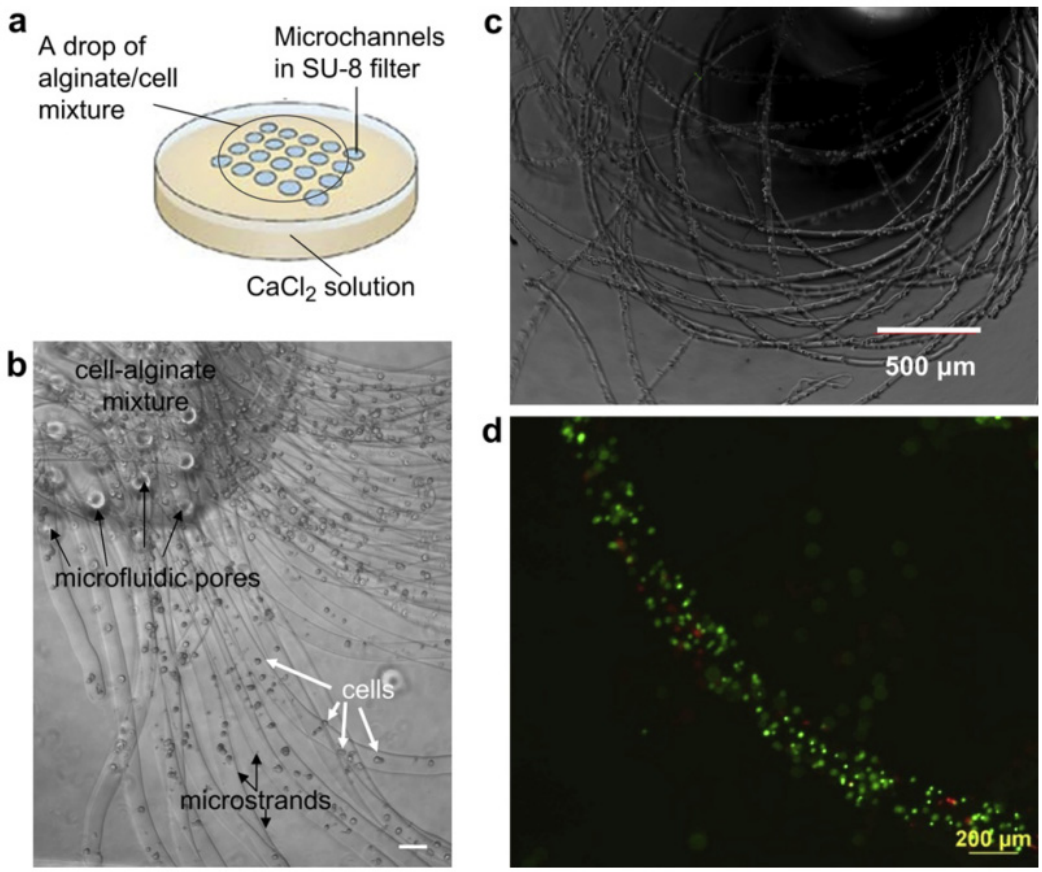

Figure 2.15 Encapsulation of mouse ES cells in alginate hydrogel microstrands. (a) Schematics of the formation of microstrands by adding one drop of cell-alginate solution onto the array of microfluidic SU-8 filter device which is floating on the top of the $CaCl_2$ solution. (b) Optical image of the array of alginate hydrogel microstrands. Scale bar ¼ 40 mm. (c) Optical image of long, continuous microstrands. (d) Fluorescent image of mouse ES cells in a microstrand stained by calcein AM/EthD-1 (green: live cells; red: dead cells) [100].

As shown in Figure 2.15, the micro-fiber alginate hydrogel was generated by placing a drop of alginate solution onto SU-8 filter. The diameter of the fabricated gel fiber can be controlled by changing the size of the microchannels in SU-8 filter. Cells were immobilized within the gel fiber during the cross-linked process. Later, the solution was replaced by the PLL solution to coat the Alginate-PLL complex layer. Finally, the inner alginate hydrogel was dissolved by sodium citric to form the APA micro strands. For the evaluation of the fabricated APA micro strands, the differentiation potential of mouse ES cells recovered from alginate/PLL aqueous micro strands were assayed compared with the one recovered from alginate gel micro strands.

The results showed that APA aqueous micro strands promoted compact ES cell organization and induced high level of PDX-1 expression which is a transcription factor essential for pancreatic development and insulin-producing β–cell maturation. Therefore, the ES cell in APA micro strands showed higher preference toward the endoderm and mesoderm lineages.

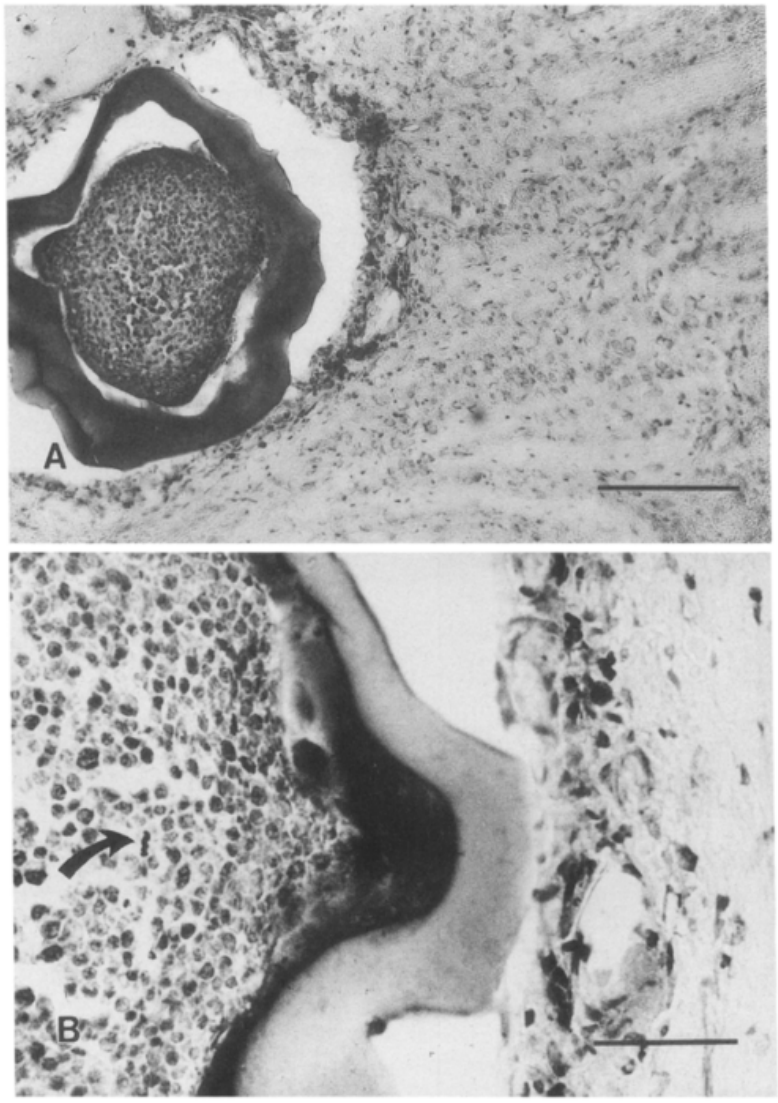

Figure 2.16 Nissl-stained section of a PC12 cell-loaded microcapsule maintained for 2 weeks in vitro followed by 4 weeks implantation in the denervated striatum of an animal which showed a significant reduction in rotation asymmetry under apomorphine challenge. Notice the closely packed. Well-preserved PC12 cells, scale bar, 200 μm. (B) A higher power micrograph shows the presence of a mitosis (arrow), scale bar, 50 μm [101].

Implantation of APA microcapsules containing varying cells also shows advantages for drug release thanks to the semi-membrane property of Alginate-PLL complex shell compared with other systems. Shelley R. Winn reported the implantation of dopamine-secreting PC12 cells in the 6-hydroxydopamine unilaterally lesioned rat model. Tyrosine hydroxylase immunopositive PC12 cells were observed 4 weeks post

implantation in all animals exhibiting a reduction in turning behavior [101]. No viable PC12 cells were seen in or around the broken capsules and no tumor formation occurred in any of the implanted animals. The results indicated the beneficial of APA microcapsules for cell implantation in vivo.

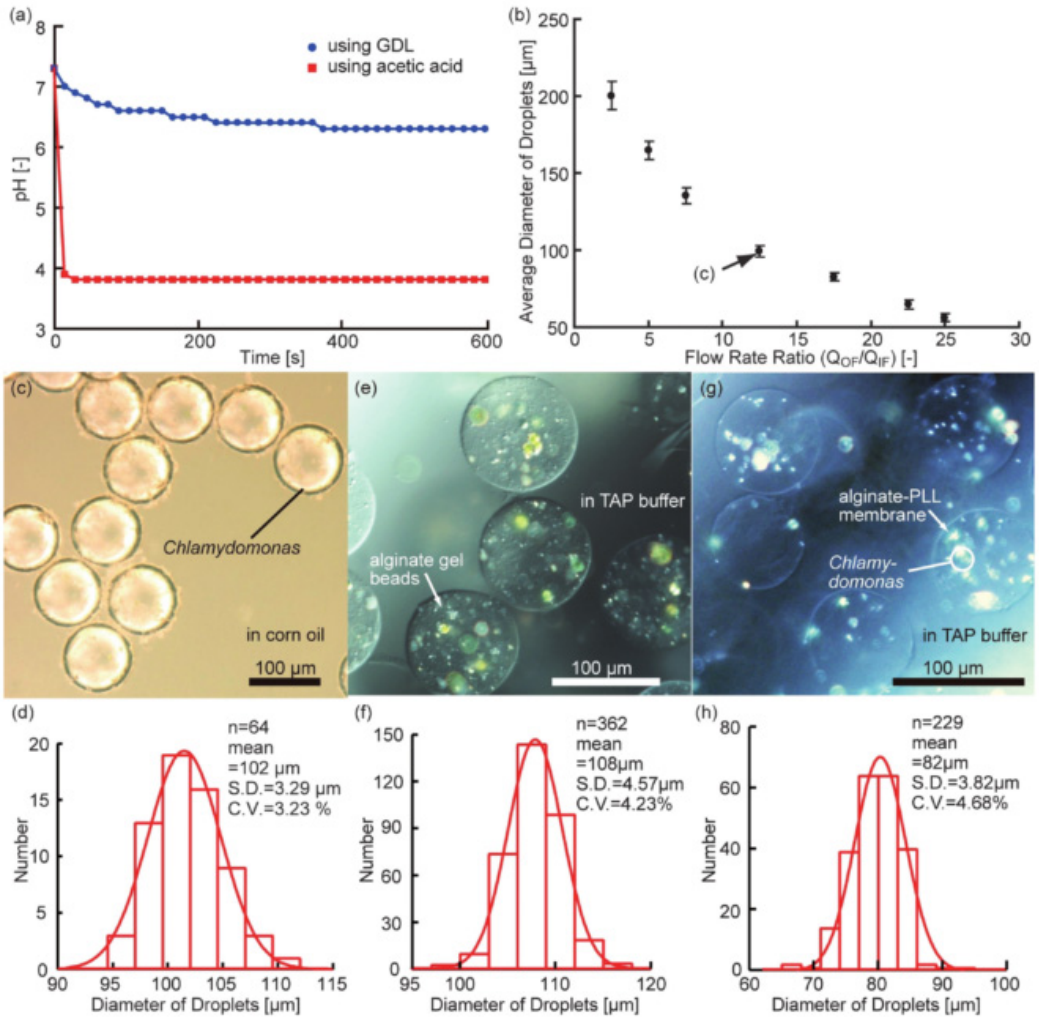

Figure 2.17 (a) plots the pH reduction after mixing equal portions of TAP buffer with GDL (150 mM) and TAP buffer containing $CaCO_3$ nano-particles (7.5 mg/ml). plots the pH reduction after mixing equal portions of TAP buffer with acetic acid (150 mM) and TAP buffer containing $CaCO_3$ nano-particles (7.5 mg/ml). AsGDL is slow hydrolyzing acid, the combination of GDLand $CaCO_3$ nano-particles is gentle gelation method for organisms. (b) Plot of the sodium alginate droplets encapsulating Chlamydomonas produced by the same AFFD with respect to the flow rate ratio (QOF/QIF,QIF ¼ 12 ml/min) (C.V. < 5%). (c) Image of monodisperse sodium alginate droplets with Chlamydomonas in corn oil. (d) Diameter distribution of sodium alginate droplets with Chlamydomonas shown in (b). Images of (e) monodisperse alginate gel beads with Chlamydomonas and (g) monodisperse microcages encapsulating Chlamydomonas made from sodium alginate droplets shown in (b). (f) and (h) Diameter distribution of alginate gel beads and microcages shown in (e) and (g), respectively. (S.D. is standard deviation and C.V. is coefficient of variation.) [102].

Morimoto et al. presented a method for forming monodisperse semi-permeable

microcapsules composed of an alginate-poly-L-lysine (PLL) membrane for the observation of encapsulated cells as shown in Figure 2.17. They evaluated the main parameters that effected the dimension of the fabricated APA microcapsules in a droplet generation system such as the velocity of the fluid and the different kind of base material components. They successfully observed the movement trajectory of the encapsulated cells during long-term culture period while maintained the viability to calculate the speed of the Chlamydomonas. What's more, other researchers also point out the potential of APA microcapsules for post-analysis of the encapsulated cells by solubilizing the alginate-PLL membrane using pronase E [103]. This will help the researchers retrieve the encapsulated bio-components for further analysis.

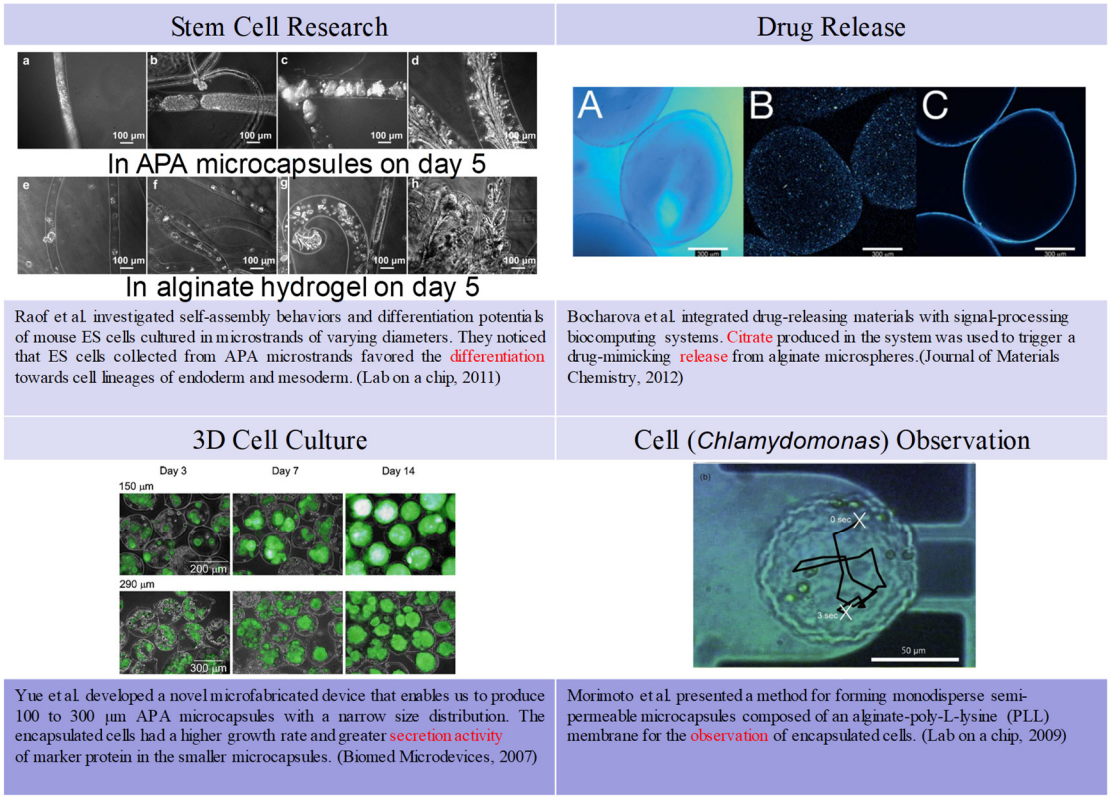

Figure 2.18 Applications of APA (Alginate/poly-L-lysine(PLL)/alginate microcapsules.

In summary, we conclude the varying applications of APA microcapsules for Stem cell research, drug release, 3D cell culture and cell implantation in vivo as shown in Figure 2.18. Generally, different cell sources could be employed in cell encapsulation technology, ranging from the islets of Langerhans, the most commonly used cell type, to novel approaches using encapsulated stem cells and hepatocytes. However, there is lack of an efficient method for shape-controlled formation of APA microcapsules due to the mechanism of alginate hydrogel formation. As you may remember, the Ca-alginate hydrogel is formed when alginate chain cross-linked with Calcium ions. Therefore, it's difficult to precisely control the shape of the fabricated alginate hydrogel structure due to the diffusion of the calcium ions in aqueous state. So far, the common methods for the generation of the APA microcapsules are based on the microfluidic

technology or special micro-nozzle device. Thus, how to solve this issue is the main challenge for the current objective.

2.5 Standard management of cell lines in the laboratory

C2C12 (Mouse myoblast cell line) NIH/3T3 (Mouse fibroblasts cell line) and RCL-18 (Mouse liver cell line) cells were cultured for experiments inside Dulbecco's Modified Eagle's Medium (DMEM, Sigma Aldrich) with 10% fetal bovine serum (FBS, Sigma Aldrich) for 72 hours, inside an incubator (37 °C, 5% CO_2). Prior to experiments, Cells were collected and all culture medium was removed. Figure 2.19 shows the morphology of the NIH/3T3 cells under 2D culture. Cells were stained green using Cell Tracker Green CMFDA (Invitrogen, CA, USA) for fluorescence detection.

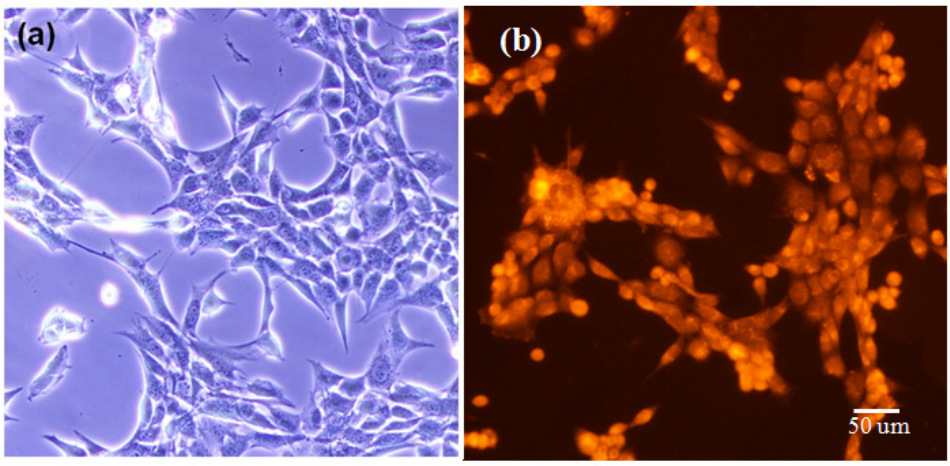

Figure 2.19 The morphology of fibroblasts (NIH/3T3) under 2D culture. (a) In growth status which is adhering on the substrate. (b) The fluorescent images of fibroblasts (NIH/3T3) located by Cell Tracker Orange.

Regarding the management of the cell line, the original cell seeds are obtained from companies or the medical department. We do the cell culture and sub-culture in our lab. The cells grow on the surface of the culture dish, adhering firmly. The cells are spindle shaped with the length about 100 μm. Prior to the experiments or the sub-culture, we need to detach the cells from the substrate by trypsin. The cells become round shape with the diameter about 20 μm. We use the cell in round shape during the experiments such as on-chip immobilization, encapsulation and assembly.

2.6 Summary

In this chapter, we introduced the typical methods for the immobilization of bio-components onto specific address in situ. As one of the recently well-established new method, electrodeposition of Ca-alginate hydrogel was presented in details. The varying applications in cell manipulation and assembly based on electrodeposition method were reviewed. We also showed the basic fabrication process for building multi-functional microelectrode device which is the necessary experimental setup for the electrodeposition method. We also showcased of the fabricated electrodeposition device for the immobilization of RLC-18 cells onto the micro-patterns area with simple geometry in our experiment.

On the other hand, we introduced the other technique for cell encapsulation using Alginate-Poly-L-lysine-alginate (APA) microcapsules. The structure mechanism of APA microcapsules and typical applications in terms of tissue engineering were briefly presented.

Generally, electrodeposition method is a power tool for 2D cell patterning and immobilization with programable shape-control ability. However, the method is so far limited to the 2D substrate surface due to its mechanism. To further overcome this limitation and apply this method for the 3D bio-assembly applications. Inducing the APA microcapsules system is a possible and promising way to achieve shape-controlled APA microcapsules since there is still lack of an efficient method to control the shape of the APA microcapsules. Therefore, in the next chapter, we will describe the proposed novel method for shape-controlled APA microcapsules fabrication based on electrodeposition.

Chapter 3
Shape-controlled high cell-density microcapsules by electrodeposition

3.1 Motivation of 3D cell structure fabrication

Recent advances in tissue engineering have relied upon development of methods to place spatially selective biological components at specific three-dimensional (3D) locations [104-106]. There is similar interest in developing methods to assemble cells within bio-scaffolds for fabrication of 3D cell structures. Current methods to assemble cells into two-dimensional (2D) or 3D structures include non-spherical polymeric microparticle in situ photo-polymerization [26, 107], cell patterning on 2D surfaces by using dielectrophoresis technique [25, 79], 3D bio-printing [22, 27], cell sheet engineering [48], and cell encapsulation units [108, 109]. Thus, many fabrication methods have been developed to immobilize and culture cells in 3D formats.

The use of alginate-poly-L-lysine (PLL) microcapsules has shown great potential in fabricating 3D cell structures with high cell density ever since Lim et al. first reported this approach for fabrication of microencapsulated islets for implantation in 1980 [108]. Lately, cell-laden Ca-alginate fibers or droplets have been transformed into 3D microcapsules to form tissue-like cell spheroids and cylindroids after long-term cultivation [99, 110]. These microcapsules provide a soft and "liquid-like" platform that mimics the embryonic microenvironment for self-assembly of cells [100]. Small molecular weight substances like nutrient and oxygen molecules can pass through the alginate-PLL membrane of microcapsules, while cells are blocked by the membrane [96, 109]. However, because of the mechanism of Ca-induced alginate gel formation, it is still difficult to precisely control the gelation process to produce alginate-PLL microcapsules with specific shape. Therefore, despite the commonly used alginate fibers or droplets generated microfluidic devices, there is still a lack of an efficient approach to achieve shape-controlled alginate-PLL microcapsules for 3D cell structure fabrication.

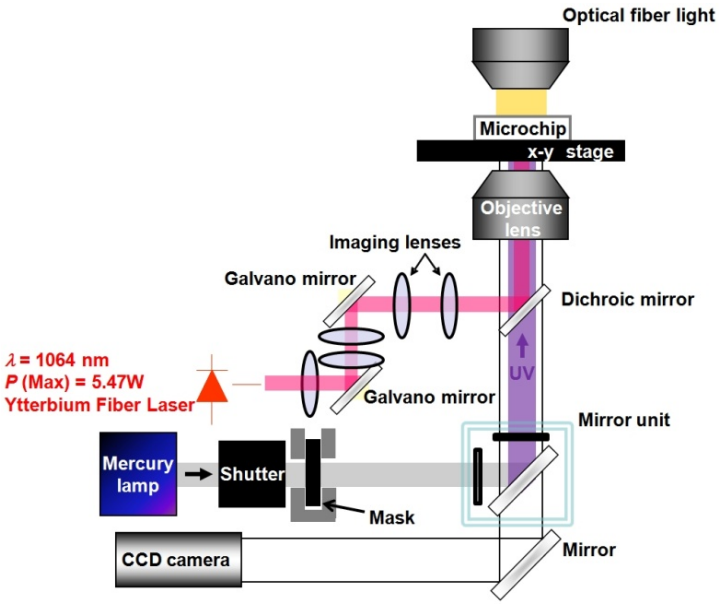

Figure 3.1 A schematic drawing of the on-chip laser manipulation and fabrication systems[75].

For production of shape-controlled alginate-PLL microcapsules, the electrodeposition method is a promising technique. Electrodeposition of Ca-alginate hydrogels on specific device plays an important role in entrapment and immobilization of biological components, such as cells and bacteria, for studying cell-cell signaling and 3D cell culture [90, 106]. Cheng et al. demonstrated a novel approach for fabrication of alginate gels inside a microfluidic system [86, 90]. In their work, a Ca-alginate composite hydrogel biofilm entrapping bacterial cells was fabricated on gold electrodes inside the microfluidic system, with its shape controlled by using electrical signals. By electrodeposition, Ca-alginate gelation can be triggered by an electrical signal, which enables us to fabricate an in-situ Ca-alginate gel membrane with controllable size and shape on microelectrodes. Consequently, other researchers have also focused on the fabrication of cell structures by depositing cell-laden alginate gel on electrodes [92, 93]. Their results show that cell viability can be maintained during culture, but cells did not spread because of the lack of cell adhesion molecules and spaces within the Ca-alginate gel. Thus, promoting cell proliferation has become the main challenge concerning the electrodeposition method for 3D cell structure fabrication.

Therefore, we introduced a new approach to solve the issue of cell proliferation in the electrodeposition method. Our approach particularly aims at the fabrication of shape-controlled alginate-PLL microcapsules for 3D cell structures based on electrodeposition. In this study, we applied the electrodeposition method to alginate-PLL microcapsule fabrication by transforming the 2D gel membrane into 3D microcapsules. A Ca-alginate gel membrane was formed on the micro-patterned fluorine-doped tin oxide (FTO) electrode, thus forming a microfabricated conductive array. The electrodeposition-based gel-membrane formation process was applied to cell encapsulation into alginate-PLL microcapsules with liquid cores (sphere, cuboid, and

rod), where cells were cultivated for 2 weeks.

3.2 Microelectrode system set up

3.2.1 System hardware setup in our lab

The microscope observation systems in our lab were shown in Figure 3.1. The main equipment is an inverted microscope (IX-71, Olympus). X-Y stage and the height of objective lens (Z-axis) were controlled for manipulating the objects. Several objective lens were used, including oil immersion objective UPLFLN 100XOI2 (Olympus, for laser manipulation and on-chip fabrication), and air objective 40X (Olympus, for on-chip fabrication). The laser was scanned on X-Y coordinate by controlling the angle of galvanometer mirror (LSA-10A-30, Harmonic Drive Systems). UV was illuminated by the mercury lamp (USH-1030L, USHIO) and the exposure time was controlled by the shutter (BSH-RIX, Sigmakoki). The microfluidic device was set on the stage. The observation was performed by the CCD camera (XC-555, Sony).

3.2.2 Materials

Sodium alginate (A2033, Sigma-Aldrich, St Louis, MO), sodium citrate tribasic dihydrate (S4641, Sigma-Aldrich, St Louis, MO), PLL hydrobromide (molecular weight 30,000–70,000 Da, Sigma-Aldrich, St Louis, MO), fluorine-doped tin oxide coated glass slide (surface resistivity ~7 Ω/sq, 735140, Sigma-Aldrich, St Louis, MO), and 4-(2-hydroxyethyl)-1-piperazineethanesulfonic acid (HEPES, 346-01373, Wako Pure Chemical Industries, Osaka, Japan) were used. Calcium carbonate ($CaCO_3$, ϕ 0.97 μm, #2300) was supplied by Sankyo Seifun Ltd (Japan). Photoresist (AZ 5214 E) was purchased from AZ Electronic Materials (Germany) GmbH. Water used to prepare the solution was deionized with a Millipore Direct-Q3 water purification system (Millipore, Worcester, MA).

Deposition solution. The deposition solution was prepared by dissolving 1% (w/v) sodium alginate in solution containing NaCl (126 mM), KCl (2.7 mM), $Na_2HPO_4 \cdot 12H_2O$ (8.1 mM), KH_2PO_4 (1.47 mM), and HEPES (21 mM). The pH was adjusted to 7.3 by adding 0.5 M NaOH solution. $CaCO_3$ (0.5%, w/v) was uniformly dispersed in the solution by using a magnetic stirrer for 24 h.

HEPES buffer solution. The HEPES buffer solution was prepared by dissolving HEPES (5 g/L) in a solution containing NaCl (8 g/L), KCl (0.37 g/L), Na_2HPO_4 (1.076 g/L), and glucose (1 g/L). The pH was adjusted to 7.3 by adding 0.5 M NaOH solution.

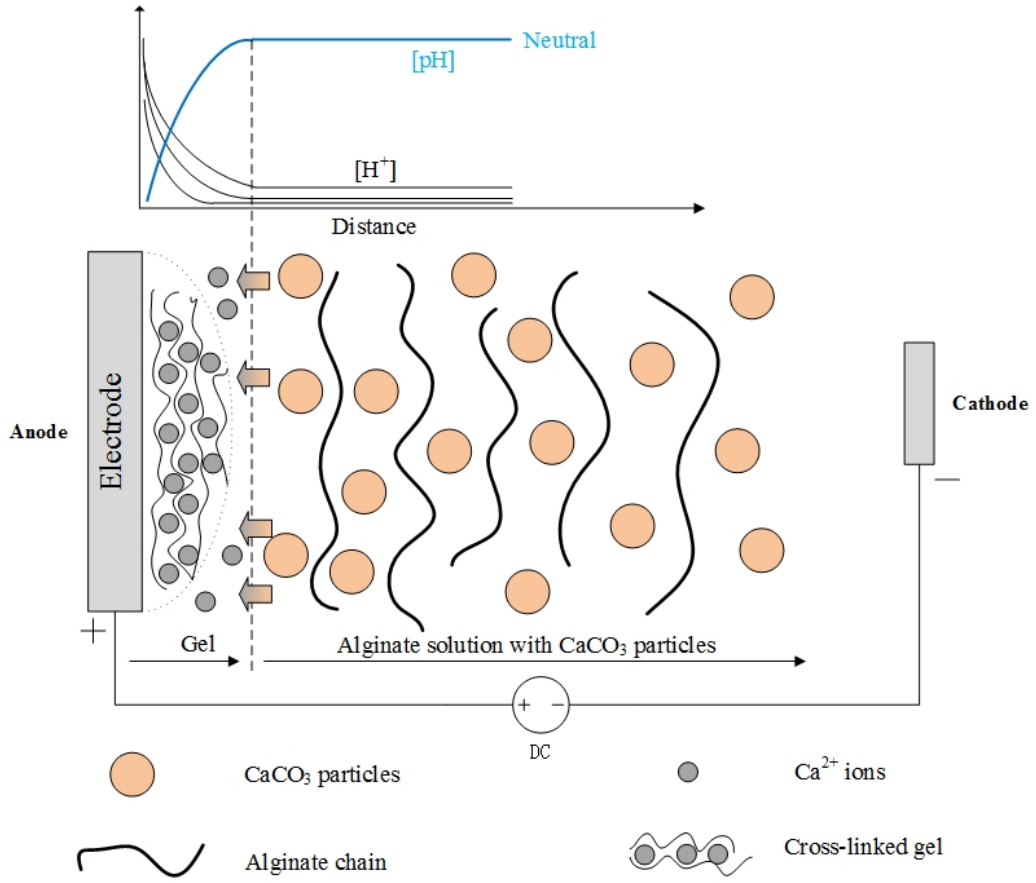

Figure 3.2 The principle of electrodeposition

Calcium chloride solution. To prepare 1.1% (w/v) calcium chloride solution, 0.55 g of $CaCl_2$ (anhydrous) was dissolved in 50 mL distilled water.

Sodium citrate solution. Sodium citrate tribasic dihydrate (1.62 g) was dissolved in 100 ml of 0.45% (w/v) NaCl solution to prepare 55 mM sodium citrate solution.

Cell viability test solution. The cell viability solution was prepared by mixing 0.8 μL calcein AM (1 mg/mL, Wako Pure Chemical Industries), 2.8 μL propidium iodide (PI, 1 mg/mL, Wako Pure Chemical Industries), and 1 mL HEPES buffer solution.

3.2.3 Fabrication of 2D Ca-alginate gel membranes on the electrode by using electrodeposition

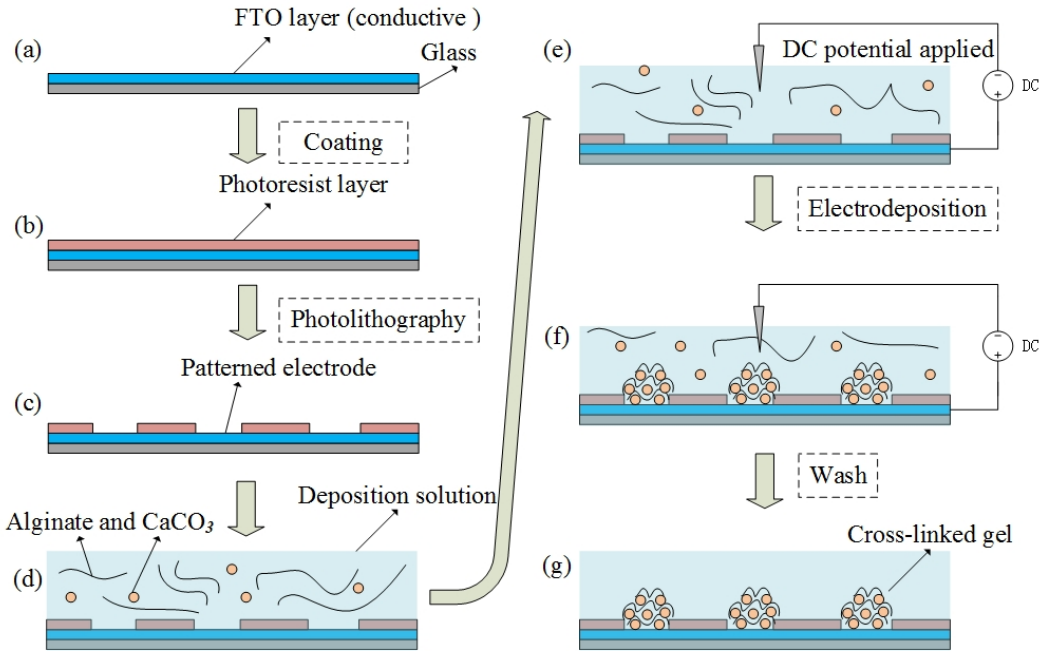

Figure 3.3 Fabrication procedure of microelectrode on FTO glass and Calcium induced cross-linked alginate hydrogel.

The electrodeposition method is a powerful tool in cell manipulation and assembly because it is a programmable method for the spatiotemporally controllable assembly of cell populations for 3D cell culture and for studying cell-cell signaling [90, 92, 106]. Alginate and chitosan are commonly used hydrogel-forming polysaccharides for electrodeposition [83, 106]. However, the pH change required to trigger the formation of the chitosan hydrogel is lethal to cells, which makes chitosan unsuitable for cell entrapment. Unlike chitosan, the electrodeposition of alginate hydrogel provides a programmable and biocompatible method for spatially selective cell entrapment and 3D cell culture [93].

The procedure for fabricating Ca-alginate gel membranes is illustrated in Figure 3.3. A schematic illustration of the mechanism for calcium alginate electrodeposition is shown in Figure 3.2. Briefly, deposition solution (500 µL) mixed with RLC-18 cells (cell density, 5×10^6 cell/mL) was placed on the patterned electrode area. One copper wire was immersed into the deposition solution (about 1 mm length) as a cathode while the other copper wire was attached to the FTO surface as an anode. Both wires were connected to a DC power supply. The distance between the copper wire (cathode) and the FTO surface (anode) was approximately 5 mm. A DC voltage (4.5 V) was applied to the FTO electrode for 15 s to trigger H^+ generation by the electrolysis of water and form a pH gradient at the anode surface ($2H_2O \rightarrow O_2 + 4H^+ + 4e^-$). Ca^{2+} was released from $CaCO_3$ particles because of encountering protons at the anode ($2H^+ + CaCO_3 \rightarrow Ca^{2+} + H_2O + CO_2$). Ca-alginate hydrogel membranes were formed on the bare

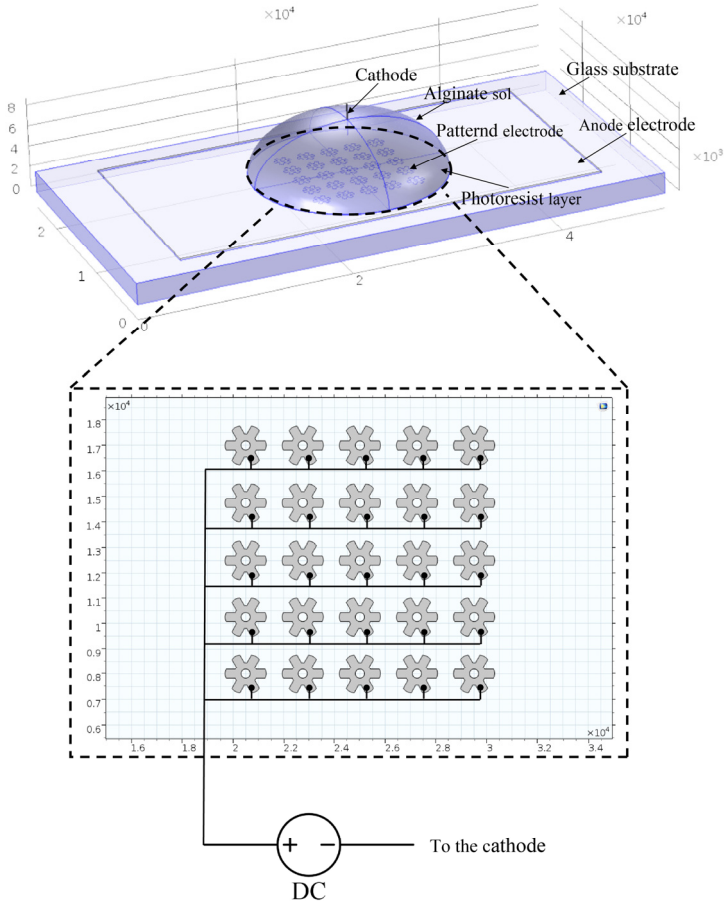

Figure 3.4 Model for numerical simulation of electric field of microelectrodes.

patterned electrode area in the presence of Ca^{2+}, because Ca^{2+} ions act as ionic bridges between l-guluronic acid residues on adjacent chain segments (Ca^{2+} + 2Alg-COO^- → Alg-COO^-–Ca^{2+}–$^-$OOC-Alg). After 15 s, the DC power supply was turned off, and the FTO electrode was immediately immersed into the HEPES buffer solution in a 10-cm petri dish to flush away the deposition solution.

3.2.4 Simulation for electric field of microelectrode

We constructed model for numerical simulation of electric field using COMSOL Multiphysics software. The schematic of the design is shown in Figure 3.4. Here, we tuned the insertion depth of cathode electrode (a copper wire that inserted into deposition solution) to check its effect on electric field distribution. By altering the parameter of insertion depth from short (1 mm) (Figure 3.5a) to long (8 mm) (Figure 3.5b), the electric field distribution has significantly been changed.

The results in Figure 3.5 indicated the electric field on the center area is higher than other areas since the center area is close to the cathode electrode. What's more, the short

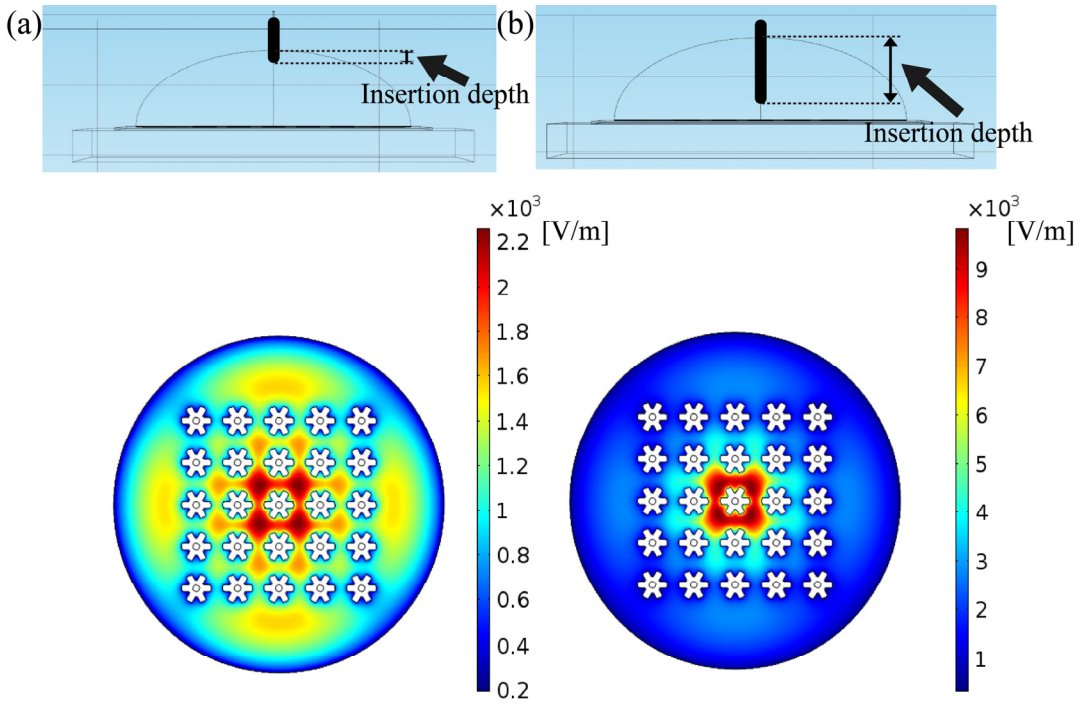

Figure 3.5 The numerical simulation of electric field distribution over the microelectrode of Figure 3.4. The results of electric field distribution independent to the insertion depth of cathode electrode which is short (1 mm) (a) or long (8 mm) (b). The applied potential is 4.5 V. The unit is V/m.

insertion depth of electrode lead to a smooth electric potential gradient (electric field at the center is 1.5 times than at the periphery) compared with the long insertion depth which lead to a steeply electric potential gradient (electric field at the center is 3 times than at the periphery). Therefore, in order to achieve a uniform electric field as much as possible, the cathode electrode (inserted copper wire) should be as far away from the anode (microelectrode of FTO glass) as possible. Thus, we choose the insertion depth of less than 2 mm in our real experiment.

3.2.5 Transformation of 2D gel structures to 3D microcapsules

In chapter 3.3.2, Ca-alginate gel structures have been fabricated onto the microelectrode. However only fixed within the gel, cells may not be able to spread during culture since there is possibly no adhere molecular inside the alginate gel [23]. Thus, the method transforming the 2D gel structures into 3D alginate-Poly-L-lysine (PLL) microcapsules are used. By this microcapsule technique, living cells encapsulated within the 3D alginate-PLL microcapsules can be promoted into 3D microtissue with high cell density as shown in Figure 3.6.

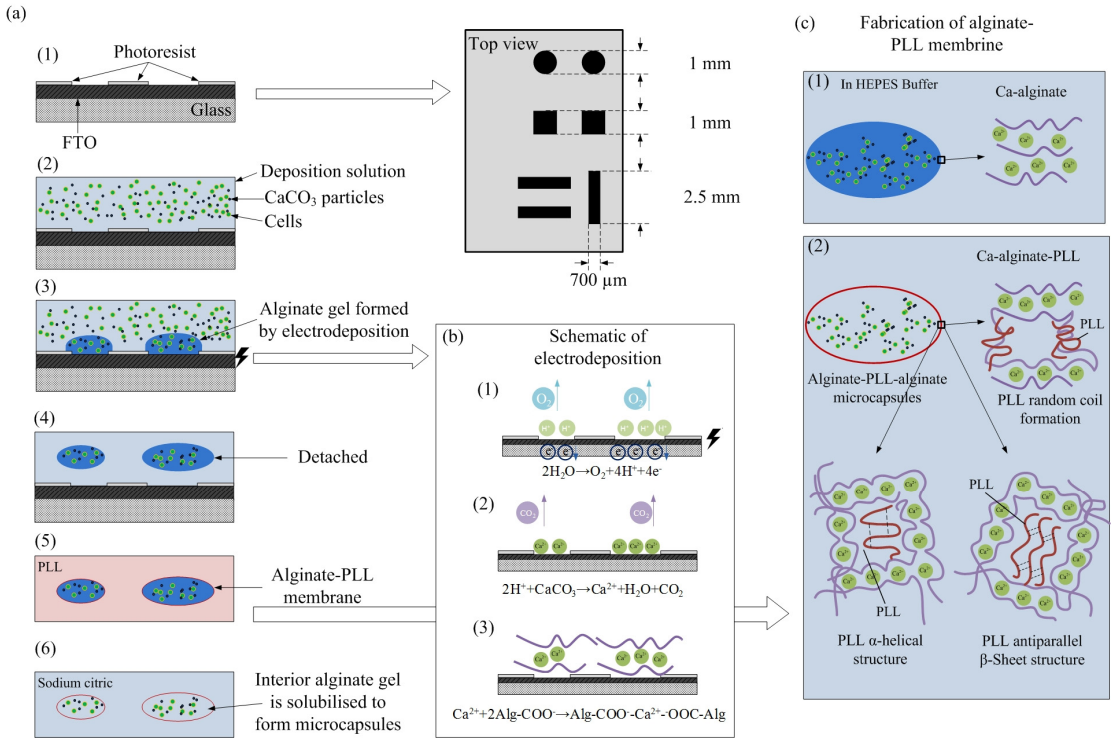

Figure 3.6 Procedure for fabricating shape-controlled alginate-poly-L-lysine (PLL) microcapsules based on electrodeposition. (1) Briefly, patterned FTO electrodes were fabricated by the photolithograph process, (2) and an alginate solution with $CaCO_3$ particles and cells was housed on FTO electrodes. (3) Alginate gel membranes were formed on FTO electrodes by electrodeposition. Schematic illustration of mechanism of calcium alginate electrodeposition. (3-1) An acid microenvironment formed by electrolysis degrades $CaCO_3$ particles to release Ca^{2+} ions (3-2), which cross-link with alginate to form the hydrogel *in situ* (3-3). (4) The formed alginate gel membranes were detached by manual pipetting. (5) A semi-permeable alginate-PLL complex membrane was formed by reacting the gel with PLL solution, (6) and the microcapsules cores were liquefied by sodium citrate to form 3D alginate-PLL microcapsules. (7) Finally, high cell-density cell structures were achieved after long-term cultivation.

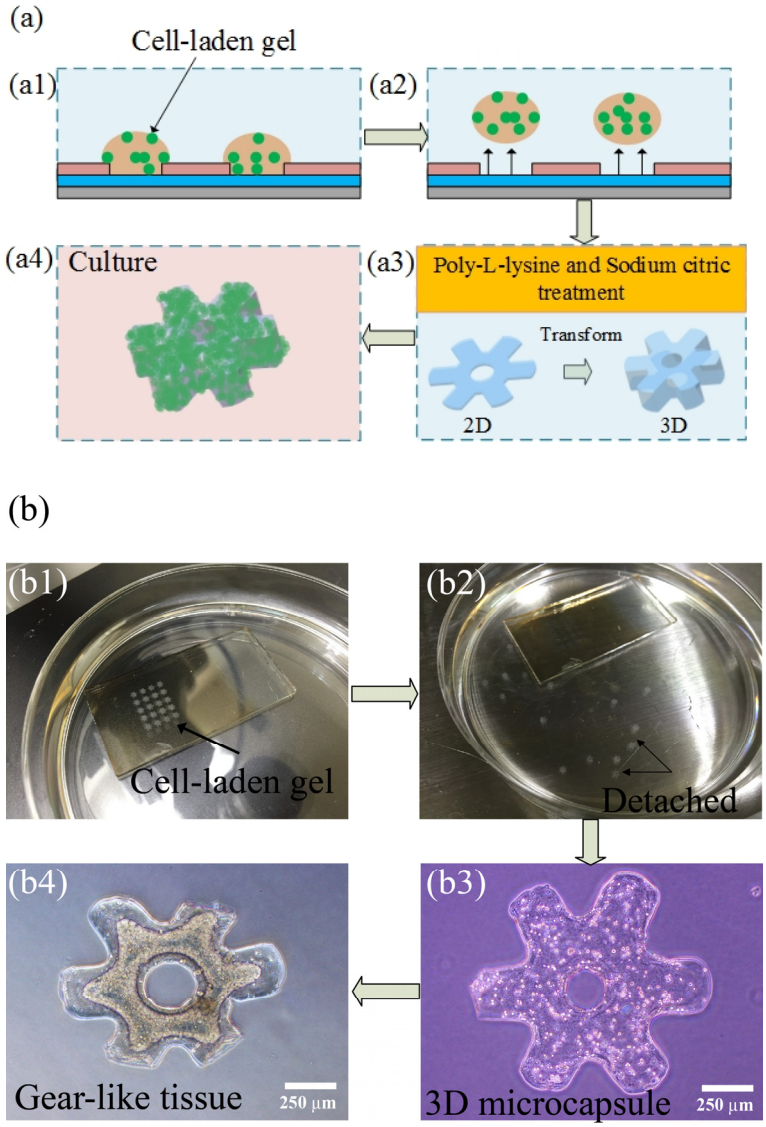

Figure 3.7 (a) A schematic drawing of strategies for fabricating gear-like tissue; (b) Corresponding fabricating results in experiment. In this experiment, we showcased a gear-like structure design for the demonstration.

The alginate-PLL encapsulation procedure used in this paper was a modification of the conventional technique [26, 29, 30]. First, as we have described in the chapter 3.3.2, cell-laden gear-like gel structures have been fabricated onto the microelectrode inside a 10 cm petri dish within HEPES buffer solution (Figure 3.7(b1)). To achieve 3D alginate-PLL gear-like microcapsules, we detached the array of gel structures from the microelectrodes by shaking the dish for 2 minutes. Due to fluid shear stress, the gel structure can be separated from the surface of microelectrode automatically Figure 3.7(b2)). After the detachment process, these gel structures were transferred into a 10 ml plastic centrifuge tube for next step. In addition, there is totally no sticking issue among the microelectrodes during the releasing process.

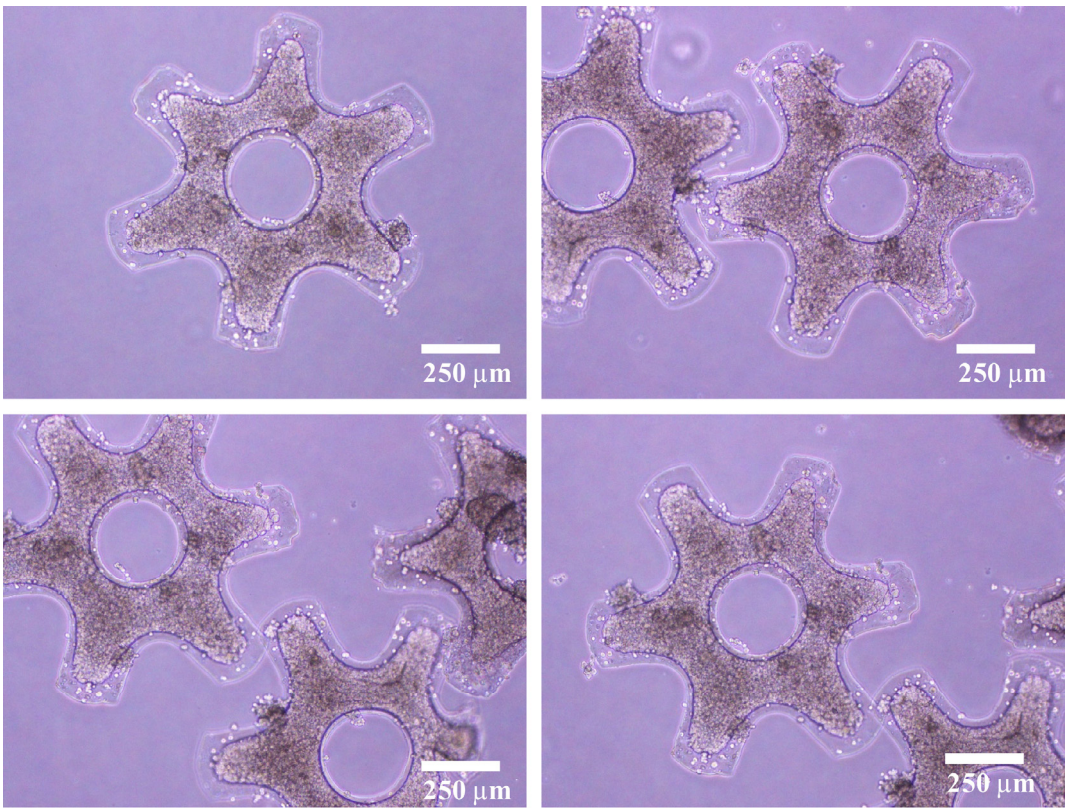

Figure 3.8 The culture results of the fabricated six-tooth gear-like tissue using RLC-18 (rat liver) cells in day 9.

Then, the gel structures were washed with 1.1 %(w/v) $CaCl_2$ solutions twice since the Ca^{2+} ions can harden the gel structures by cross-linking with alginate secondly. Follow by a treatment of a 0.05 %(w/v) PLL solution (molecular weight 30,000–70,000, Sigma-Aldrich) for 5 min, thus an alginate-PLL complex layer was formed around the gel structures. This alginate-PLL complex layer is a semi-permeable membrane which allows small molecular weight substances such as oxygen pass through while high molecular weight substances such as proteins and cells are blocked. By this way, the nutrient and oxygen can be transported into inner cells of the fabricated alginate-PLL gel structures.

Then, the gel structures were washed with 1.1 %(w/v) $CaCl_2$ solutions again to remove the extra PLL solution. Follow by a treatment of 0.03 %(w/v) sodium alginate solution for 4 min, alginate was reacted with PLL to form an outer PLL-alginate complex layer. This step is necessary because the PLL may have poison effect when directly contact with cells.

Then, the alginate-PLL-alginate gel structures were treat with 55 mM sodium citrate solution for 6 min. This process can liquefy the inner alginate structures to finally achieve 3D alginate-PLL-alginate microcapsules. The microcapsules were then washed several times by HEPES buffer solution to remove the extra sodium citric and then

transferred into 35 mm tissue culture dish for further cultivation at 37 °C in a humidified 5 % CO_2 incubator (Figure 3.7(b3-b4)).

The current results of improved method are shown in Figure 3.8. The shape of six-tooth gear-like tissue is achieved after 9-day culture. As the results, the outer and inner diameters of the gear-like tissue are about 975 ± 25 μm and 320 ± 10 μm respectively ($N > 5$, measured by ImageJ). We also increased initial cell density of the deposition solution to reduce the incubation period. Therefore, the gear-like tissue can be produced within one-week culture.

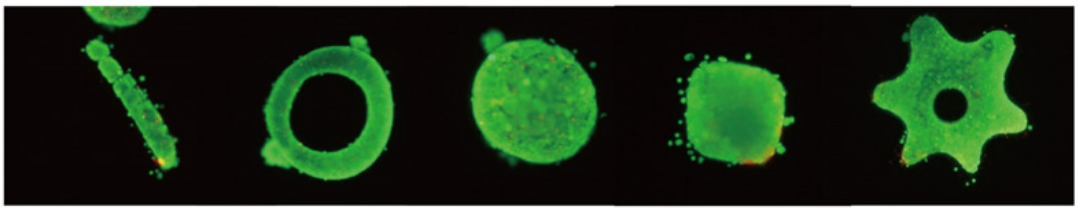

Figure 3.9 Fabrication results of 3D microtissue (RLC-18 Rat liver cells) with different shapes

So far, varying shapes of microtissues using RLC-18 rat liver cells have been fabricated on microelectrode device successfully and the shape of microtissue can be simply controlled by changing the design of microelectrode patterns as shown in Figure 3.9. Thus, the contribution of this work includes: 1) This work describes the technique of electrodeposition in generating 3D microtissue as a product of shape control. 2) Using the common electrodeposition approach, deposition of calcium alginate gel structures has previously been restricted to a 2D surface; however, this work demonstrates overcoming this limitation to fabricate 3D microtissue. 3) Compared with other methods for fabrication of 3D tissue architecture [21, 111], micro-scale tissue can be fabricated by our approach owing to the resolution of the electrodeposition method (~200 μm). Additionally, these microstructures can be easily transferred by a 1-ml pipette for further applications. Therefore, our method provides a suitable platform for construction of 3D high cell-density structures using shape-controlled alginate-PLL microcapsules. This platform has potential to stimulate new uses for microencapsulation technology in various applications such as in tissue engineering.

3.3 Evaluation of the morphology and cell viability of the fabricated APA microcapsules

3.3.1 Shrinkage phenomenon of Alginate gel structures

Fabrication results of 3D hydrogel-PLL microcapsules are shown in Figure 3.10(a). Sphere, cuboid, and rod microcapsules were observed from different angles (Figure 3.10(c–e)), which were confirmed by rotating the microcapsules. The black granules remaining on the interior surface represent $CaCO_3$ particles.

The architecture of these alginate hydrogel-PLL microcapsules includes a central core of Ca^{2+}-cross-linked alginate gel that can provide an aqueous microenvironment and a two-layer shell consisting of a PLL inner layer and sodium alginate outer layer, as shown in Figure 3.10(b). The alginate-PLL semi-membrane permits passage of low molecular weight substances, such as nutrients and oxygen, to the core and passage of metabolic products from the core, while retaining the core material within the microcapsule [109].

The success rate of transforming 2D alginate hydrogel membranes into 3D alginate hydrogel-PLL microcapsules was relatively high (approximately 85%). However, if bubbles were present in gel structures after electrodeposition, conversion to alginate-PLL microcapsules may fail because the bubbles create holes in the gel structure. Therefore, the applied voltage and deposition time should be maintained within an optimum range to avoid bubble formation.

When performing the PLL coating and alginate coating steps, the chemical reactions result in aggregation. Consequently, prior to the addition of the PLL or alginate solution, the centrifuge tube was gently shaken to prevent aggregation.

In the present study, the average core diameter of the microspheres was approximately 630 μm, as shown in Figure 3.10(f). The average core length of the microcube was approximately 500 μm, as shown in Figure 3.10(g). The length of the rod was approximately 1800 μm, while its width was approximately 240 μm (Figure 3.10(h)). Compared with the initial size of the micro-pattern, the size of microcapsules was decreased to approximately half. This shrinkage of calcium alginate gels after gel formation is a general phenomenon also observed in other studies [110].

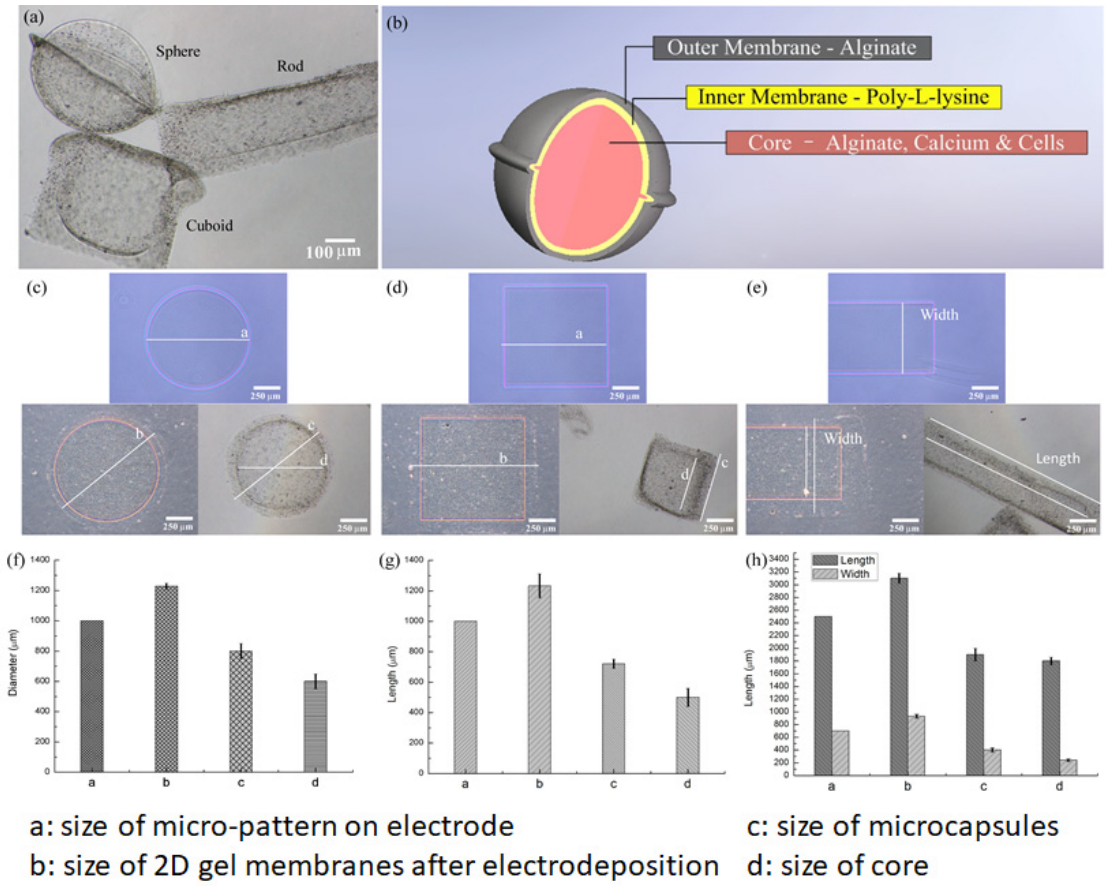

Figure 3.10 (a) Fabrication of 3D shape-controlled alginate-PLL microcapsules in sphere, cuboid, and rod shapes (cell not loaded). (b) Diagram shows the structure of alginate-PLL capsules, which includes an aqueous core loaded with cells and a two-layer shell consisting of a PLL inner layer and sodium alginate outer layer. (c–e) Bright field images of micro-patterned alginate hydrogel membranes formed by electrodeposition and 3D microcapsules in sphere, cuboid, and rod shapes, respectively. (f–h) Size distribution of micro-pattern, gel membrane, microcapsules and core in sphere, cuboid, and rod shapes,

To quantitatively analyze this shrinkage phenomenon and investigate the relationship between sizes of 2D gel structures generated after electrodeposition and those of 3D microcapsules, the following four parameters were measured for each spherical, cubic, and rod microcapsules as shown in Figure 3.10(c–h):

a: size of micro-pattern on electrode

b: size of 2D gel membranes after electrodeposition

c: size of microcapsules

d: size of core

Parameter c represents the total size of microcapsule, while parameter d only represents the size of core as shown in Figure 3.10(c–e). The edge area of gel structures was not transformed into the microcapsule and consistently remained 2D (Figure

3.10(a)). This phenomenon may be caused by the edge area of these 2D gel structures after electrodeposition being too thin. After being coated with PLL and dissolution of the alginate inside, these thin areas stick together.

Table 3.1 Parameter ratios dependent on the shape of alginate-PLL microcapsules

Alginate-PLL capsules	***Ratio: b/a***	***Ratio: d/b***
Sphere	1.22 ± 0.02x	0.49 ± 0.03x
Cuboid	1.23 ± 0.05x	0.41 ± 0.02x
Rod	1.24 ± 0.03x	0.42 ± 0.02x*

Table 3.1 shows parameter ratios dependent on the shape of alginate-PLL microcapsules. The b/a ratio is defined as the dimensional resolution, where parameters a and b denote sizes of circular, square, and rectangular micro-patterns and corresponding sizes of Ca-alginate hydrogels produced by these micro-patterns, respectively. The d/b ratio is also defined as the dimensional resolution, where parameter d denotes the core size of the circular, square, and rectangular shapes. The d/b ratio shows a small range from 0.40x to 0.50x, which indicates that size of microcapsules can be controlled using our method. Therefore, these results validate the feasibility of our approach to fabricate shape-controlled alginate-PLL microcapsules. Furthermore, it is noteworthy that prepared alginate-PLL microcapsules were strong enough to be handled with tweezers.

3.3.2 Evaluation of cell viability

RLC-18 cells were successfully encapsulated within 3D microcapsules for long-term culture to form structures with high cell-density (similar to that found *in vivo*: 10^8–10^9 cells cm^{-3}). However, according to our culture results, after 9-day cultivation, there was still much space that was unoccupied by cells [112]. Therefore, to reduce culture time, we reduced the size of the micro-patterns and eventually achieved cell structures with

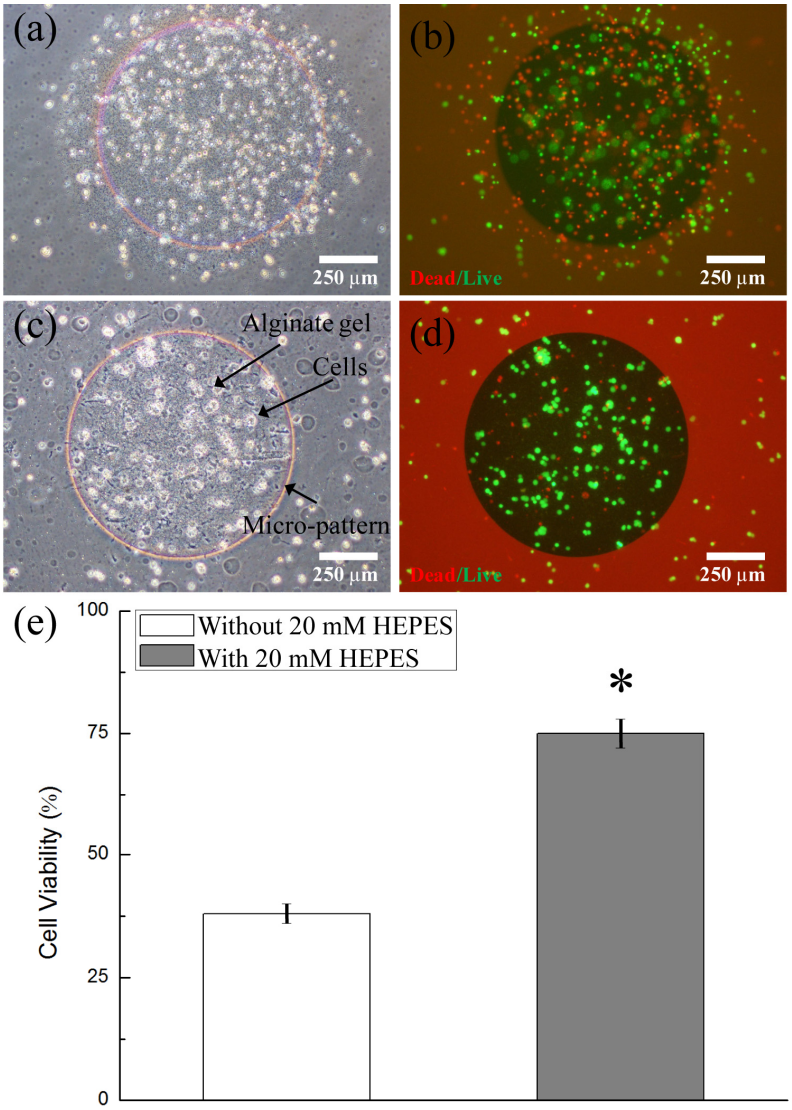

Figure 3.11 (a) Bright field and (b) fluorescent micrographs of RLC-18 cells entrapped in 2D electrodeposited Ca-alginate gel membranes without addition of 20 mM HEPES to the deposition solution. (c) Bright field and (d) fluorescent micrographs of RLC-18 cells entrapped in 2D electrodeposited Ca-alginate gel membranes with addition of 20 mM HEPES. The photoresist layer also shows red fluorescence. (e) Significantly increased percentage of live cells was observed after addition of HEPES to the deposition solution (*, $p < 0.05$).

sizes less than 500 μm in diameters within 2 weeks (Figure 3.12(a)). Results of long-term culture within the current microcapsules are shown in Figure 3.12(b-d). After 2-week cultivation, 3D cell structures (sphere, cuboid, and rod) were fully occupied by cells at high cell density.

During electrodeposition, an acid gradient is generated around the electrode that may have a lethal effect on cells viability. Thus, cell viability was studied soon after electrodeposition. Cell viability was found to be maintained at approximately 75% by

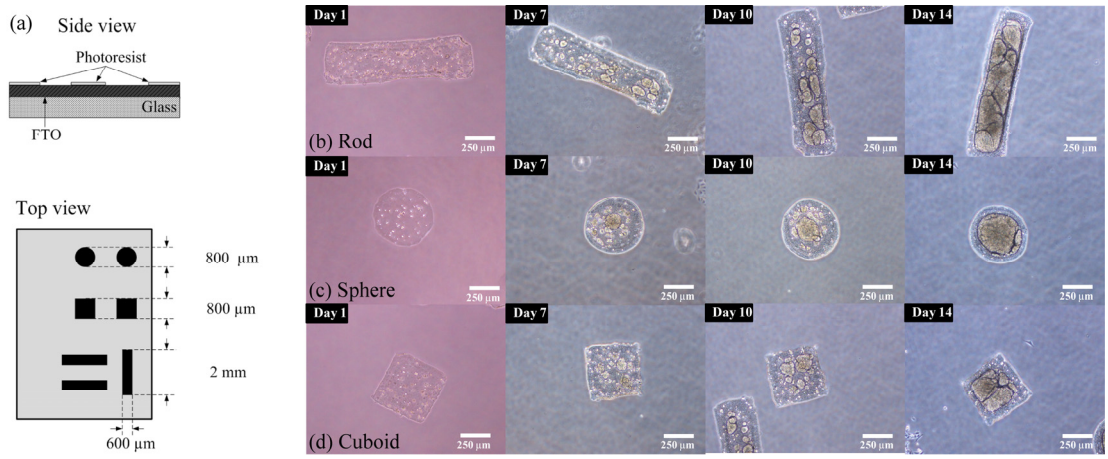

Figure 3.12 (a) Size of micro-pattern electrode used for 3D cell structure fabrication. Cell encapsulation and growth in alginate-PLL microcapsules with different geometries for 2 weeks to form 3D high cell-density structures. Cell growth in 200-µm diameter microcapsules with rod shape (b). Cell growth in 400 µm-diameter microcapsules with sphere shape (c). Cell growth in 340-µm length microcapsules with cuboid shape (d).

adding 20 mM HEPES to the deposition solution (Figure 3.11). Compared with other groups, for example, Cheng et al. [113] reported more than 80% cell viability after immobilization and culturing of myeloma cells by using electrodeposition of calcium alginate gel. However, cancer cells are not sensitive to changes in pH compared to normal cells [114]. Shi et al.[82] reported the electroaddressing of *Escherichia coli* cells by deposition with Ca-alginate hydrogels. Here, we successfully maintained cell viability by co-deposition with a normal cell line (RLC-18 cells) through the electrodeposition process. Therefore, we confirm the feasibility of the current method for immobilizing normal cells without compromising cell viability under physiological conditions.

Figure 3.13 shows cell viability in 17-day cultured 3D cell structures assessed using the live/dead assay kit; the viability was approximately 96%. No necrotic area, caused by high cell-density due to cell proliferation and tissue contraction, was found in the central tissue because the microcapsule size was optimal for nutrient transportation. These results also indicate that presence of residual $CaCO_3$ particles within microcapsules has not caused serious toxic effect on encapsulated cells. However, direct contact with $CaCO_3$ may cause cell inflammation. To remove the possible side effects of residual $CaCO_3$, nano-$CaCO_3$ may go through the PLL-alginate semi-membrane instead of being entrapped within the microcapsules. Furthermore, since our system allows precise control over the size of 3D microcapsules, it is possible to fabricate cell structures that respond to varying cell lines.

Figure 3.14 shows fabricated microelectrodes used in this study. In total, there are 42 predefined microelectrodes on the FTO glass slide, including 20 circular, 10 square, and 12 rectangular patterned microelectrodes. The throughput of the approach

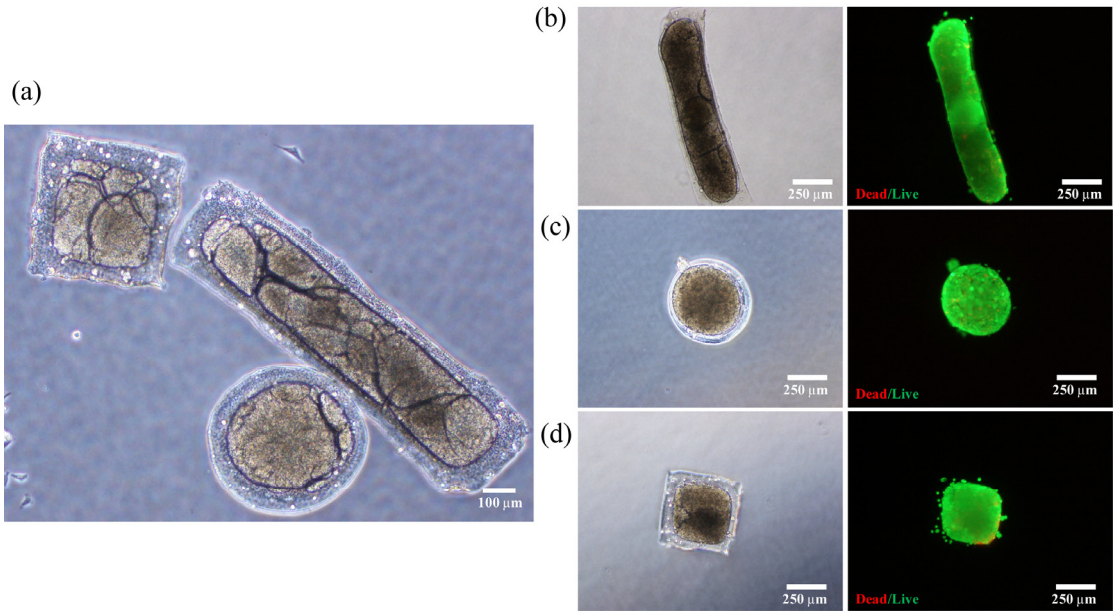

Figure 3.13 (a) Bright field image of 3D high cell-density structure in sphere, cuboid, and rod shapes. (b–d) Cell viability of 17-day cultured 3D tissue as assessed by using the live/dead assay kit.

described in this paper for cell encapsulation can be increased by increasing number of microelectrodes since deposition time of electrodeposition process is independent to the number of microelectrodes. Cell-encapsulated 3D microcapsules can potentially be applied to tissue engineering. It has been reported that hepatocyte cylindroids have high cell activity and maintain highly differentiated functions [115]. Shape-controlled microcapsules of 100-μm size have various advantages, including high nutrient and oxygen transport and high cell activity. The technique describe in this paper for fabrication of shape-controlled 3D cell structures will be useful for application to tissue engineering and cell transplantation.

The present method requires only generally regarded safe chemicals and can be performed without sophisticated techniques. The electrodeposition method presented here for fabrication of 3D cell structures is simple, as demonstrated by the following points: (1) The electrodeposition technique is now reasonably well established, and electrodeposition of gel structures on 2D electrodes has been well characterized in related studies [84, 116]. (2) The detachment process of gel structures from 2D surfaces can be easily achieved by pipetting or shaking as discussed. (3) The gel structures are strong enough to maintain their morphology without any defect while going through all processes. (4) The gel structures or microcapsules can be transferred simply by a 1-ml pipette. (5) Failures are mainly caused by bubble interference, which can be avoided by using a suitable DC potential during electrodeposition. Because of its simplicity, this method based on electrodeposition is applicable to the construction of shape-controlled microtissue.

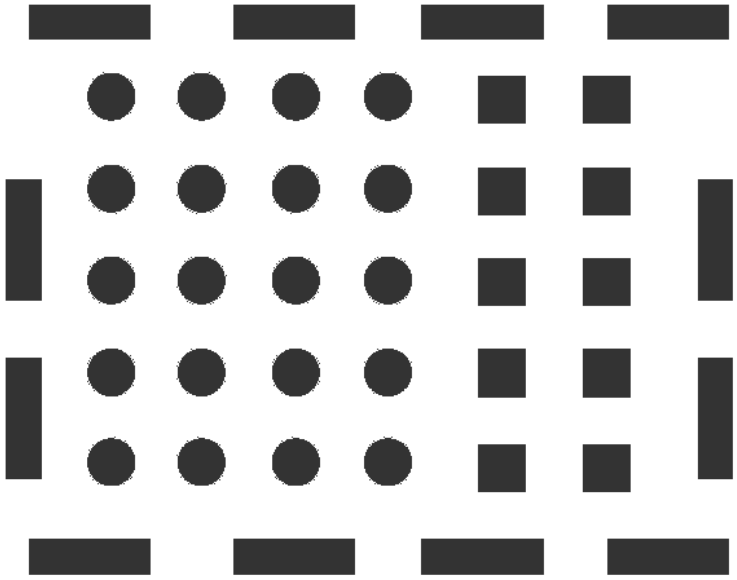

Figure 3.14 (a) Images of fabricated microelectrodes used in current experiment with twenty circular, ten squares and twelve rectangle patterns. (Black area is the conductive area of microelectrode and white area is covered by the photoresist material).

3.4 Summary

In summary, we applied the electrodeposition method to produce 3D high cell-density shape-controlled microcapsules. Achievements of our approach include generation of 3D alginate-PLL microcapsules with specific shape by electrodeposition, successfully encapsulation of living cells, rat liver cell RLC-18, into these microcapsules (sphere, cuboid, and rod shape), and generation of structures with high cell-density by 2 weeks of culture. This method enabled formation of precise micro-scale tissues during tissue formation. Use of this method to achieve specific 3D cell structures will create new opportunities for application of microcapsule technology to tissue engineering.

Chapter 4
Three-dimensional Hepatic Lobule-Like Tissue Constructs by Cell-microcapsule Technology

4.1 Motivation of hepatic lobule-Like tissue constructs

In vitro biofabrication of multicellular aggregates has been used in tissue research as a compromise between conventional two-dimensional (2D) cultures and the complexity of artificial organs for pharmacological assays [117] and toxicological studies [118]. Until now, the cell-containing modules used to build three-dimensional (3D) cell models have taken the form of cell spheroids [119], cell microfibers [120], and cell sheets [121]. Among the various methods used to generated cell-containing modules, the fabrication of alginate-poly-L-lysine (PLL)-alginate (APA) microcapsules as one of the typical cell microcapsules was first established in 1980 by F. Lim and has been widely used for cell entrapment and drug delivery for over 30 years [1, 108, 110, 122-124]. The architecture of the APA microcapsules includes a central core of dissolved Ca^{2+}-cross-linked alginate gel that can provide an aqueous microenvironment and an alginate-PLL complex shell that acts like a semi-membrane. This semi-membrane permits the passage of low molecular weight substances, such as glucose and oxygen, to the core and passage of metabolic products from the core, while retaining the microencapsulated islets or drugs within the microcapsule. Thus, the APA microcapsules provide a soft and "liquid-like" system platform in which the cells can be promoted into high-cell density aggregation after long-term culture. In addition, the PLL-alginate complex shell can further be dissolved by treatment with 1.6% sodium citrate solution to recover the encapsulated cells or to release the drugs [100]. However, because of the gelation mechanism of the calcium-alginate hydrogel (calcium ions cross-link with alginate), it is difficult to prepare APA microcapsules with a specific shape and size [125]. This disadvantage limits the utilization of the APA microcapsules for further applications in tissue engineering as a bio-scaffold.

Electrodeposition method has recently been established [86, 90, 116]. It is used to deposit a calcium-alginate gel film at specific electrode addresses with a pre-designed shape and size. Many research groups have performed work to immobilize cells, bacteria, and other bio-components within the alginate gel for cell-cell signaling and cell culture studies based on the electrodeposition method [82, 92]. The mechanism of electrodeposition is used to release calcium ions from the region of the micro-electrode surface via electrolysis (H^+ is released from the anode and reacts with $CaCO_3$ particles to release calcium ions). Thus, these calcium ions can immediately react with alginate around the electrode to form an alginate hydrogel film. Simultaneously, the bio-components are immobilized within the gel film for further applications. The advantages of the electrodeposition method include: 1) high bio-component immobilization resolution (~20 μm) [90] and 2) the use of simple equipment to apply potentials. Despite these advantages, the major challenges related to 3D cell model fabrication based on electrodeposition remain. Few of these approaches have been adopted in 3D cell tissue constructs for the following reasons: 1) most fabrication is restricted to a 2D surface as a biofilm because of the principle of electrodeposition, 2) there is an acid area generated around the electrode (H^+ ions released), which may affect the viability of immobilized cells, and 3) cells embedded within the calcium-alginate film have a low proliferation rate due to a lack of extracellular matrix (ECM) and room.

Thus, it is crucial to establish a new approach for the coupling of APA microcapsule modules and deposited shape-controlled alginate hydrogels in a combination format. From this perspective, we proposed a novel method to fabricate 3D multilayer hepatic lobule-like tissue based on electrodeposition and microcapsule techniques. The design of a micro-electrode device, which was previously used for preparing microtissue in sphere, cuboid, and rod shapes [98], was modified to obtain suitable dimensions for preparing hepatic lobule-shaped microtissue (HLSM). The micro-pattern electrode was fabricated by photolithography. The arrayed micro-pattern electrode is capable of simultaneous formation of alginate gel film *in situ* with a hepatic lobule shape based on the electrodeposition method. These cell-containing gel films were further detached from the substrate and treated with PLL and sodium citrate solution to form 3D microcapsules. Cells encapsulated within the microcapsules eventually fully occupied all spaces to achieve HLSM in two weeks.

In addition to the fabrication details of the HLSM, which can be found in our previous report [126], the current work is novel because the morphology, growth, and functionality of the RLC-18 hepatic lobule-shaped microtissue (HLSM) was compared to that of RLC-18 cell spheroids, which are commonly used cell models. In addition, 3D 4-layerd hepatic lobule-like tissue was further assembled by establishing a simple micro-manipulation system. This study aims to clarify that the bio-function of the HLSM with similar shape to native tissue may differ from the normal cell spheroid quantitatively. In addition, our method is capable of providing a suitable platform for

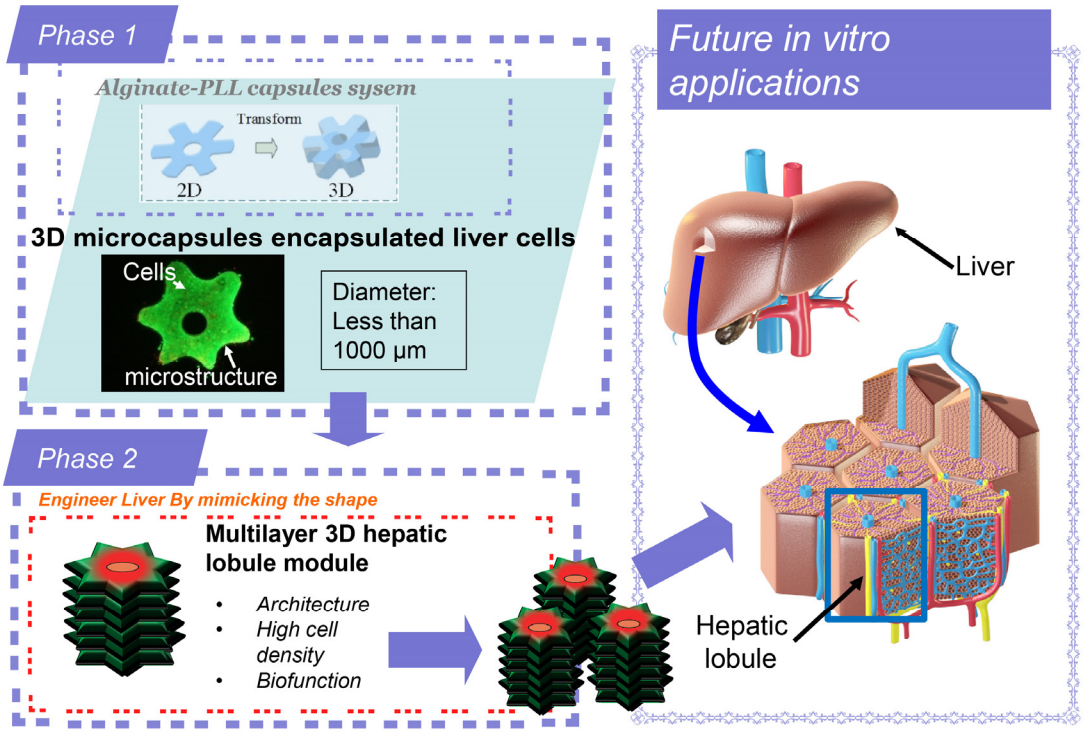

Figure 4.1 Microcapsules-based procedure for fabrication of the multilayer 3D hepatic lobule-like tissue. Phase 1: Fabrication of the HLSM to mimic the shape of hepatic lobules with bio-function. Phase 2: Assembly of the single HLSM into 3D hepatic lobule-like tissue for future *in vitro* applications of artificial liver fabrication.

3D cell model fabrication for future *in vitro* applications for artificial liver fabrication. The whole research map was shown in Figure 4.1.

The contributions of this work include: (1) the combined method of cell microcapsule technology for generating 3D microtissue to mimic the shape of the hepatic lobule, (2) microtissue with a hepatic lobule shape and spheroids were compared quantitatively based on albumin secretion and cell number during long-term culture, and (3) a simple micro-manipulator system was established to assemble the single microtissue into 3D multilayer hepatic lobule-like tissue. Therefore, we believe our method provides a suitable platform for constructing a 3D cell model by cell microcapsule technology. This platform has the potential to stimulate new uses for microencapsulation technology in various applications such as in tissue engineering.

In the previous chapter, shape controlled microtissues were fabricated on microelectrode device. In this chapter, we improved upon the previous method and then fabricated 3D multilayered hepatic lobule model with HLSM as basic building block.

In order to define the shapes of gel structures, a microelectrode device with separated patterning and fabrication areas was fabricated. Size control for microtissue was demonstrated. These hepatic lobule microtissue can be further assembled into more complex 3D structures and could become functional components of artificial liver.

4.2 Integrated microelectrode devices

4.2.1 Electrodeposition method

The general mechanism of calcium alginate electrodeposition for cell entrapment is shown in Figure 4.2. First, the electrical signal triggers H^+ generation by the electrolysis of water to form a pH gradient at the anode surface. The reaction can be described as:

$$2H_2O \rightarrow O_2+4H^++4e^-$$

Second, Ca^{2+} ions are released via $CaCO_3$ particles by reacting with H^+. The reactions can be described as:

$$2H^++CaCO_3 \rightarrow Ca^{2+}+H_2O+CO_2$$

Third, the released calcium ions interact with the G block of the alginate to form the ‘‘egg-box’’ junction and cross-link the polymer chain. The reactions can be described as:

$$Ca^{2+}+2Alg\text{-}COO^- \rightarrow Alg\text{-}COO^-\text{-}Ca^{2+}\text{-}^-OOC\text{-}Alg$$

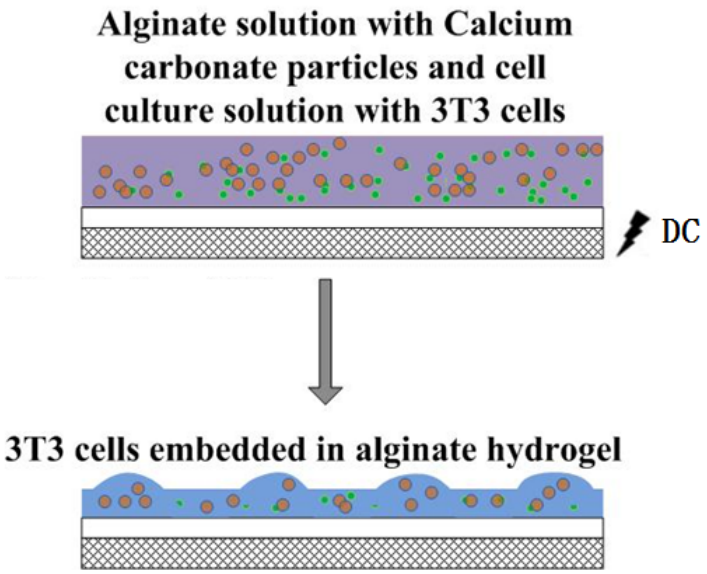

Figure 4.2 A schematic drawing of entrapment of 3T3 cells as an example inside alginate hydrogel

structures.

For electrodeposition, the deposition solution was prepared by dissolving 1% w/v alginate sodium (80 – 120 cP, Wako) in PBS buffer, and 0.5% w/v $CaCO_3$ (310034, Sigma-Aldrich) was uniformly dispersed in the solution using magnetic stirrer for 24h.

4.2.2 Fabrication of micro-patterned electrode

Microelectrodes are key elements in cell entrapment for electrodeposition. Firstly, we chose fluorine-doped tin oxide (FTO) as a conductive material because it is transparent. The glass was coated with thin ITO and was used to fabricate microelectrodes. The thickness of the ITO layer is 150 nm. The fabrication method was based on photolithography. The photoresist AZ (5214-E, Clariant (Japan) K.K.) was used as the protective layer.

The photolithographic technique was used to construct the electro-device in this experiment, as previously described [98]. Briefly, fluorine-doped tin oxide (FTO) glass

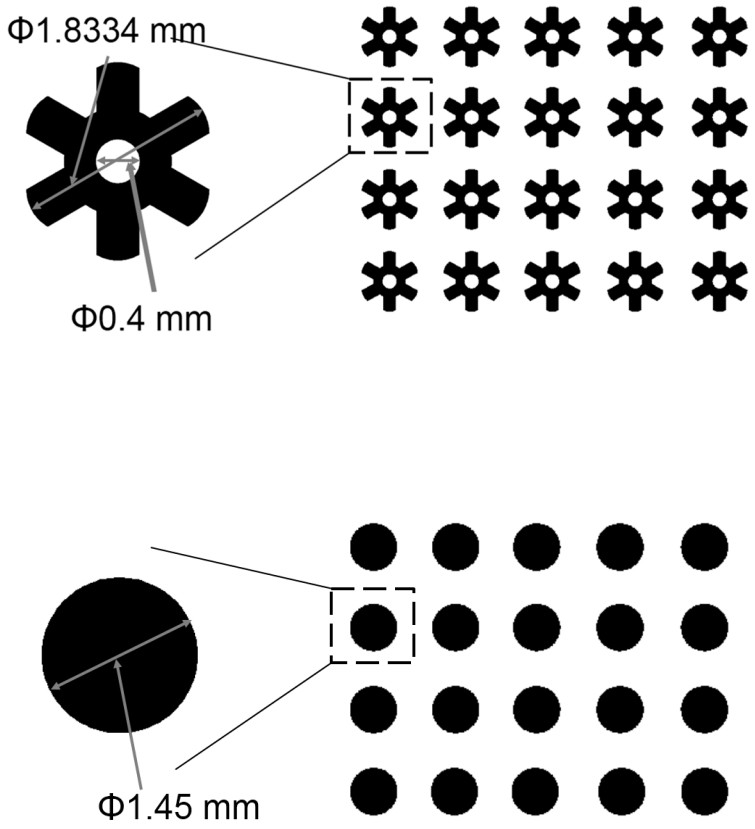

Figure 4.3 (a) Images of fabricated microelectrodes used in current experiment with twenty patterns for the HLSM and spheroids on each FTO glass slide. (Black area is the conductive area of microelectrode and white area is covered by the photoresist material).

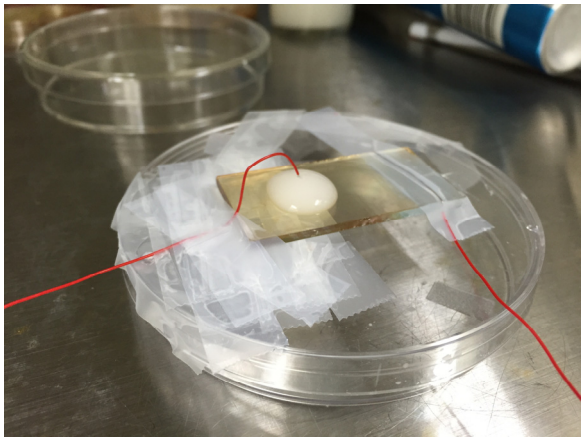

Figure 4.4 (a) Experimental setup of electro-device for depositing of Calcium alginate hydrogel.

slides (2.5 cm × 5 cm) were washed with isopropyl alcohol and Milli-Q water using an ultrasonic cleaner. The photoresist (AZ 5214E) was coated on the surface of FTO glass with 1.4 μm thickness.

The patterned-electrode was fabricated using a micro pattern generator (μPG 101, Heidelberg, German) based on our AutoCAD design of micro-electrodes. In the present work, micro-patterns of hepatic lobule and circular shapes were prepared as shown in Figure 4.3 to fabricate the HLSM and cell spheroids for comparison. The outer diameter of the hepatic lobule pattern was 1.8334 mm and the inner diameter was 0.4 mm. The diameter of the circular pattern was 1 mm. To quantitatively analyze the morphology, growth, and functionality of the RLC-18 HLSM compared with those of the cell spheroid, the designed micro-electrodes for HLSM and the spheroid had the same initial area of 1.651 mm^2.

4.2.3 Experimental setup for electrodeposition

To fabricate the HLSM and spheroids, the FTO glass slide with micro-electrodes was first set up horizontally. A copper wire (No. 359-835, RS Components Ltd, German) from the anode of a DC power supply was connected to the FTO conductive surface by tape. The pre-prepared RLC-18 cell suspension was centrifuged and washed with PBS once to remove the DMEM, which may interfere with the electrodeposition reaction. Then, the cell suspension was centrifuged again, mixed with 700 μl deposition solution, and evenly dispersed by gently pipetting. Thus, 500 μl of 700 μl deposition solution was taken and dropped onto the micro-electrode area like a hemispheroid. The other copper wire from the cathode of the DC power supply was inserted into the "hemispheroid" from the central top and was fixed by tape. The inserted length of the wire was as short as possible (around 1 mm).

The experimental setup is shown in Figure 4.4. It is noteworthy that the

concentration of insoluble $CaCO_3$ inside the deposition solution slightly changed because of natural settling. In our experiment, the deposition solution was stirred again and heated in a 37 °C water bath for 30 min. Then, 700 µl of deposition solution from the upper solution was immediately taken to perform electrodeposition, as described. The deposition solution could be stored for up to 14 days at room temperature (20 to 25°C) [127].

The FTO glass slide was recycled because the AZ photoresist layer can be easily removed by alcohol washing. However, the chemical reaction may permanently change the property of the surface of the micro-electrode via oxidation. Therefore, it is better to change the address of the micro-electrode on the FTO slide for each experiment.

4.3 Fabrication of the RLC-18 HLSM and spheroid

4.3.1 Material and solution preparation

We used sodium alginate (Medium viscosity, A2033), sodium citrate tribasic dihydrate (S4641), poly-L-lysine hydrobromide (molecular weight 30,000–70,000), fluorine doped tin oxide coated glass slide (surface resistivity ~7 Ω/sq, 735140) (Sigma-Aldrich) and HEPES (346-01373) (Wako Pure Chemical Industries). Calcium carbonate ($CaCO_3$) (0.97 µm, #2300) were kindly supplied from Sankyo-seifun Ltd (Japan). Photoresist (AZ5214-E) was purchased from AZ electronic material GmbH. Cell Counting Kit-8 (CCK8) was purchased from Dojindo Ltd (Japan). Rat albumin enzyme-linked immunosorbent assay (ELISA) Quantitation kit (ERA3201-1) was purchased from Assaypro Inc (USA). The water used to prepare the solution was deionized with a Millipore Direct-Q3 water purification system (Millipore, Worcester, MA).

Deposition solution

The deposition solution was prepared by dissolving 1% w/v alginate sodium in solution containing NaCl (126 mM), KCl (2.7 mM), $Na_2HPO_4 \cdot 12H_2O$ (8.1 mM), KH_2PO_4 (1.47 mM) and HEPES (21 mM).The pH was adjusted to 7.3 by adding 0.5M NaOH solution. $CaCO_3$ (0.5% w/v) was uniformly dispersed in the solution using a magnetic stirrer for 24h.

HEPES buffer solution

The HEPES buffer solution was prepared by dissolving HEPES (5g/L) in solution containing NaCl (8 g/L), KCl (0.37 g/L), Na_2HPO_4 (1.076 g/L) and glucose (1 g/L). pH was adjusted to 7.3 by adding 0.5M NaOH solution.

Calcium chloride solution

To prepare 1.1% calcium chloride solution, 0.55 g of $CaCl_2$ (anhydrous) was dissolved in 50 ml of distilled water.

PLL solution

Poly-L-lysine hydrobromide (25 mg) was dissolved in 50 ml of 0.9% w/v NaCl solution (0.05% PLL solution).

Sodium citrate solution

Sodium citrate tribasic dihydrate (1.62 g) was dissolved in 100 ml of 0.45% w/v NaCl solution (55mM sodium citrate solution).

Cell viability test solution

The cell viability solution was a mixture of 0.8 μL calcein AM (1 mg/mL, Wako), 2.8 μL propidium iodide (PI) (1 mg/mL, Wako) and 1 mL HEPES buffer solution.

4.3.2 Fabrication protocols

For the fabrication process, a DC voltage (4.5 V) was applied to the FTO electrode for 15 s to generate the calcium-alginate hydrogel film embedded with RLC-18 cells on the region of micro-electrode based on the mechanism of electrodeposition [106]. Briefly, H^+ is generated by the electrolysis of water formed in an acidic microenvironment at the anode surface ($2H_2O \rightarrow O_2+4H^++4e^-$). Ca^{2+} is released from $CaCO_3$ particles due to the proton encounter at the anode ($2H^++CaCO_3 \rightarrow Ca^{2+}+H_2O+CO_2$). The calcium alginate hydrogel films are formed when calcium ions cross-link with alginate immediately ($Ca^{2+}+2Alg\text{-}COO^- \rightarrow Alg\text{-}COO^-\text{-}Ca^{2+}\text{-}^-OOC\text{-}Alg$). After 15 s, the DC power supply was turned off and the FTO electrode was immediately immersed into the HEPES buffer solution inside a 10 cm petri dish. By gently shaking the dish, the extra unsolidified deposition solution was removed. After 2~3 min shaking until the gel film could be clearly seen, the HEPES buffer solution was changed to fresh solution. Then, the gel films were detached from the FTO surface by gently pipetting. After the detachment, the FTO glass and most of the HEPES buffer solution in the dish were retrieved. A sufficient amount (~10 ml) of 1.1% $CaCl_2$ solution was added to the dish to harden the detached gel structures. This process takes approximately 2 min while shaking the dish gently. Thus, these hardened gel structures were transferred into a 10 ml centrifuge tube with a 1 ml pipette for further processing.

After transferring these gel structures to the 10 ml plastic centrifuge tube, the structures were washed with 1.1% (w/v) $CaCl_2$ solutions once again. Then, the supernatant was removed by an aspirator. PLL solution (1 ml, 0.05% (w/v)) was added to react with the Ca-alginate gel structures for 5 min. Then, the PLL solution was

removed and 2 ml 1.1% $CaCl_2$ solution was added to wash the structures. Then, the supernatant was removed. HEPES buffer (2 ml) and 2 ml of 0.03% w/v alginate solution were added to the tube for 4 min. Then, the supernatant was removed. Sodium citrate solution (2 ml, 55 mM) was added to dissolve the inner alginate for 6 min. Finally, the gel structures were washed with HEPES buffer solution twice and transferred to a culture dish for long-term cultivation at 37 °C in a humidified 5% CO_2 incubator.

4.4 Evaluation of the RLC-18 HLSM and spheroid

4.4.1 Characterization of the RLC-18 HLSM and spheroids

Table 4.1 Characterization of the HLSM and spheroids measured by different methods

	HLSM	Spheroid	Measurement methods
Area of micro-electrode	1.651 mm^2	1.651 mm^2	Measured by AutoCAD (Area calculation function based on DXF file of design)
Diameter	975 ± 25 µm (Outer) 320 ± 10 µm (Inner)	840 ± 30 µm	Measured by ImageJ based on 2D optical images
Height	300 ± 22 µm	400 ± 16 µm	Measured by confocal laser scanning microscope using FITC-labeled PLL [126]
Area (Top view)	0.350 ± 0.02 mm^2	0.550 ± 0.02 mm^2	Measured by ImageJ (Area calculation function based on 2D optical images)
Volume	0.11 mm^3	0.15 mm^3	Calculated by the volume equation (1-2)
Surface area	1.99 mm^2	1.50 mm^2	Calculated by the surface area equation (3-4)

Table 4.1 shows the characterization results of the HLSM and spheroid measured by different methods. The initial design for the micro-electrode area of the HLSM and spheroids was 1.651 mm^2 measured by AutoCAD. The outer and inner diameters of the

HLSM were approximate 975 ± 25 μm and 320 ± 10 μm, respectively, as shown in Figure 4.5A. The diameter of the spheroid was approximately 840 ± 30 μm.

After transforming the 2D gel film into 3D microcapsules (described above), the base area (top view) was calculated to be 0.350 ± 0.02 mm^2 in the HLSM and 0.550 ± 0.02 mm^2 in the spheroid. Compared with the initial area (1.651 mm^2) of the micro-pattern, the base area of microcapsules was decreased by approximately a quarter because the deposited alginate gel shrank after reacting with calcium ions, a common phenomenon [110].

The height of the HLSM was approximately 300 ± 22 μm (N = 8) measured by confocal microscope using a FITC-labeled PLL-alginate shell for laser scanning, as shown in Figure 4.5B. This result can also be verified by the optical image shown in Figure 4.5A. The height of the spheroid was approximately 400 ± 16 μm (N = 10) measured by the same method. The difference in the height can be attributed to the different shape of the structures when they were transformed from 2D gel film into 3D microcapsules.

The volume of the HLSM and spheroid were 0.11 mm^3 and 0.15 mm^3, respectively, calculated by the volume equation shown below:

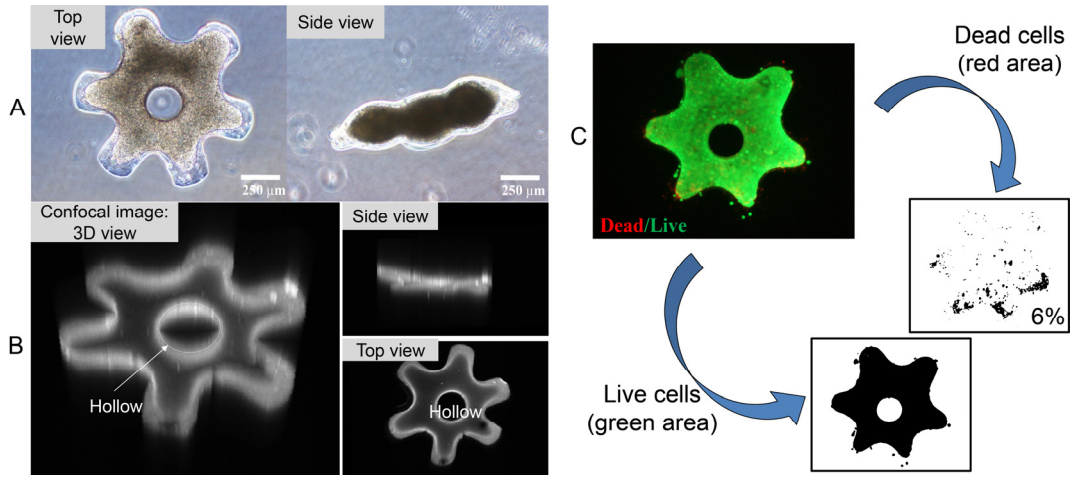

Figure 4.5 (a). Fabrication results for the HLSM after two weeks of culture. (A) Optical images of the HLSM with tissue-like cell density. The outer and inner diameters were approximately 975 ± 25 μm and 320 ± 10 μm, respectively (N>5, measured by ImageJ). (B) The confocal images show the 3D view of the HLSM. The height was approximately 302 ± 22 μm (N>8). (C) The fluorescence image shows the cell viability of the HLSM. The red area (dead cells) occupied approximately 6% of the whole area within the HLSM, indicating that viability was at least over 90% (By measuring the red (dead cells) and green (live cells) fluorescent areas in each image by ImageJ, N>5).

HLSM: $$V = S \cdot H \quad (1)$$

Spheroids: $$\mathrm{V} = \frac{4}{3}\pi SH \quad (2)$$

where S and H are the base area and the height, respectively.

The surface area of the HLSM and spheroid were 1.99 mm^2 and 1.50 mm^2, respectively, calculated by the surface area equation shown below:

HLSM: $$S = 2S + C \cdot H \quad (3)$$

Spheroids: $$\mathrm{S} = 4\pi\left(\frac{a^p b^p + a^p c^p + b^p c^p}{3}\right)^{\frac{1}{p}} \quad (4)$$

where C is the perimeter of HLSM including the inner part and outer part. (a = b) are a pair of equal semi-axes and c is a distinct third semi-axis of the spheroid (ellipsoids). p ≈1.6075 yields a relative error of at most 1.061% for this approximate formula.

The culture results of RLC-18 HLSM and spheroids on days 1, 4, 6, 8, 10, 12, 14, and 16 are shown in Figure 4.6. Initially, the distributed cells began to form many small aggregates on day 6. After continuous culture, the cell aggregates had a trend of fully occupying the inner surface of the alginate-PLL membrane and eventually occupied all the room within the microcapsules on day 14. Interestingly, after 14 days the alginate-PLL shell could not further maintain the cells within the HLSM. The cells would break though the membrane and continue to grow outside as a cluster. However, this phenomenon mostly occurred in spheroids on day 20 (data not shown). This result may

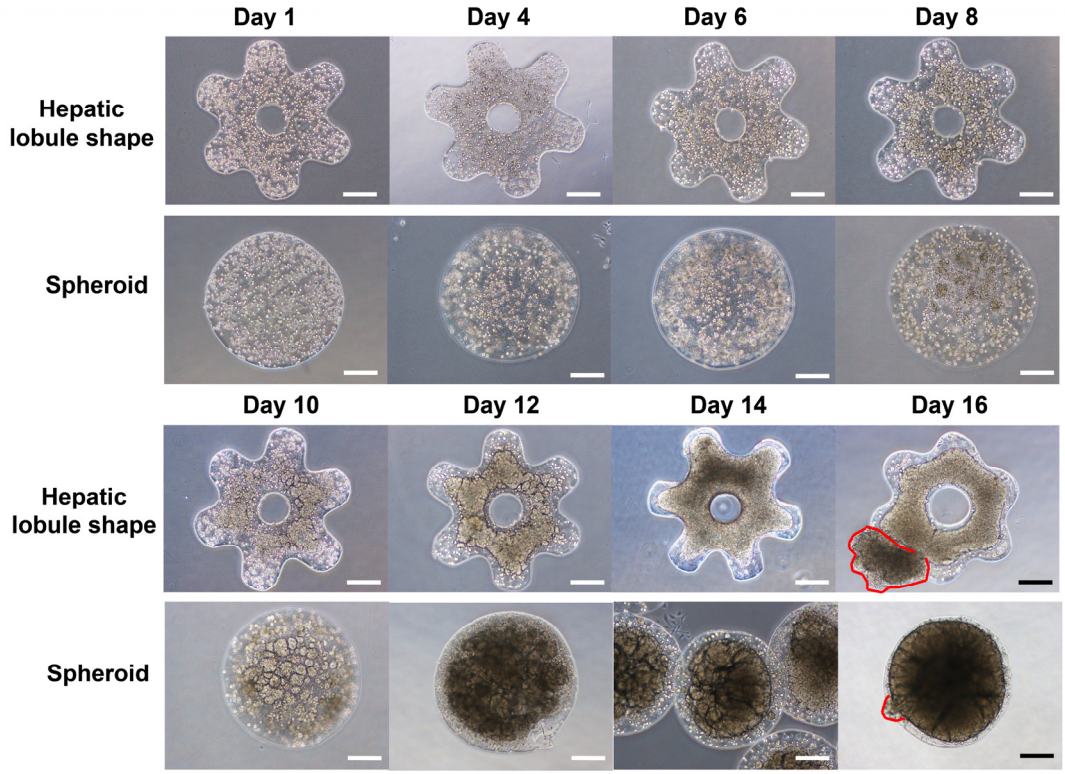

Figure 4.6 . Cell culture results for the HLSM and spheroids on days 1, 4, 6, 8, 10, 12, 14, and 16. The initial cell density in deposition solution was around 1×10^7 cells/ml. Scale bar represents 250 μm. The cell densities of the HLSM and spheroid were approximately 1.3×10^8 cells/cm^3 and 1.08×10^8 cells/cm^3 on day 14. Beyond day 14, the cell may break through the Alginate-PLL complex shell to form the cell cluster outside as indicated by red mark.

also verify our calculation results of the structure volume shown in Table 1, because the spheroids had a larger volume (0.15 mm^3) than the HLSM (0.11 mm^3) for cells to further occupy beyond day 16.

4.4.2 Cell number counting and viability assay

We used a Cell Counting Kit-8 (CCK8) to determine the cell number in the fabricated microtissue. This kit allows for sensitive colorimetric assays for the determination of the number of viable cells in cell proliferation. The detection sensitivity of CCK-8 is higher than other tetrazolium salts such as MTT, XTT, MTS, or WST-1, according to the technical manual. Following the protocol, we first prepared standard samples that contained known numbers of viable cells to create a calibration curve. The procedure for cell counting included: 1) Inoculation of individual microtissue of the HLSM or spheroid (100 μl/well) in a 96-well plate. 2) Adding 10 μl of the CCK-8 solution to each well of the plate. 3) Incubating the plate for 3 h in the

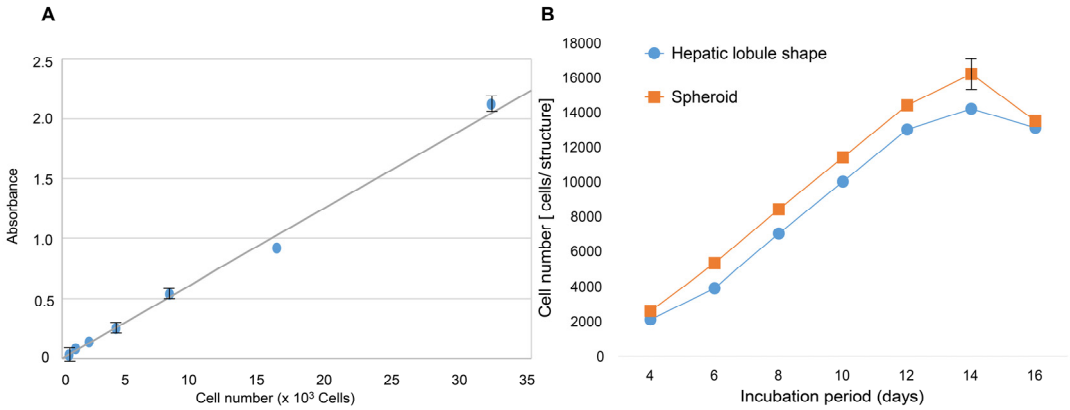

Figure 4.7 (A) The calibration curve of a linear fitting model (f(x) = p1*x, p1 = 0.006497) shows the relationship between the RLC-18 cell numbers and absorbance (OD) using the CCK8 assay. (B) Change in the cell numbers of the RLC-18 HLSM and spheroids during the incubation period.

incubator. 4) Measuring absorbance immediately at 450 nm using a microplate reader (Infinite F50 plate readers, TECAN) to determine the cell number of each microtissue.

In order to confirm if the presented method is suitable for use in biological applications, cell viability of the fabricated microtissue was checked on day 14. The fabricated structures were washed once with HEPES buffer solution and then immersed into the cell viability test solution for 30 min in an incubator. Then, the structures were washed with HEPES buffer solution again. A fluorescent microscope was used to observe the samples.

Figure 4.5C shows the fluorescence results for cell viability within the HLSM on day 14. By separating the RGB image, it is shown that the red area (dead cells) occupied approximately 6% of the whole area. The cell spheroids have also been measured in previous work and showed similar results to the HLSM [98]. This result indicates that our method can be used to fabricate the microtissue while also maintaining viability after long-term culture. Because we used the normal mammalian cell line, we believe this method is also capable of encapsulating other bio-components such as cancer cells and bacteria while maintaining their viability during long-term culture.

Figure 4.7A shows the calibration curve of a linear fitting model to indicate the relationship between the RLC-18 cell numbers and absorbance (OD) using the CCK8 assay. Based on the calibration curve, the cell number was determined by measuring the OD value. Figure 4.7B shows the changes in cell numbers per structure of the HLSM and spheroid.

Figure 4.7B shows that the cell numbers in HLSM and spheroids on day 14 of

culture increased to approximately 9 and 11 times the initial cell numbers (~1500 cells/structure), respectively. Consequently, the cell numbers per structure in HLSM and spheroids reached approximately 1.42×10^4 and 1.62×10^4 cells/structure, respectively. Hence, the cell density of the HLSM and spheroids can be calculated using the relationship between volume and cell number. The cell density was approximately 1.3×10^8 cells/cm^3 and 1.08×10^8 cells/cm^3 for the HLSM and spheroids, respectively, indicating that the fabricated microtissue had a high cell-density. Interestingly, the cell numbers in the spheroid on day 14 of culture were 1.4-fold higher than that in the HLSM on day 14. This result was consistent with the following finding: the volume in the spheroid was larger than that of HLSM, even though we used the micro-electrode with exactly the same area for both designs (Table 4.1). Therefore, the spheroid with larger volume may provide more room for cell proliferation.

4.4.3 Albumin secretion and urea synthesis

A rat albumin ELISA quantitation kit was used to measure albumin levels during the culture period (at 4, 6, 8, 10, 12, 14, and 16 days). Before the assay, the fabricated microtissue was washed with PBS and fresh medium was added; after 24 h, this medium was withdrawn and aliquots were temporarily stored at -20 °C. There were two groups of the HLSM and two groups of the spheroids, which consisted of 19 HLSMs and 26 spheroids from four independent cell preparations. The levels of albumin measured at each time point were normalized to each microtissue or the cell number. The urea level in the medium was determined using the urea assay kit (DIUR-100). The levels of urea measured at each time point were normalized to each microtissue or the cell number.

Figure 4.8A shows that the albumin-secretion activities per HLSM structure were almost the same as those of the spheroid before day 10; however, starting on day 12, the activities of the HLSM were significantly higher than those of the spheroids, with a maximum of 1.6-fold the activity on day 14 ($p = 0.0059$; $n = 4$). According to the culture results shown in Figure 4.6, the cells were beginning to fully occupy the microcapsules from day 12.

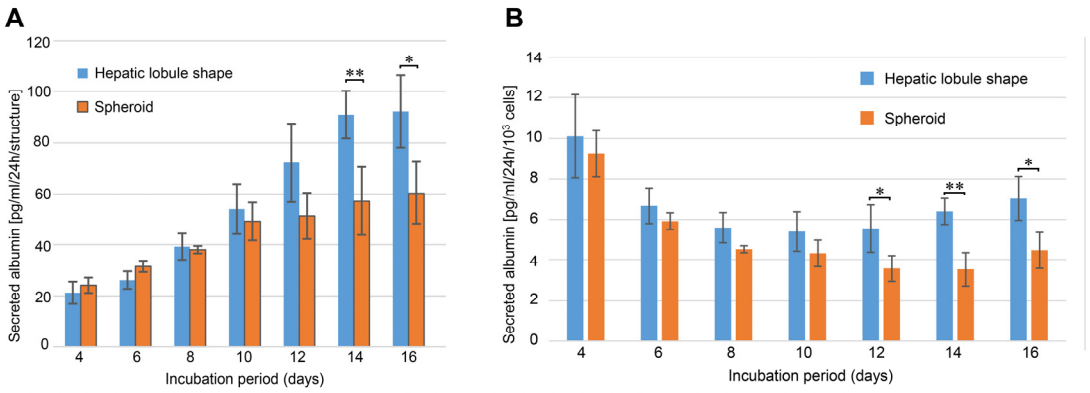

Figure 4.8 Albumin secretion per structure (A) and per cells (B) of the RLC-18 HLSM and spheroids. The data represent the mean ± standard derivation of at least three experiments from four independent cell preparations. ∗ $p < 0.05$; ∗∗ $p < 0.01$.

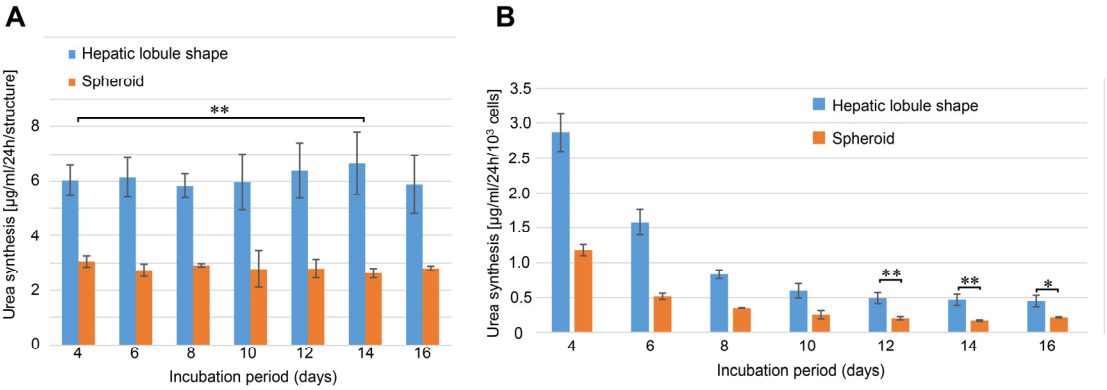

Figure 4.9 Urea synthesis per structure (A) and per cells (B) of the RLC-18 HLSM and spheroids. The data represent the mean ± standard derivation of at least three experiments from four independent cell preparations. ∗ $p < 0.05$; ∗∗ $p < 0.01$.

Figure 4.8B shows the albumin secretion per cell of the RLC-18 HLSM and spheroids. First, there was a declining trend in albumin secretion in both structures. Second, cells cultured within HLSM showed significantly higher activity as compared with cells cultured within spheroids at days 12, 14, and 16 (p = 0.0251, 0.0015, and 0.0105; n = 4, respectively) and showed ~1.8-fold higher activity as compared with cells cultured within spheroids on day 14. This result indicated that the albumin secretion of the HLSM was higher than that of the spheroids both per structure and per cell.

Figure 4.9A shows urea secretion per structure into the medium. The HLSM showed significantly higher urea-synthesis levels as compared with the cell spheroids from day 4 until the end of the experiment (day 16). Figure 4.9B shows the urea secretion per cell of the HLSM and spheroids. A significant decrease in urea synthesis was observed between days 4 and 8 for all cultures. Cells cultured within HLSM showed significantly higher urea syntheses than cells cultured within spheroids at days

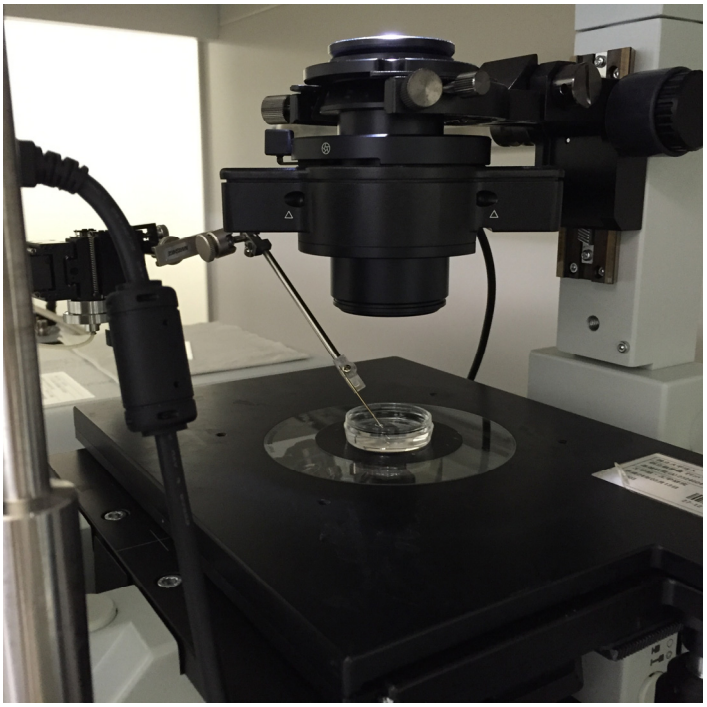

Figure 4.10 (a) Experimental setup of the micro-manipulator system for 3D multilayer hepatic lobule-like tissue assembly.

12, 14, and 16 (p = 0.000528, 0.00606, and 0.010689; n = 4, respectively). These results clearly demonstrated the effectiveness of the PLL-alginate microcapsule system and the HLSM formed in preserving *in vitro* hepatocyte functions.

4.5 Assembly of four-layered hepatic lobule-like tissue by micromanipulator

To demonstrate the feasibility of the current method for 3D-cell-model fabrication, a simple micromanipulator system was built to assemble the HLSM into a 3D multilayer hepatic lobule-like tissue to mimic the native tissue as shown in Figure 4.11. The assembly technique used in this study was a modified method [128]. Briefly, the glass micropipette was defined (G-1000; Narashige International Inc., East Meadow, NY, USA), heated, and pulled in micrometer dimensions (P-2000; Sutter Instrument, Novato, CA, USA) as a main manipulator. The main manipulator orientation can be adjusted along the X-, Y-, and Z-axes prior to assembly. The main manipulator first moves downward to contact the microcapsules in the central position. Air is manually injected into the solution through a 1-mL pipette to create bubbles, which lead to a regular rising movement that is utilized to assemble the four-layered hepatic lobule-like tissue fabricated in an open environment.

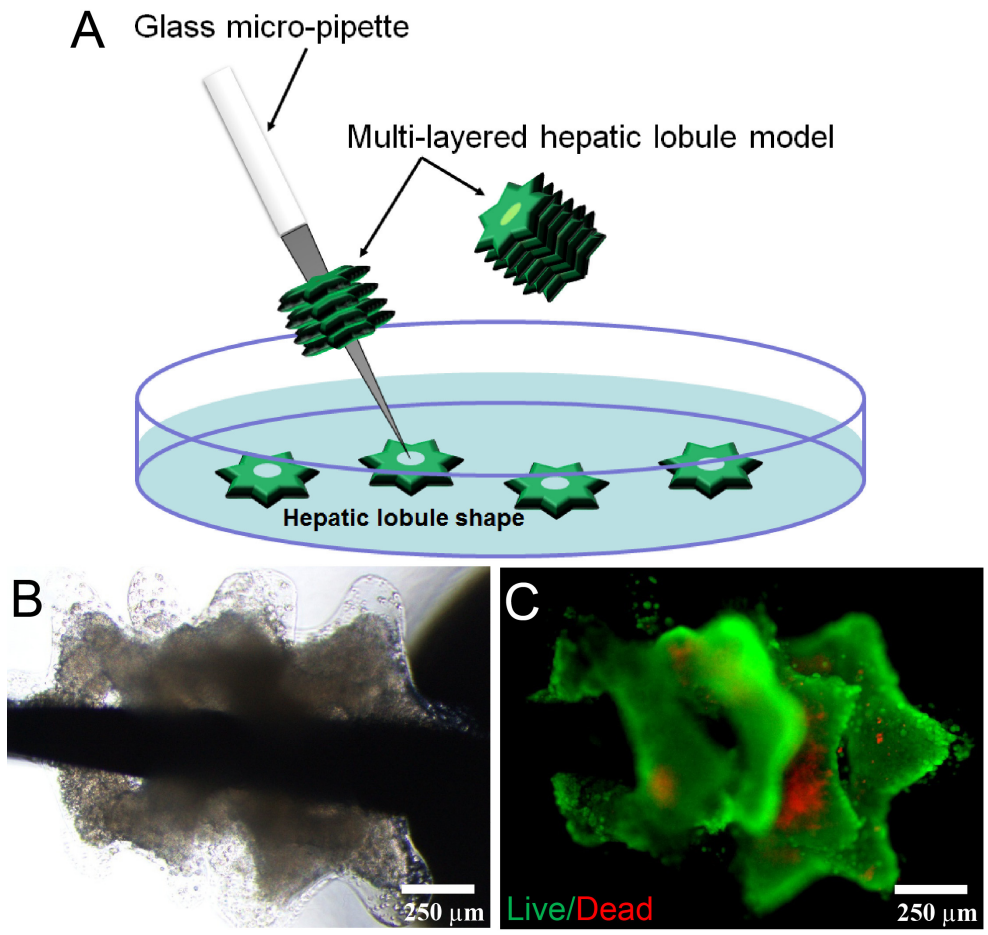

Figure 4.11 (A) Concept for assembly of multilayer HLSM with repetitive single-step contact micromanipulator. The glass micropipette moves downward to contact the microtissue in the center position (the central vein of the HLSM). Air is manually injected into the solution through a pipette to create bubbles near this microtissue (not shown in figure). These bubbles lead to a regular rising movement of the microtissue, which is utilized to load the microtissue onto the main manipulator. This one-step pick-up procedure was repeated to assemble the multilayer HLSM. (B) Bright image of assembled four-layered HLSM. (C) Cell viability of the four-layered HLSM assessed by live/dead assay.

The four-layered hepatic lobule-like tissue was manually assembled by a repetitive one-step micromanipulator. The optical and fluorescence images are shown in Figure 4.11B and Figure 4.11C, and the experimental setup is shown in Figure 4.10. The movie of the assembly process can be found in the supplementary information. It took a total of 10 min to assemble the 3D four-layered tissue, which exhibited cell viability >80%. The cell density was 1.2 X 10^8 cells/cm^3 (calculated using the relationship between volume and cell number at day of 16). Unlike other assembly methods [2], ours was sufficiently repeatable and can be used to easily assemble many single micromodules into a 3D cell model. For example, Huaping Wang's group develops a versatile method that engineers permeable 3D microtissues into tissue specific microscopic architectures. The customized, arbitrarily shaped hollow micromodules are prepared by photocopolymerizing poly (ethylene glycol) diacrylate (PEGDA) with acryloyl-PEG-

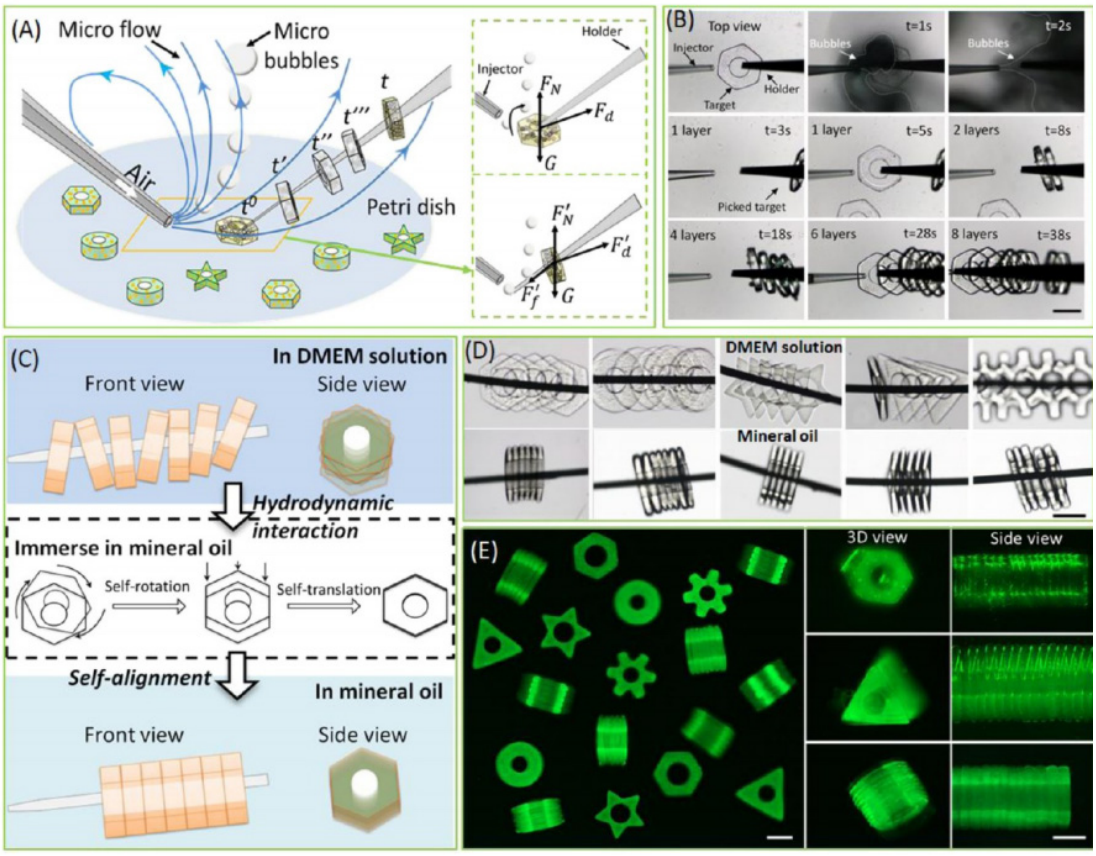

Figure 4.12 . (A) Schematic of the sequential pickup of micromodules based on microbubble injection. (B) Selective pickup of cell-laden micromodules with the hexagonal structure from the DMEM solution. (C) Schematic of the self-alignment of picked-up micromodules based on hydrophilic and hydrophobic interactions. Driven by surface tension during the interaction, the micromodules self-rotate and self-translate into an integrated geometry. (D) Optical images of the picked-up micromodules before and after self-alignment. The micromodules with different postures in the DMEM solution assumed a uniform posture when immersed in mineral oil. (E) Fluorescence image demonstrating the assembly results of 3D microstructures with different tissue-specific morphologies after the release from the holder. The micromodules were fabricated from the PEGDA prepolymer solution with 5 mM RGDS and 0.2% (v/v) fluorescent microspheres. Scale bars: 200 μm in (B), 300 μm in (D), and 300 μm in (E) [2].

Arg-Gly-Asp-Ser (RGDS). These micromodules are spatially reorganized and self-aligned by a facile assembly process based on hydrodynamic interactions, forming an integrated geometry with tissue-specific morphology and a vessel-mimetic lumen. The RGD linkages create cell-adhesive structures in the PEGDA hydrogel, greatly increasing the long-term cell viability in 3D microtissue cultures [2, 129]. However, compared with our proposed methods, the cells encapsulated within the RGD-modified PEGDA hydrogels seems to only grow on the outer surface of the fabricated micro-structures. Thus, how to further promote the formation of 3D microtissue by removing the PEGDA scaffold might be the main challenge for them.

4.6 Discussion

In this study, we demonstrated a new method for forming 3D multilayer hepatic lobule-like tissue using PLL-alginate microcapsules that closely mimic the *in vivo* structure of the hepatic lobule. Hepatocytes are anchorage-dependent cells that are notoriously difficult to maintain *in vitro* [130]. To preserve hepatic functions *in vitro*, various methods for culturing hepatocytes have been proposed, including dielectrophoresis-based liver cell patterning [111], cylindrical multicellular aggregation [115], stacking of cell sheets [131], 3D cell culture [132], and sandwich co-cultures with 3T3 fibroblasts [133]. These studies demonstrated the significance of cell-matrix and cell-cell interactions. Unlike previous studies, this study demonstrated the following three advantages: 1) successful adaption of electrodeposition to generate 3D-cell-tissue constructs, 2) incorporation of PLL in the alginate hydrogel as an ECM to promote cell adhesion and proliferation, and 3) morphological and functional characterization of the 3D hepatic lobule-like tissue construct developed in this study as compared with the RLC-18 cell spheroid that had been commonly utilized as a 3D tissue-like model.

Yamazaki et al. reported that spheroids cultured in the microwell chip with a bottom surface made of honeycomb film showed an enhanced proliferation rate, because the oxygen permeability of the honeycomb film is higher than that of other materials [134]. Therefore, limited oxygen may be an important factor that limits the functionality of and proliferation rate in microtissues. However, in their work, the albumin-secretion activities per cell of HepG2 spheroids in both chips were almost the same. This result indicated that beyond the external factors, the shape of the microtissue is essential. The possible key parameter that enhances cell functionality involves controlling cell orientation to form a microtissue that has a maximum transfer efficiency of oxygen and nutrients. Therefore, the purpose of measuring albumin secretion by the HLSM and spheroid in this work included: 1) to quantitatively examine the functionality of the HLSM, which has a similar shape to our native tissue as compared with the normal cell spheroid; and 2) to demonstrate that the 3D cell model assembled by a single functional HLSM is also biofunctional.

Quantitative analysis illustrated that the characteristic morphology of the microtissue contributed to enhanced hepatocyte viability and functionality. Albumin secretion and urea synthesis were significantly upregulated in the HLSM. A possible explanation is that in the HLSM, the central “vein” provides a hollow structure that supports efficient mass transfer of oxygen, nutrients, and waste, contributing to the sustained proliferation of cells and functionality of the HLSM. Additionally, the surface area of the HLSM was 1.99 mm^2 larger than that of the spheroid, which was 1.50 mm^2 (Table 4.1). This result indicated that the HLSM had more surface area for enhancing the nutrient- and waste-exchange rates with culture medium. In Figure 4.8A, the amount of albumin secreted by the "structure" was low, but began to increase gradually. By

contrast, in Figure 4.8B, the amount of albumin secreted by the "cells" was high, and then began decreasing. The possible explanations for this phenomenon are as follows. Albumin secretion and cell proliferation are considered unrelated processes and generally move in the opposite direction [135]. The results shown in Figure 4.7b and Figure 4.8B support this theory. In Figure 4.8B, at 4 days the growth of cells in sparse culture can fully access to the culture medium, where the cells exhibited the highest albumin-secretion activities. From days 6 to 12, when the cells in the microcapsules occupied all the available substrate (the inner PLL surface) and began to form multiple large cell aggregates, the cell activities decreased. Usually, peak albumin secretion coincides with cell confluence, which is also characterized by decreased cell proliferation. As shown in Figure 4.8A, the albumin secretion reached its peak on day 14, accompanied by decreased cell proliferation according to data in Figure 4.7A. However, from day 12 to 16, cells reached confluence and stopped growing, while albumin increased again. The possible reason is that some cells broke through the PLL membrane at day 16, as shown in Figure 4.6. The cells outside the microcapsules increased the contact surface with culture medium. This may lead to the increased albumin secretion. During the culture periods, the hepatocytes showed appreciable levels of urea synthesis, which were stable and did not change when expressed per structure (Figure 4.9A). However, when expressed per cell, the levels gradually and progressively declined in both types of structure (Figure 4.9B). We believe that the possible reason for this behavior is similar to that already described above for the albumin secretion. This result is consistent with a report that the 3D hepatocytes micro-organoids are critical for preserving hepatocyte function [130]. Although the urea production in our case appears lower than the conventional works that cultured hepatocytes on a modified alginate scaffold [136, 137]. The possible reason is that the urea production from 2D culture may be higher than that from 3D dense culture [130].

The reason why we stop culture the fabricated APA microcapsules both in HLSM and spheroid shapes is that as shown in Fig. S11, at the day of 18, the encapsulated cells broke through the alginate-PLL complex membrane and attached to the bottom surface of the culture dish for 2D proliferation. Therefore, we could not further culture them for the quantitative analysis although the albumin secretion is still increasing.

Generally, cell spheroids with a diameter >300 μm do not allow survival of inner-core cells, which usually die by necrosis. However, we did not observe central necrosis occurring in our case according to live/dead assay results following culture. A possible explanation is that unlike conventional cell spheroids cultured in a liquid-drop system or other surface-treatment methods in which the cells grow from the inside to the outside naturally, cells within microcapsules grow from the outside (the PLL inner surface) to the inside. We believe that this might help to avoid the central necrosis phenomenon.

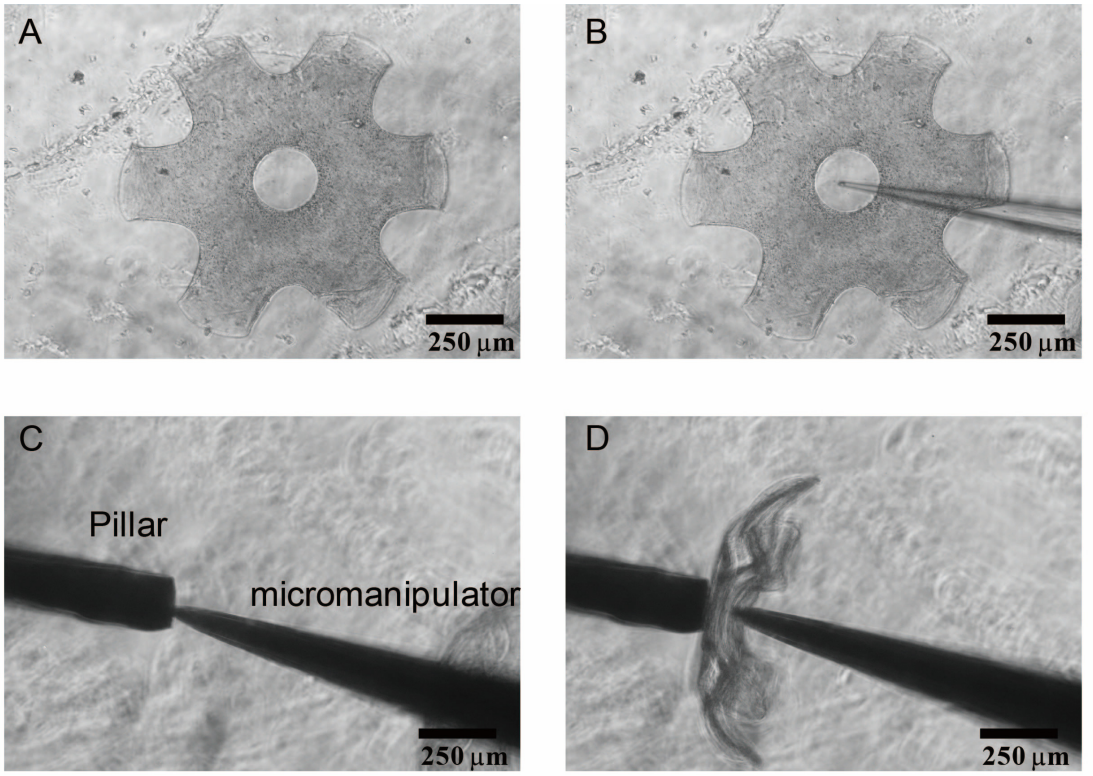

Figure 4.13 (A) Fabrication result of the HLSM without cells. (B) Micromanipulator attached to the center of the HLSM for loading. (C) Micromanipulator contacts with the pillar. (D) Transferring the HLSM onto the pillar.

As shown in Figure 4.11, a four-layered hepatic lobule model was constructed to demonstrate the feasibility of the proposed method for 3D multilayered tissue constructs in tissue engineering applications. The biofunctionality was confirmed by comparing the HLSM with normal cell spheroids. In future, we plan to build polydimethylsiloxane (PDMS) with pillars to better investigate the functional and histological characteristics of the assembled 3D multilayered tissue. We intend to load the HLSM onto the pillar that is made of a titanium wire, using a one-step micromanipulator. The preliminary experimental results can be found in Figure 4.13. By means of such pillar as a substrate, “sandwich” hepatic cord-like tissue co-cultured with 3T3 feeder cells for long-term preservation of liver-specific functions will be assembled and evaluated, comparing them with monocultures of hepatocytes in 3-dimension. The other challenge of the current method for cellular implantation is how to merge the multilayered cell structures. One possible solution to this issue would be to stabilize the multilayered hepatic lobule model by a secondary crosslinking step simply by immersing it into alginate solution, in a fashion similar to that of the assembled multilayered PEG structure [138]. As another option, alginate-PLL membrane-free transplantation of the hepatic lobule mode would be possible after chemically dissolving the alginate-PLL membrane [100], that would enhance the

supply of oxygen and nutrients and merge cells together for syngeneic transplantation. However, without the alginate-PLL membrane, the tissue shape may not be maintained.

Therefore, the purpose of building the micromanipulation system was to demonstrate the feasibility of the current method for fabricating a 3D cell model, such as a hepatic lobule-like tissue, by using the single HLSM as a building block. Compared with other commonly used cell-containing hydrogels, such as alginate hydrogel [139], poly(ethylene glycol) diacrylate [140], and collagen [21], the microcapsules fabricated by the electrodeposition and microcapsule techniques have advantages, including: 1) high cell density similar to our native tissue, 2) biofunctional 3D cultures, and 3) shape-control capability based on the design of the microelectrode. Therefore, this constitutes a promising technique for fabricating complex 3D cell models using varying microcapsules to encapsulate different cell lines for further applications in tissue engineering.

4.7 Summary

In summary, this paper presented the fabrication of HLSM as a building block for 3D multilayer hepatic lobule-like tissue constructs. RLC-18 cells were successfully encapsulated within the HLSM and compared with cell spheroids, exhibiting improved cell functionality over 12 days. A repetitive one-step micromanipulator system was established to fabricate four-layered hepatic lobule-like tissue from the HLSM. Our technology to fabricate a complex 3D cell model with biofunctionality enabled precise control of cellular alignment and orientation in three dimensions. Our findings may significantly impact the development of in vitro 3D models for broader applications, including those involving tissue engineering, cell transport, and drug delivery.

Chapter 5
In Vitro Mimicking the Morphology of Hepatic Lobule Tissue Based on Cellular Ca-alginate hydrogel sheets

5.1 Motivation of cell sheet fabrication

Various liver tissue engineering approaches currently under development, with applications ranging from artificial liver organ transplantation to cell-based therapies, rely on the ability to encapsulate hepatocytes in three-dimensional (3D) scaffolds. Hydrogels are attractive scaffolds for 3D cell culture and tissue engineering due to their tissue-like water content, injectability, and tunable properties. Extensive efforts have been made to allow the control of various hydrogel formations, such as thermoresponsive gel, photo-crosslinkable gel and chemical-crosslinkable gel; this control could facilitate drug release [141], cell assembly In vitro [142, 143], tissue formation [26, 144, 145] and subsequent transplantation [146].

A hydrogel made from an acidic polysaccharide of sodium alginate, which can ionically cross-linked with multivalent cations (e.g., Ca^{2+}, Fe^{3+}), is widely used to entrap and immobilize cells [106], as well as bacterial [90] and other bio-components. The “cell containing alginate hydrogel modules” take the form of cell droplets [119, 147-149], cell microfibers [130, 150] and cell sheets [82, 93]. Challenges remain concerning the application of this hydrogel in tissue engineering; first, cell proliferation rate is slow within the gel due to a lack of cell adhesion molecules, although some researchers have indicated that the incorporation of RGD peptides can help cell adhesion [151]. Second, it is difficult to control the formation of a complex alginate hydrogel structure due to the diffusion of the multivalent cations in solution. Microfluidic technology and specialized devices with nozzle arrays are the common method to generate these structures [99, 100, 152].

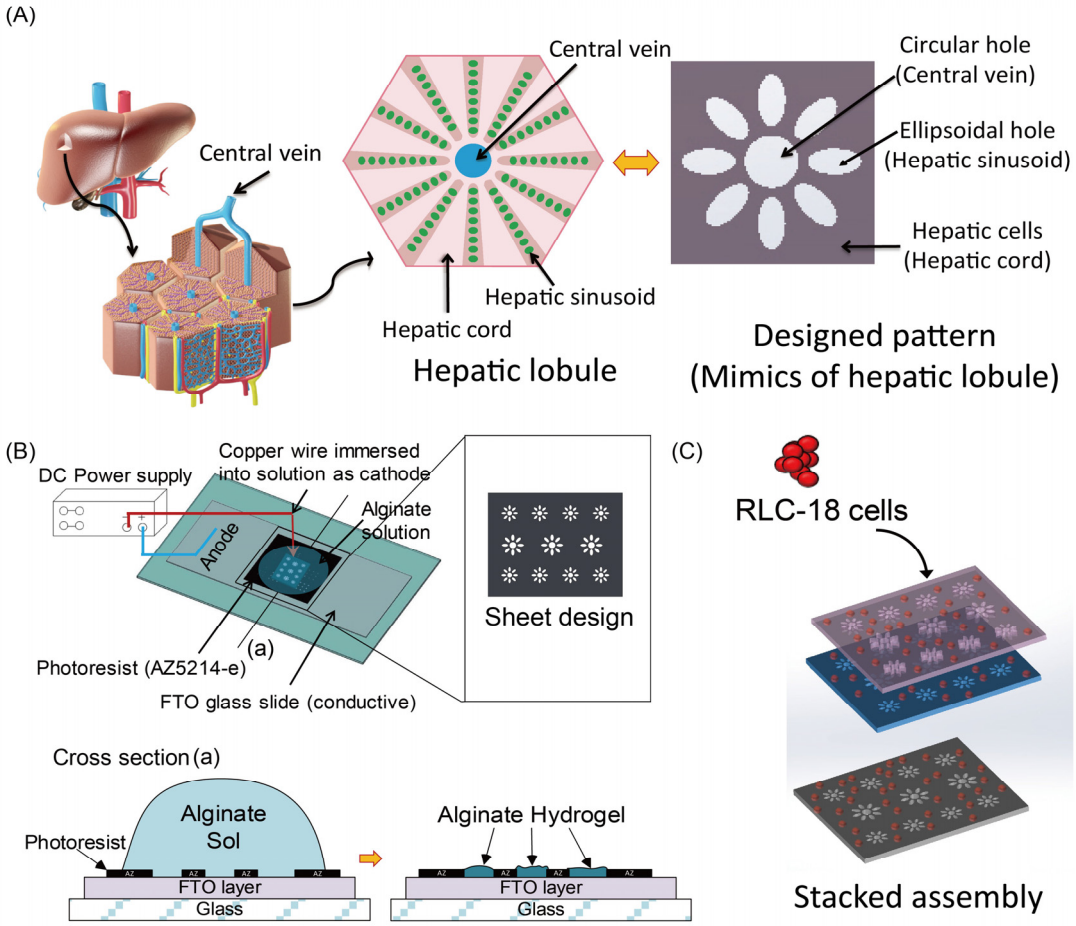

Figure 5.1 (A) The structure of the hepatic lobule as the functional units of the liver (left), and the two-dimensional microarchitecture of the hepatic lobule (right). (B) We developed a micro-patterned electrode device using a photolithography technique. Two kinds of hepatic lobule patterns were designed with different outer diameters (1.5 mm and 2.0 mm). A DC voltage was applied to the device to trigger the electrodeposition process. The cross section (a) shows the changes before and after the electrodeposition process. The alginate solution goes through the gelation process to form an alginate hydrogel structure on an FTO layer based on the principle of electrodeposition. (C) The fabricated alginate cell sheets are further detached and stacked to form multi-layered hepatic lobule tissue.

Recently, electrodeposition has been well established [90, 153, 154]. This method is widely utilized to deposit alginate or chitosan gel film onto a specific area of 2D substrate for cell-cell signal studies [89, 93]. The mechanism of electrodeposition is used to release calcium ions from the region of the micro-electrode surface via electrolysis (H^+ is released from the anode and reacts with $CaCO_3$ particles to release calcium ions). Thus, these calcium ions can immediately react with alginate around the electrode to form an alginate hydrogel film. Simultaneously, bio-components are immobilized within the gel film for use in further applications [154]. The advantages of electrodeposition include the fact that the complex patterns to a resolution of <100

μm can be achieved [90]. Thus, this method successfully overcomes the shape control limitations of alginate gel. In our previous report [145], we demonstrated that issues with cell proliferation within alginate gel can be solved through an improved electrodeposition method which produces high cell-density microtissue. However, some challenges remain, limiting the use of electrodeposition in further applications of tissue engineering. Generally, the method restricts placement of fabricated alginate sheets to a 2D electrode. This limitation raises the question of whether the fabricated cell sheet could be detached and assembled for 3D tissue formation. In addition, the detached alginate sheets can curl themselves due to their flexibility and insufficiently cross-linked Ca-alginate structure [90], making them unsuitable building blocks for 3D stacking assembly. As a result, it is necessary to fabricate the gel sheet on a flat surface.

In the current study, we propose a method to fabricate Ca-alginate cell sheets for hepatic lobule tissue constructs based on the electrodeposition method. The centimeter-scale cell sheets were produced with pre-designed hepatic lobule patterns. After a one-day culture, we successfully detached the sheets from the 2D electrode substrate without any structural defect and stacked them into 3D multilayer hepatic lobule tissue within a PDMS mold. Cell proliferation and functionality of the fabricated Ca-alginate cell sheet were quantitatively compared to that of regular 2D culture. This study aims to clarify that alginate cell sheets created by electrodeposition can potentially be utilized for 3D tissue constructs. A research map is shown in Figure 5.1.

This work is potentially significant for a number of reasons. First, we demonstrate that alginate sheet fabrication with hepatic lobule patterns using electrodeposition can be potentially utilized for 3D tissue constructs. Second, an easy method is proposed to detach the sheet from a flat surface without any defect. We also show that the detached sheets can be transferred simply using a 1-ml pipette, then stacked into a multi-layered tissue. We believe our method provides a suitable platform for constructing a 3D cell model by stacking alginate cell sheets using electrodeposition. This platform has the potential to uncover new uses for electrodeposition in various applications such as in cell–ECM interactions, structure–function relationships, tissue morphogenesis, and modular tissue reconstructions.

5.2 Material and methods

5.2.1 Materials and solution preparation

We used sodium alginate (Medium viscosity, A2033), fluorine doped tin oxide coated glass slide (surface resistivity ~7 Ω/sq, 735140) (Sigma-Aldrich) and HEPES (346-01373) (Wako Pure Chemical Industries). Calcium carbonate ($CaCO_3$) (0.97 μm, #2300) were kindly supplied from Sankyo-seifun Ltd (Japan). Photoresist (AZ5214-E)

were purchased from AZ electronic material GmbH. Cell Counting Kit-8 (CCK8) was purchased from Dojindo Ltd (Japan). Rat albumin enzyme-linked immunosorbent assay (ELISA) Quantitation kit (ERA3201-1) was purchased from Assaypro Inc (USA). The water used to prepare the solution was deionized with a Millipore Direct-Q3 water purification system (Millipore, Worcester, MA).

The deposition solution was prepared by dissolving 1% w/v alginate sodium in solution containing NaCl (126 mM), KCl (2.7 mM), $Na_2HPO_4 \cdot 12H_2O$ (8.1 mM), KH_2PO_4 (1.47 mM) and HEPES (21 mM). The pH was adjusted to 7.3 by adding 0.5M NaOH solution. $CaCO_3$ (0.5% w/v) was uniformly dispersed in the solution using magnetic stirrer for 24h.

The HEPES buffer solution was prepared by dissolving HEPES (5g/L) in solution containing NaCl (8 g/L), KCl (0.37 g/L), Na_2HPO_4 (1.076 g/L) and glucose (1 g/L). pH was adjusted to 7.3 by adding 0.5M NaOH solution.

To prepare 1.1% calcium chloride solution, 0.55 g of $CaCl_2$ (anhydrous) is dissolved in 50 ml of distilled water.

The cell viability solution was a mixture of 0.8 μL calcein AM (1 mg/mL, Wako), 2.8 μL propidium iodide (PI) (1 mg/mL, Wako) and 1 mL HEPES buffer solution.

5.2.2 Fabrication of micro-patterned electrode

The photolithographic technique was used to construct the electro-device in this experiment. Briefly, fluorine-doped tin oxide (FTO) glass slides (2.5 cm × 5 cm) were washed with isopropyl alcohol and Milli-Q water using an ultrasonic cleaner. The photoresist (AZ 5214E) was coated onto the surface of FTO glass with 1.4-μm thickness.

The micro-patterns were designed to mimic liver lobule morphology as shown in Figure 5.1A. The length of the sheet is 1.2 cm and the width is 0.95 cm. There are two types of hepatic lobule pattern utilized in the current work: one with a diameter of 1.5 mm and the other of 2 mm. The hepatic lobule is a building block of the liver consisting of a portal triad, hepatocytes arranged in linear cords between a capillary network (hepatic sinusoid), and a central vein. The peculiarity of liver sinusoids consists in the fact that blood infuses the liver lobule unidirectionally, entering the portal area and ending its pathway in the central vein. When compared with liver histology, the circular hole of the micro-pattern mimics the central vein. Around the central vein, eight ellipsoidal holes represent hepatic sinusoids as communication paths between the portal vessels and central vein. The other area on the alginate sheet embedded with hepatic cells mimics the hepatic cord. The patterned-electrode was fabricated using a laser writing device (μPG 101, Heidelberg, German) based on our AutoCAD design of micro-electrodes.

5.2.3 Electrodeposition of Ca-alginate gel sheet

To fabricate the Ca-alginate gel sheet with hepatic lobule patterns using the electrodeposition method, the following steps were performed:

1) The prepared RLC-18 cells were centrifuged and washed with HEPES buffer twice to fully remove the culture medium since the DMEM may interfere with the electrodeposition chemical reaction and generate bubbles. Then, 700 µl deposition solution was mixed with the centrifuged RLC-18 cells by gently pipetting.

2) 500 µl deposition solution was taken from the mixed 700 µl cell deposition solution to be placed onto the electrode area, as shown in figure 1B.

3) A DC power supply was connected to the device using two copper wires. One copper wire was immersed into the deposition solution as a cathode at a depth of about 1 mm. The other copper wire was attached to the surface of the FTO glass as an anode.

4) A DC voltage was applied to the FTO electrode to trigger electrolysis and start the electro-deposition process. The Ca-alginate gel sheet was deposited onto the patterned electrode area based on the electrodeposition principle as shown in Fig. 2A.

5) After 15 s, the DC power supply was turned off immediately and extra non-cross-linked alginate solution was removed by a pipette. Then, the FTO glass was transferred into HEPES solution for washing.

6) The FTO glass was gently shaken for several minutes until the boundary of the hepatic lobule pattern on the gel sheet could be clearly identified under an optical microscope.

Before the experiment, the deposition solution was stirred again to evenly disperse the $CaCO_3$ particles and heated to 37 °C. In the meantime, 1 ml of the pre-prepared RLC-18 cell suspension (cell concentration: 10^7 cells/ml) was centrifuged and washed with phosphate-buffered saline (PBS) twice to remove the DMEM, which might have interfered with the electrodeposition reaction. The cell suspension was then centrifuged again, mixed with 700 µL of the heated deposition solution, and evenly dispersed by gently pipetting. Finally, 500 µL of the 700 µL deposition solution was dropped onto the microelectrode area as shown in Figure 5.2B.

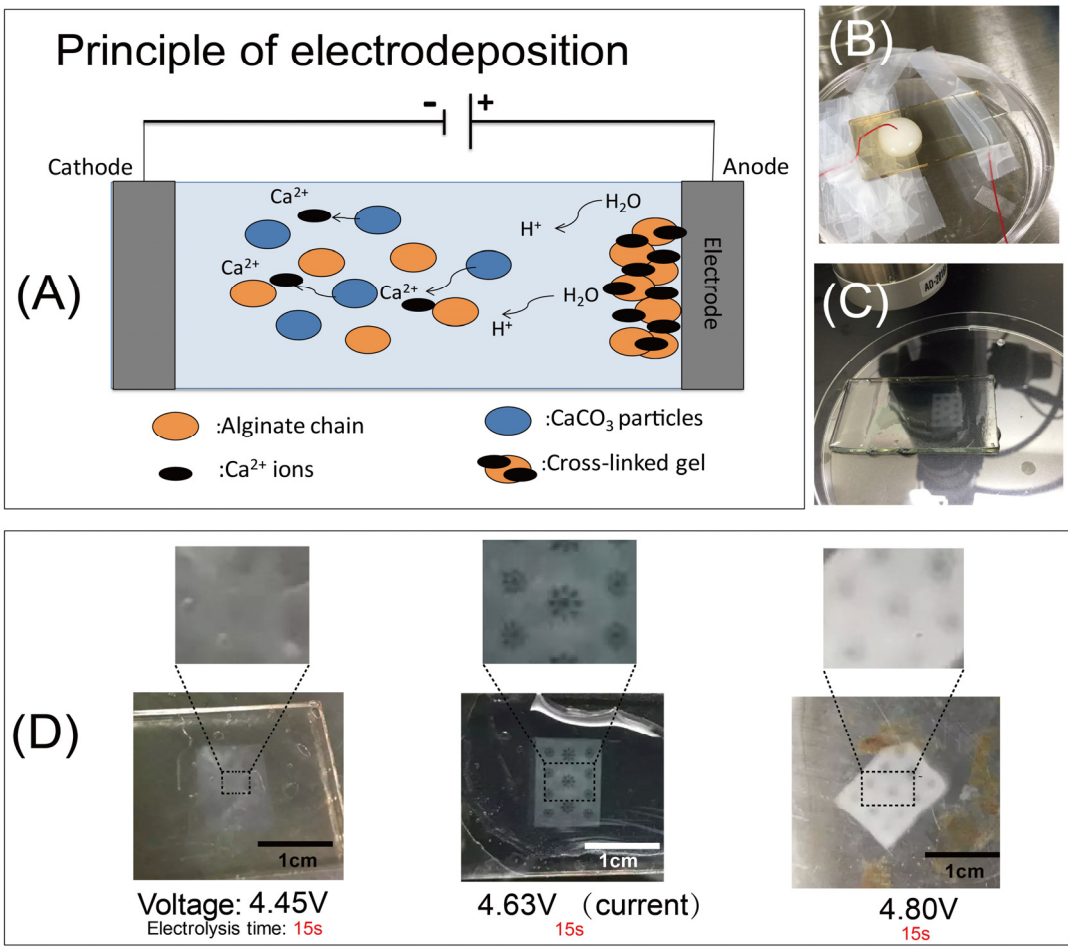

Figure 5.2 (A) The principle of electrodeposition. (B) The experimental setup before electrodeposition; A DC power supply was utilized to trigger the electrodeposition process by attaching the anode to the FTO glass and immersing the cathode into the deposition solution (Red wire). (C) The Ca-alginate gel sheet was deposited onto the micro-electrode area corresponding to the design. (D) The effect of the applied voltage on the stability of the gel sheet structure. A lower voltage leads to an unstable gel sheet generation due to the insufficient cross-link of Ca-alginate chain (Left image); A higher voltage leads to a thick gel sheet generation without the hepatic lobule pattern due to the diffusion of Ca^{2+} ions (Right image).

A DC voltage of 4.63 v was applied for 15 s to trigger the electrodeposition process. The concept of the electrodeposition principle is shown in Figure 5.2A. Briefly, H^+ is generated by the electrolysis of water formed in an acidic microenvironment at the anode surface ($2H_2O \rightarrow O_2+4H^++4e^-$). Ca^{2+} is released from $CaCO_3$ particles as they encounter protons at the anode ($2H^++CaCO_3 \rightarrow Ca^{2+}+H_2O+CO_2$). The calcium alginate hydrogel films are formed when calcium ions cross-link with alginate immediately ($Ca^{2+}+2Alg\text{-}COO^- \rightarrow Alg\text{-}COO^-\text{-}Ca^{2+}\text{-}^-OOC\text{-}Alg$). Therefore, the shape of the gel sheet can be altered by changing the design of the micro-electrode.

Figure 5.2C shows the fabricated Ca-alginate gel sheet after washing with HEPES solution for 2 min. In Figure 5.2D, we show cases where a lower voltage was used, which leads to unstable gel sheet generation due to insufficient cross-linking of Ca-alginate chains; and cases where a higher voltage was used which leads to generation of a thick gel sheet without the hepatic lobule pattern due to the diffusion of Ca^{2+} ions.

5.2.4 Detachment of the fabricated gel sheet from the substrate

The detachment method process is shown in Figure 5.3A. After washing (see '5)' above), 1.1% $CaCl_2$ solution was dropped onto the gel sheet for 15 min; Ca^{2+} ions harden the gel structure by cross-linking with alginate chains. The CaCl2 solution was then removed and the FTO glass immersed in HEPES solution or DMEM solution (the latter if using cells) at 37 °C in a humidified 5% CO_2 incubator. After 24 h, the gel sheet detached from the FTO glass substrate automatically.

Figure 5.3A shows the detachment procedure of the fabricated gel sheet from the FTO glass substrate. As described in the previous section, the gel sheet was fabricated onto the micro-electrode (Figure 5.3AII). Then, 1.1% $CaCl_2$ solution was dropped onto the gel sheet to harden the gel structure (Figure 5.3AIII). After 15 min, the $CaCl_2$ solution was removed and the FTO glass with the gel sheet was immersed in the culture medium for further incubation. After 24 h, the gel sheet can be easily detached from the FTO glass by shaking (Figure 5.3AIIII). Without the 24-h incubation, it is difficult to detach the gel sheet without any defect either by shaking or pipetting. The fabricated gel sheet will strongly adhere to the FTO glass after $CaCl_2$ treatment due to surface tension.

In fact, we have tried several methods to detach the fabricated gel sheets, including:

1) As we described above, treating the fabricated gel sheet with $CaCl_2$ and culturing within DMEM for 24 h. Then, the gel sheet can be detached simply and easily by shaking the dish. This is the recommended method.

2) Detaching the gel sheet soon after electrodeposition without $CaCl_2$ treatment. The gel sheet can be detached simply by shaking. However, the detached gel sheet will curl itself automatically with or without the later $CaCl_2$ treatment.

3) Treating the fabricated gel sheet with $CaCl_2$ and starting the detachment immediately. The gel sheet can be detached by gently pipetting. The video of this detachment process can be found in the supplementary material. This method requires

more than 2 min to detach one gel sheet. In addition, pipetting may bring damage to the gel sheet, which leads to a structure defect.

4) Treating the fabricated gel sheet with $CaCl_2$ and then immersing the sheets into cell viability test solution for 30 min. The gel sheet can be easily detached by shaking. A possible reason is that the Calcein-AM and PI are capable of weakening the Calcium-alginate chain. However, the PI may have a poisonous effect on cells.

Another possible solution to the detachment issue is to treat the FTO glass with oxygen plasma to make the surface hydrophilic. However, after O_2 plasma treatment, we found that the dropped deposition solution spread all over the FTO surface instead of remaining within the micro-electrode area.

The fabricated gel sheet before and after detachment is shown in Figure 5.3B and Figure 5.3C, respectively. Fluorescence beads were utilized to replace the liver cell to demonstrate the fabricated hepatic lobule patterns. To eliminate the effect of fluorescence beads on the results of electrodeposition in relation to the measurements and errors, carboxylate microspheres with small diameter (0.5 μm) were prepared to replace cells. According to our experimental data, we found that the fluorescence beads have no effect on the Ca-alginate electrodeposition. The hepatic lobule pattern with a 1.5 mm diameter was imaged using fluorescence microscopy before and after detachment (Fig 5.3BII and 5.3CII respectively). The results corresponding to the 1.5 mm diameter were measured to be 1567 ± 133 μm in diameter ($n > 10$). The hepatic lobule pattern with 2 mm diameter was imaged using fluorescence microscopy before and after the detachment (Fig. 5.3BIII and Fig. 5.3CIII respectively). The results corresponding to the 2 mm diameter were measured to be 2028 ± 61 μm in diameter ($n > 4$). The shape and size of the fabricated hepatic lobule pattern were as same as the initial electrode design as shown in Fig. 5.3A. Therefore, the proposed method has the advantage of allowing fabrication of the flat Ca-alginate gel sheet with a precise predesigned micro-pattern and flat surface. Compared with the common alginate gel containing cell module, e.g., alginate droplet [147], alginate fiber [150] and Ca-alginate 3D printing system [155], the current study proposes an alternative way to fabricate 2D alginate gel sheet for 3D complex tissue constructs in the tissue engineering field.

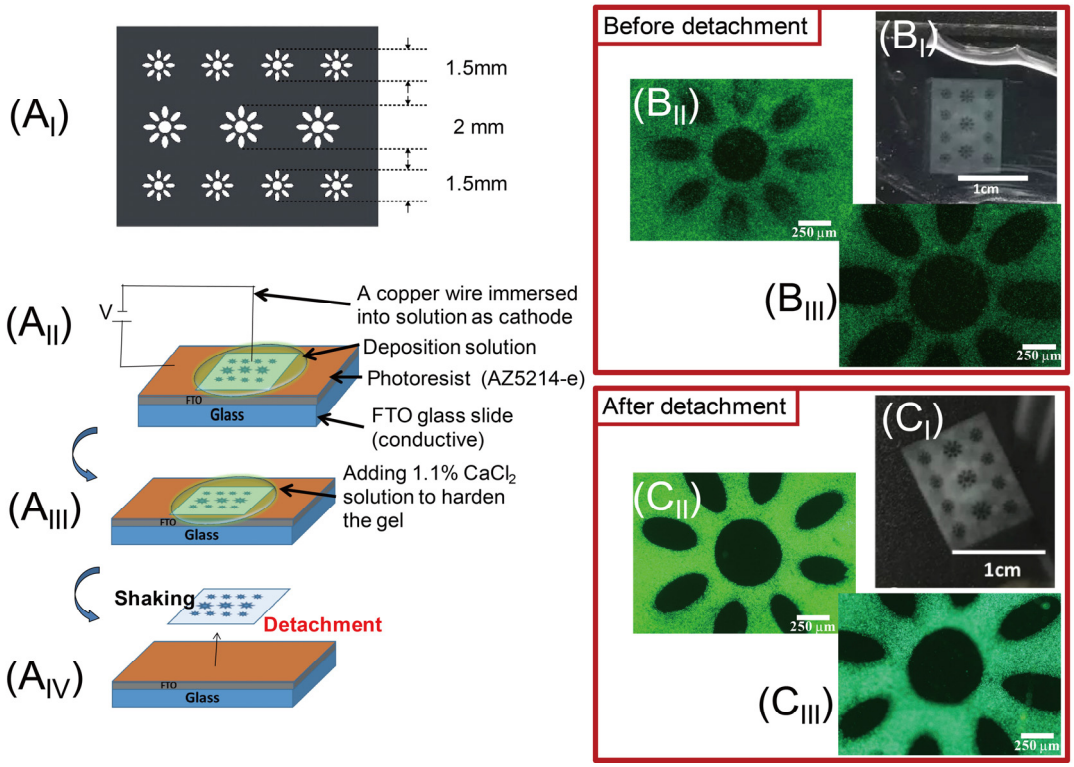

Figure 5.3 (A) The principle of electrodeposition. (B) The experimental setup before electrodeposition; A DC power supply was utilized to trigger the electrodeposition process by attaching the anode to the FTO glass and immersing the cathode into the deposition solution (Red wire). (C) The Ca-alginate gel sheet was deposited onto the micro-electrode area corresponding to the design. (D) The effect of the applied voltage on the stability of the gel sheet structure. A lower voltage leads to an unstable gel sheet generation due to the insufficient cross-link of Ca-alginate chain (Left image); A higher voltage leads to a thick gel sheet generation without the hepatic lobule pattern due to the diffusion of Ca^{2+} ions (Right image).

5.3 Evaluation of the fabricated Ca-alginate gel sheets

5.3.1 Viability assay for RLC-18 cells within alginate sheets

In order to confirm whether the presented method is suitable for use in biological applications, cell viability of the fabricated alginate sheet was checked soon after electrodeposition and on day 4 of the culture period. The fabricated structures were washed once with HEPES buffer solution and then immersed into the cell viability test solution for 30 min in an incubator. Then, the structures were washed with HEPES buffer solution again. A fluorescence microscope was used to observe the samples. Cell

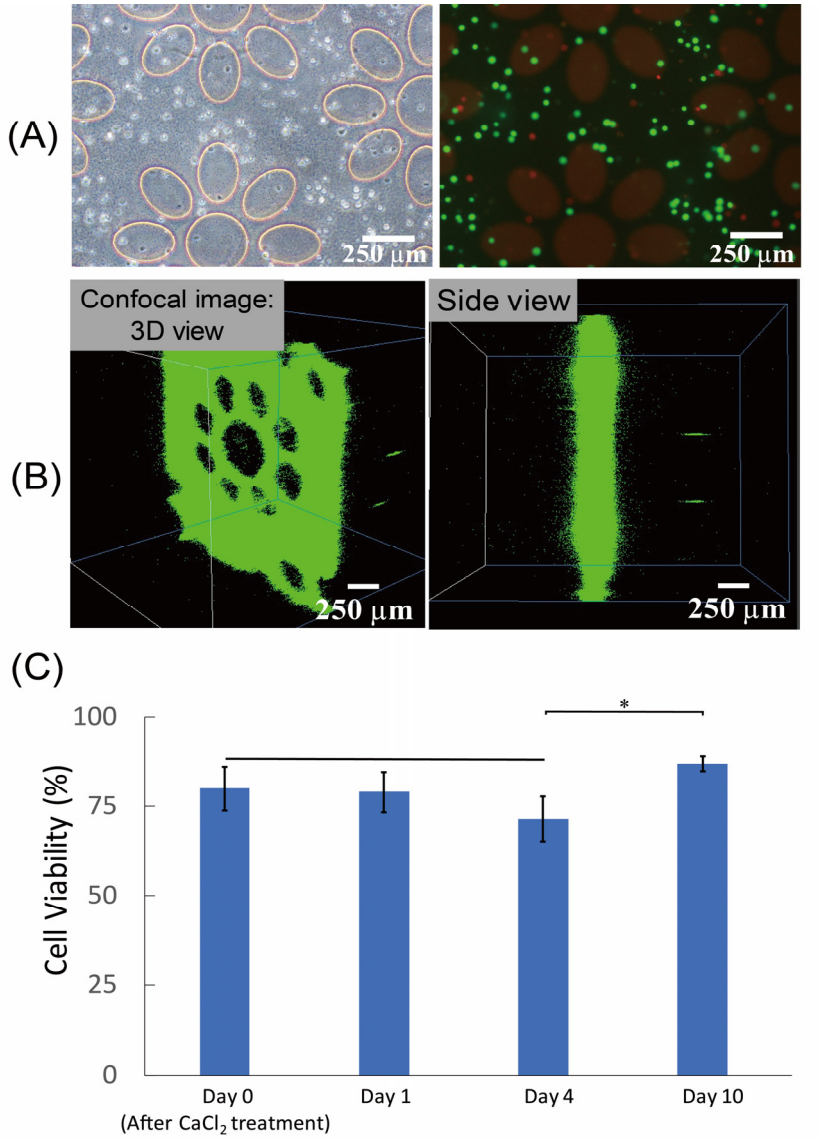

Figure 5.4 (A) Cell viability soon after electrodeposition on FTO glass was ascertained using light and fluorescence microscopy. Viability was measured to be 80 % by counting the number of live and dead cells. (B) The confocal images show the 3D view of the gel sheet. The height was approximately 302 ± 22 μm (N>3). (note that the patterns used here are old versions) (C) Cell viability was checked after Ca^{2+} treatment (time 0 of the culture), Day 1, Day 4 and Day 10. There is no significant change in cell viability during Day 0, Day 1 and Day 4. Cell viability of Day 10 was significantly upregulated compared with the one of Day 4.

viability was measured by calculating the viable and dead cells in each frame.

Figure 5.4A shows the optical and fluorescence microscopy images of cell viability soon after the electrodeposition process. RLC-18 cells were entrapped within the Ca-alginate hydrogel and assayed using the live/dead kit. By calculating the number of live and dead cells (green and red respectively), the cell viability was measured to be ~80%.

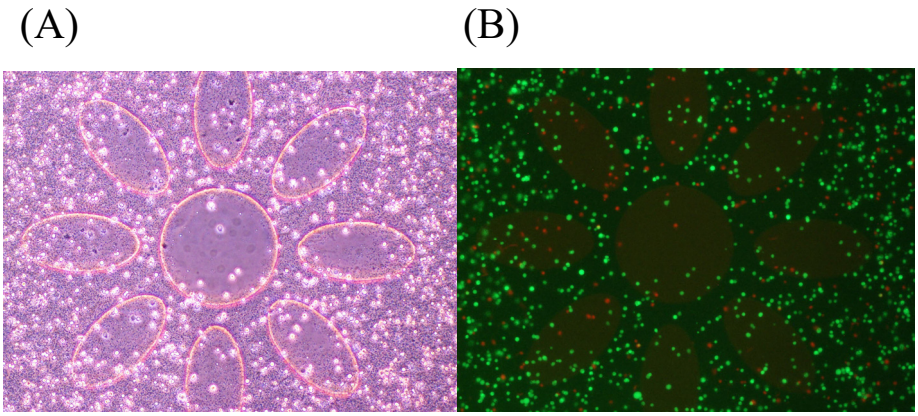

Figure 5.5 (a) Optical image of the hepatic lobule pattern (1.5 mm diameter) after $CaCl_2$ treatment. (b) Cell viability was checked under fluorescence mode using Calcein-AM and PI kit soon after the $CaCl_2$ treatment. (AZ photoresist material also showed red color under 561 nm wavelength UV light)

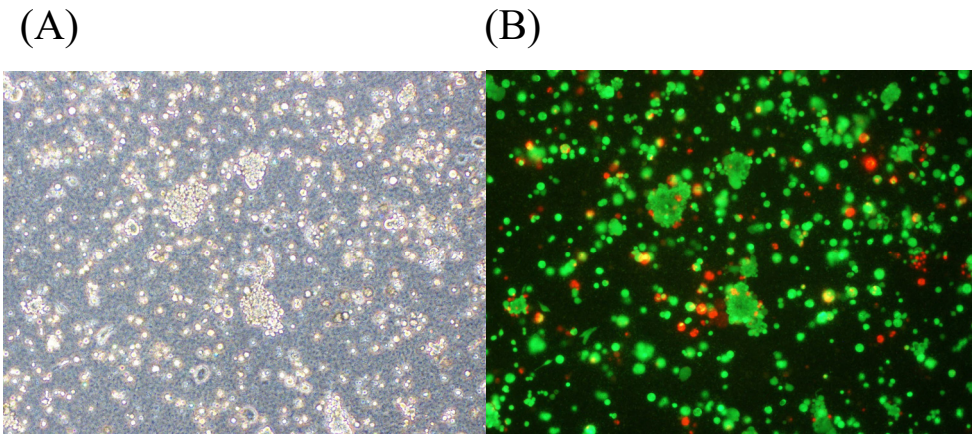

Figure 5.6 (a) Optical image of the RlC-18 cell morphology within Ca-alginate sheet cultured for 10-days. (b) Cell viability was checked under fluorescence mode using Calcein-AM and PI kit.

Figure 5.4B shows the 3D image of the fabricated alginate sheet under 3D laser confocal microscope. The RLC-18 cells were replaced by fluorescent beads for laser scanning. The thickness of the alginate sheet was approximately 302 ± 22 μm (N>3).

Figure 5.4C shows the cell viability after Ca^{2+} treatment (time 0 of the culture), Day 1, Day 4 and Day 10. There is no significant change in cell viability during Day 0, Day 1 and Day 4. Cell viability of Day 10 was significantly upregulated compared with the one of Day 4. The possible reason is that the cells within alginate hydrogel kept proliferating and started to form cell aggregates during the culture period. On the other hand, most of cells were maintained to be alive thanks to the bio-combability of the alginate hydrogel. Optical and fluorescence images of the RlC-18 cell morphology within Ca-alginate sheet after $CaCl_2$ treatment and cultured for 10-days were shown in Figure 5.5 and Figure 5.6 respectively.

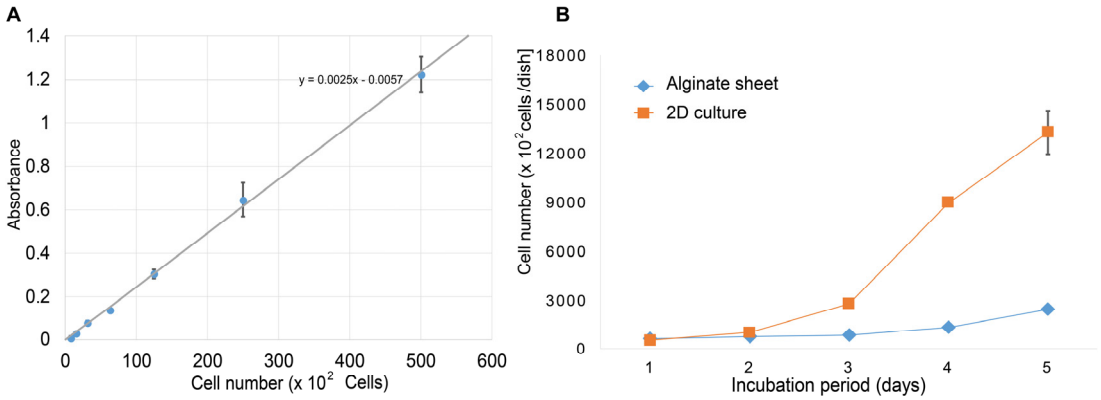

Figure 5.7 (A) The calibration curve of a linear-fitting model [f(x) = (p1 × x) – 0.0057; p1 = 0.0025] shows the relationship between the RLC-18 cell number and absorbance (OD) using the CCK8 assay. (B) Change in the cell number of the alginate cell sheet and 2D culture group during the incubation period (note that one dish only contained one alginate sheet).

5.3.2 Cell number counting

Cell Counting Kit-8 (CCK8) was utilized to measure the cell number of fabricated alginate sheets and a 2D culture control group. CCK8 is sensitive in the detection of viable cells similar to other tetrazolium salts such as MTT and MTS.

We also have constructed the calibration curve based on the relationship between the known cell number and absorbance value. The procedure for cell counting involved: 1) Incubation of individual sheet or diluted cell suspension of 2D culture (100 µl/well) in a 96-well plate. 2) Adding 10 µl of the CCK8 solution to each well of the plate. 3) Incubating the plate for 3 h in the incubator. 4) Immediately measuring absorbance at 450 nm using a microplate reader (Infinite F50 plate readers, TECAN) to determine the cell number of each microtissue.

Figure 5.7AFigure 5.9 shows the calibration curve of a linear-fitting model generated by the known cell number. Figure 5.7B shows the cell number of alginate sheet and 2D culture groups during the incubation period (day 1, 2, 3, 4 and 5).

RLC-18 cells within the alginate sheets had an initial cell number of ~6×10^4 cells and finally reached ~25×10^4 cells on day 5, a four-fold increase. On the other hand, the RLC-18 2D culture group increased from an initial ~5×10^4 cells to ~133×10^4 cells on day 5 – a 25-fold increase.

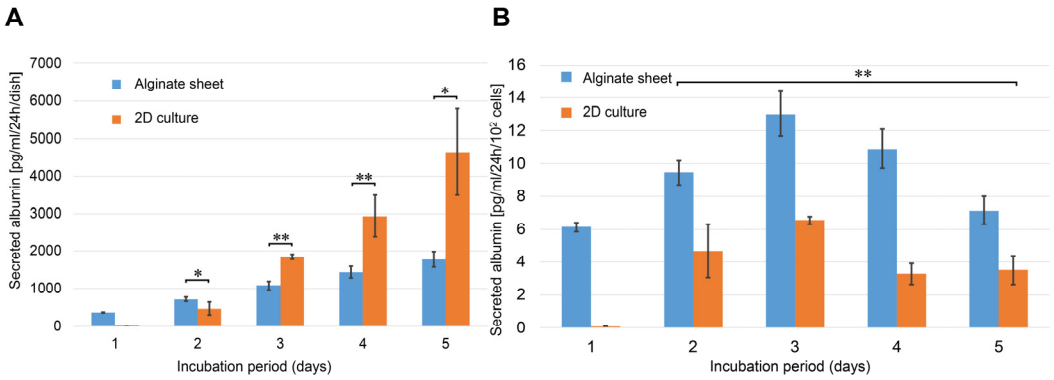

Figure 5.8 Albumin secretion per dish (A) and per 100 cells (B) of the alginate sheet and 2D culture. Data represent the mean ± standard derivation of at least three experiments from four independent cell preparations. *p < 0.05; **p < 0.01 (note that one dish only contained one alginate sheet).

From the results, we believe the cells entered the logarithmic phase from day 3, resulting in an increase in cell proliferation. However, on day 3, cell proliferation rate within the alginate sheets is still slow even after entering the logarithmic phase. Other researchers also found this phenomenon, indicating the lack of adherence molecules inside the hydrogel as a major reason [92]. Recently, this issue was countered by incorporation of RGD peptides [156] and microcapsule technique to promote cell proliferation [126].

5.3.3 Albumin secretion assay

A rat albumin ELISA quantitation kit was used to measure albumin levels during the culture period (at 1, 2, 3, 4 and 5 days). Before the assay, the fabricated alginate sheets were washed with PBS and fresh medium was added; after 24 h, this medium was withdrawn and aliquots were temporarily stored at -20 °C. The levels of albumin measured at each time point were normalized to each dish or the cell number.

The purposes of measuring the albumin secretion here include the fact that albumin is considered an important feature of well-differentiated hepatocytes, and that cells cultured within alginate sheets may have an advantage over conventional 2D culture in terms of bio-functionality.

Figure 5.8A shows the albumin secretion per dish of the alginate sheets and 2D culture. Albumin secretion showed an increasing trend during 5-days culture because the cell number is increasing. Initially, albumin secretion from alginate sheets was almost the same as that seen in 2D culture, but from day 3, the albumin secretion of the latter was significantly higher than that of the alginate sheets, and was 2.6 times higher on day 5 (p = 0.01616, n = 4). A possible explanation of this phenomenon is that cell proliferation in 2D culture was higher than that of the Ca-alginate, as shown in Figure 5.7B.

Figure 5.8B shows the albumin secretion per 100 cells of the RLC-18 alginate sheets and 2D culture. The cells within the alginate gel showed a significantly higher albumin activity than cells cultured in 2D shapes and reached a maximum value at day 3. This result indicates that the cells growing in 3D culture dramatically increase their activity and regain biofunctionality. Usually, peak albumin secretion coincides with cell confluence, which is also characterized by decreased cell proliferation. The peak albumin secretion in Figure 5.8B also suggests that the cells entered the logarithmic phase of proliferation on day 3. During the culture periods, the hepatocytes showed appreciable levels of albumin secretion ~6-12 pg/10^2 cells compared with that of 0-6 pg/10^2 cells under 2D culture. This result is consistent with a report that the 3D hepatocytes micro-organoids are critical for preserving hepatocyte function and other three-dimensional systems [21, 130].

5.4 Assembly of 2-layered hepatic lobule-like tissue

The ability to generate 3D multilayered cellular hydrogel structures is critical to the engineering of spatially complex liver tissues. Thus, we performed a simple experiment to demonstrate that reliable handling and assembly techniques, including cell sheet detachment, transfer and stacking, were applied in our method. We used a modified method here based on W. Lee's work [121]. Briefly, the detached cell sheets were collected using a modified pipette in a randomly folded configuration. The folded cell sheet spontaneously unfolded when released into the PDMS mold. The transferred cell sheets sank to the bottom of the PDMS mold when aspirating the surrounding medium. The transfer and stacking steps were repeated to assemble multi-layered hepatic lobule tissue. The dimension of the PDMS mold was designed to fit the size of the fabricated cell sheet to maximize the alignment resolution.

Figure 5.9 shows the results of cell sheets embedded with hepatic cells before assembly. On day 1, the deposited alginate gel structures were imaged and incubated. On day 3, before detachment, the cells started to adhere onto the bare area of the FTO glass surface. After detachment, hepatic lobule patterns were preserved without any defect while embedded with RLC-18 liver cells. Here, we used a high initial cell density (10^7 cells/ml in deposition solution) to address the cell proliferation issue within the alginate gel. On day 4, we collected the cell sheet and further transferred them into the PDMS mold for assembly layer by layer. By day 6, the hepatic cells merged together to mimic the hepatic cord while the ellipsoidal holes could still be clearly identified.

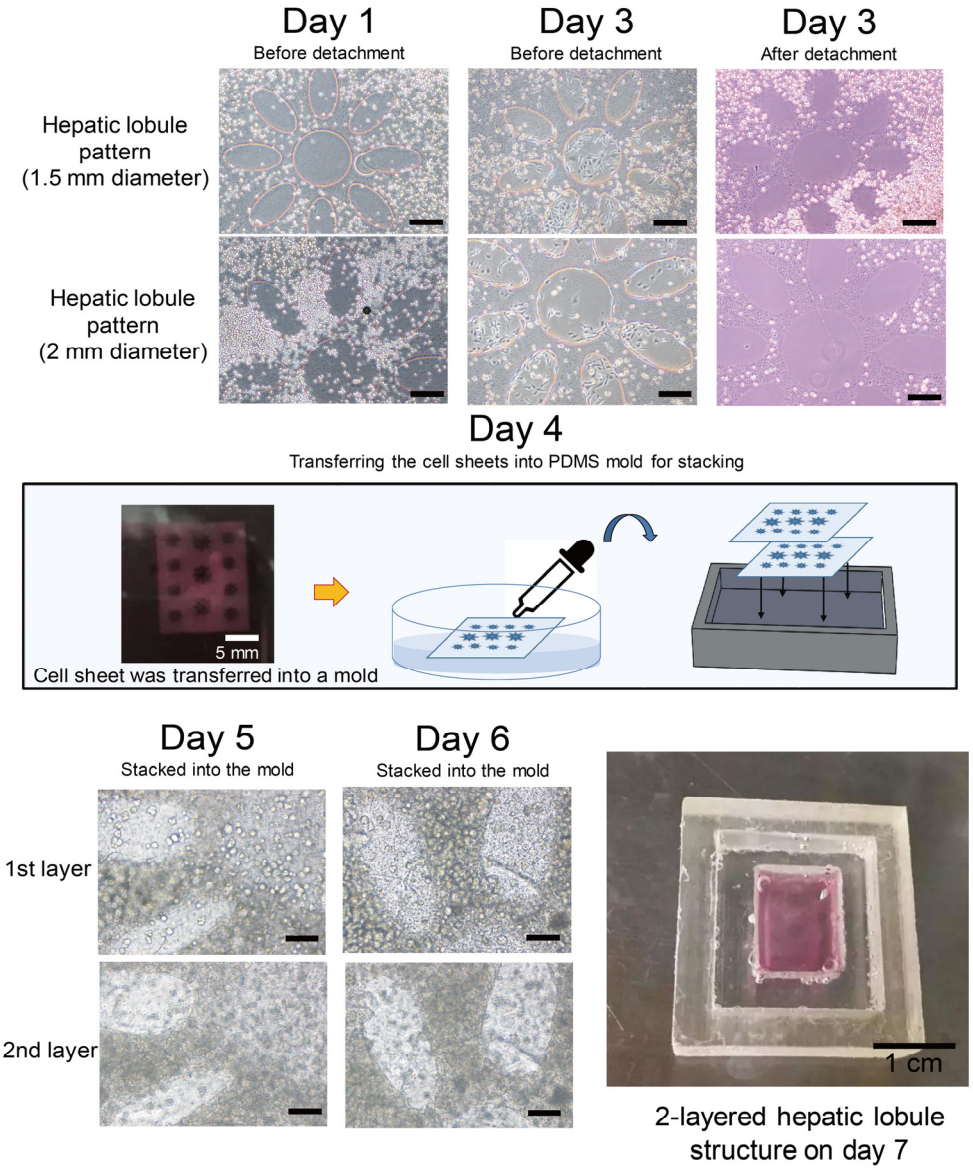

Figure 5.9 Hepatic lobule patterns of cell sheets on FTO glass was observed under a light microscope on day 1. Hepatic lobule patterns with 1.5 mm and 2 mm diameters were observed before and after detachment on day 3. The fluorescence microscopy image shows cell viability within the cell sheet on day 4; the detached cell sheets were stacked into the PDMS mold to form a 2-layered hepatic lobule model. Light microscopy images show the 1st and 2nd layer of assembled 2-layered hepatic lobule model on day 5 and day 6. Scale bars: 250 µm.

Figure 5.10 shows the additional experiment for confirmation of the hepatic lobule patterns alignment after the stacked assembly. Alginate sheets containing liver cells were assembled into a pre-defined PDMS mode layer by layer to form a 2-layered hepatic lobule structure as we mentioned above. The optical and fluorescence images of 1st layer and 2nd layer were obtained by only adjusting the Z position of the microscope respectively. The results show that the patterns were aligned during stacking to form an uninterrupted central vein. The alignment error is less than 200 µm.

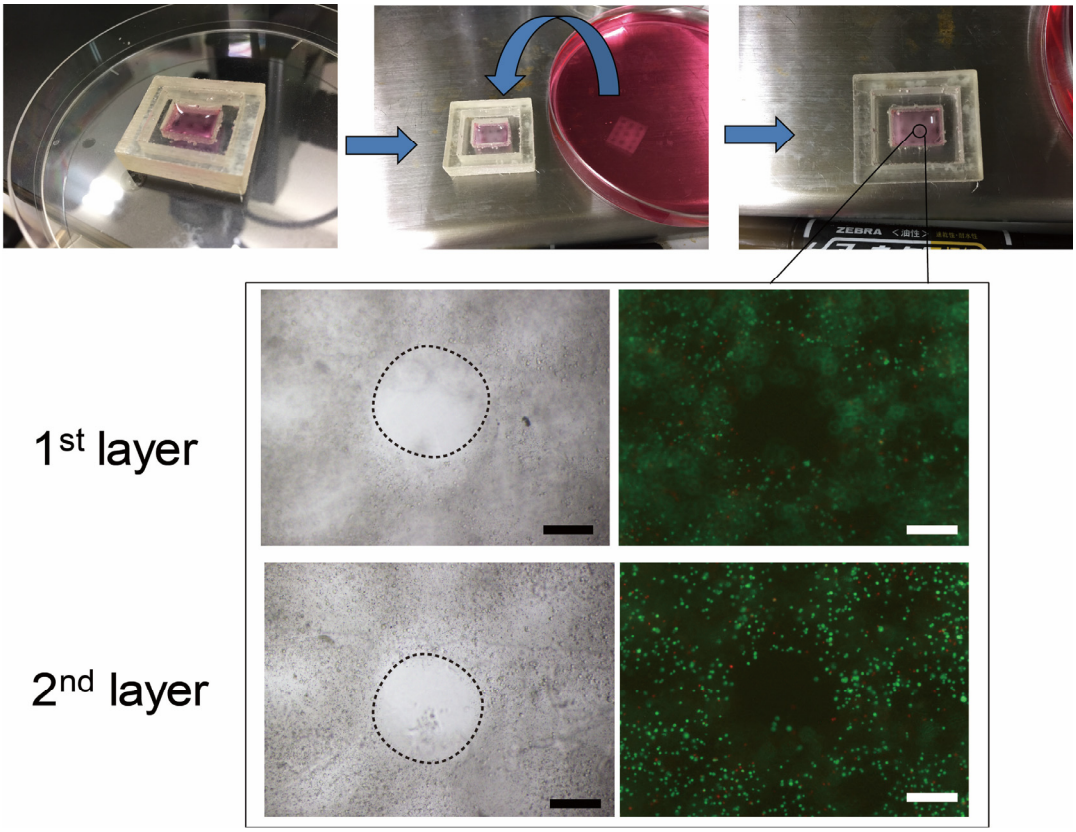

Figure 5.10 Alginate sheet containing liver cells was assembled into a pre-defined PDMS mode layer by layer to form a 2-layered hepatic lobule structure. The optical and fluorescence images of 1st layer and 2nd layer under microscope show that the patterns were aligned during stacking to form an uninterrupted central vein. The circular dash line indicates the inner edge of the alginate cell sheet. The alignment error is less than 200 μm.

Therefore, the proposed method provides a suitable and easy approach for bio-fabrication of multilayered hepatic lobule tissue in vitro.

The purpose of assembling the alginate sheets into a multi-layered structure was to demonstrate the feasibility of the method in fabricating a 3D cell model such as the hepatic lobule-like tissue by using alginate cell sheets as building blocks. When compared to similar work , our method differs from that used by Je-kyun Park's group [121] with respect to the improved electrodeposition method used for the fabrication of precise and shape-controlled micro-patterns; and from that used by Tomokazu Matue's group [93] with respect to the movability of the detached flat cell sheet for further 3D tissue formation. In addition, our method shows advantages of micro-level high resolution and simplicity compared with commonly utilized 3D alginate cell-containing fiber printing techniques for 3D tissue reconstruction [129, 155]. Although the current fabricated structure only mimics the morphology of the hepatic lobule tissue because it cannot be perfused. However, the holes in the sheets are useful in ensuring proper exchange of oxygen, nutrients, and catabolites between cells and culture medium; thus, we believe, the construct may offer considerable benefits in terms of survival and

functional performance. Therefore, the proposed technique has the potential for the design of three-dimensional lobule-like constructs by stacking varying deposited alginate sheets with complex micro-patterns and different cell lines for further applications in tissue engineering.

5.5 Summary

In summary, this paper presents a method for the fabrication of Ca-alginate cell sheets as building blocks for mimicking the morphology of hepatic lobule tissue. The alginate RLC-18 cell sheets with hepatic lobule micro-patterns were first deposited onto an electrode surface based on the electrodeposition method. After a one-day culture, the RLC-18 cells sheets were detached from 2D substrate and further assembled into a pre-designed PDMS mold. The fabricated cell sheets can be easily transferred by a 1 ml pipette and stacked layer by layer to form 3D hepatic lobule tissue. The developed method provides a new “bottom-up” paradigm to build 3D macroscopic liver tissue similar to that in vivo. The assembled hepatic lobule structure holds great promise to be improved further as in vitro models of liver organs and promote the novel applications of electrodeposition methods in tissue engineering.

Chapter 6
Conclusions and Future Works

3D cell structure assembly provides a promising way to build artificial tissues. Based on reviewing the current problems and needs for tissue engineering, especially the current construction methods and the microtechnologies, the motivation of assembly 3D cellular structures was pointed out. 3D cellular structures provide a similar environment for cells as in the real tissues, which enhance the cell proliferation and cell-cell interaction during building artificial tissues. Brief reviews on microtechnologies for tissue engineering are highlighted. The main issues for fabricating cell-laden alginate hydrogel structures are pointed out, and our methods were proposed.

We introduced a new approach to solve the issue of cell proliferation in the electrodeposition method. Our approach particularly aims at the fabrication of shape-controlled alginate-PLL microcapsules for 3D cell structures based on electrodeposition. In this study, we applied the electrodeposition method to alginate-PLL microcapsule fabrication by transforming the 2D gel membrane into 3D microcapsules. A Ca-alginate gel membrane was formed on the micro-patterned fluorine-doped tin oxide (FTO) electrode, thus forming a microfabricated conductive array. The electrodeposition-based gel-membrane formation process was applied to cell encapsulation into alginate-PLL microcapsules with liquid cores (sphere, cuboid, and rod), where cells were cultivated for 2 weeks.

we proposed a novel method to fabricate 3D multilayer hepatic lobule-like tissue based on electrodeposition and microcapsule techniques. The design of a micro-electrode device, which was previously used for preparing microtissue in sphere, cuboid, and rod shapes, was modified to obtain suitable dimensions for preparing hepatic lobule-shaped microtissue (HLSM). The micro-pattern electrode was fabricated by photolithography. The arrayed micro-pattern electrode is capable of simultaneous formation of alginate gel film *in situ* with a hepatic lobule shape based on the electrodeposition method. These cell-containing gel films were further detached from the substrate and treated with PLL and sodium citrate solution to form 3D microcapsules. Cells encapsulated within the microcapsules eventually fully occupied all spaces to achieve HLSM in two weeks.

A method to fabricate Ca-alginate cell sheets for hepatic lobule tissue constructs based on the electrodeposition method was proposed. The centimeter-scale cell sheets were produced with pre-designed hepatic lobule patterns. After a one-day culture, we successfully detached the sheets from the 2D electrode substrate without any structural defect and stacked them into 3D multilayer hepatic lobule tissue within a PDMS mold. Cell proliferation and functionality of the fabricated Ca-alginate cell sheet were quantitatively compared to that of regular 2D culture. This study aims to clarify that alginate cell sheets created by electrodeposition can potentially be utilized for 3D tissue constructs.

This is a very interesting and challenging research to apply the sodium citrate in our current approaches which can dissolve the inner alginate core through the alginate-PLL shell and create a liquid microenvironment in which cell can be promoted into real tissue-like structures. With these tissue-like unites with controllable shapes, the basic on-chip fabrication, assembly, manipulation and assembly approaches give us many possibilities on constructing complex 3D cell structures as shown in Figure 6.1 and we believe we can realize an artificial tissue in the future with the scientists' continuous work. It will help us to finally develop the functional artificial organs and to deal with the incurable organ lost disease better.

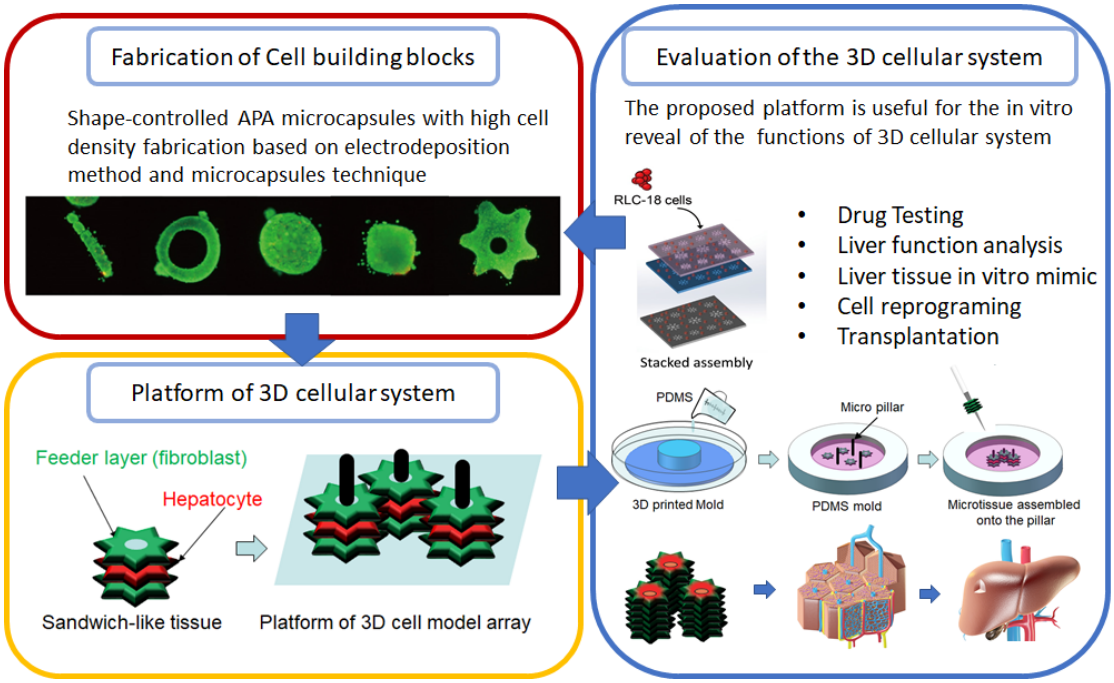

Figure 6.1 Future work and conclusion of the current work for the in vitro mimicking of the hepatic lobule tissue. The proposed platform is a useful tool for the evaluation of 3D cellular system and have potentials for the applications of drug test, liver function analysis, cell reprogramming and transplantation.

References

[1] G. A. P. Juárez, M. Spasojevic, M. M. Faas, and P. de Vos, "Immunological and technical considerations in application of alginate-based microencapsulation systems," *Frontiers in bioengineering and biotechnology,* vol. 2, 2014.

[2] H. Wang, J. Cui, Z. Zheng, Q. Shi, T. Sun, X. Liu*, et al.*, "Assembly of RGD-Modified Hydrogel Micromodules into Permeable Three-Dimensional Hollow Microtissues Mimicking in Vivo Tissue Structures," *ACS applied materials & interfaces,* vol. 9, pp. 41669-41679, 2017.

[3] R. Langer and J. P. Vacanti, "Tissue engineering," *Science,* vol. 260, pp. 920-926, May 14 1993.

[4] C. A. Vacanti, "The history of tissue engineering," *Journal of Cellular and Molecular Medicine,* vol. 10, pp. 569-576, Jul-Sep 2006.

[5] Y. Jun, E. Kang, S. Chae, and S.-H. Lee, "Microfluidic spinning of micro-and nano-scale fibers for tissue engineering," *Lab on a Chip,* vol. 14, pp. 2145-2160, 2014.

[6] D. Karamichos, C. B. Rich, A. E. K. Hutcheon, R. Ren, B. Saitta, V. Trinkaus-Randall*, et al.*, "Self-Assembled Matrix by Umbilical Cord Stem Cells," *Journal of Functional Biomaterials,* vol. 2, pp. 213-229, 2011.

[7] V. Mironov, T. Boland, T. Trusk, G. Forgacs, and R. R. Markwald, "Organ printing: computer-aided jet-based 3D tissue engineering," *Trends in Biotechnology,* vol. 21, pp. 157-161, Apr 2003.

[8] G. Mazzoleni, D. Di Lorenzo, and N. Steimberg, "Modelling tissues in 3D: the next future of pharmaco-toxicology and food research?," *Genes and Nutrition,* vol. 4, pp. 13-22, Mar 2009.

[9] Z. J. Gartner and C. R. Bertozzi, "Programmed assembly of 3-dimensional microtissues with defined cellular connectivity," *Proceedings of the National Academy of Sciences,* vol. 106, pp. 4606-4610, March 24 2009.

[10] D. Huh, G. A. Hamilton, and D. E. Ingber, "From 3D cell culture to organs-on-chips," *Trends in Cell Biology,* vol. 21, pp. 745-754, Dec 2011.

[11] U. A. Stock and J. P. Vacanti, "Tissue engineering: Current state and prospects," *Annual Review of Medicine,* vol. 52, pp. 443-451, 2001 2001.

[12] A. G. Mikos, S. W. Herring, P. Ochareon, J. Elisseeff, H. H. Lu, R. Kandel*, et al.*, "Engineering complex tissues," *Tissue Engineering,* vol. 12, pp. 3307-3339, Dec 2006.

[13] E. J. Suuronen, H. Sheardown, K. D. Newman, C. R. McLaughlin, and M. Griffith, "Building In Vitro Models of Organs," in *International Review of Cytology*. vol. Volume 244, W. J. Kwang, Ed., ed: Academic Press, 2005, pp. 137-173.

[14] W. J. Zhang, W. Liu, L. Cui, and Y. L. Cao, "Tissue engineering of blood vessel," *Journal of Cellular and Molecular Medicine,* vol. 11, pp. 945-957, Sep-Oct 2007.

[15] G. Karp, *Cell and Molecular Biology: Concepts and Experiments*: John Wiley & Sons, 2009.

[16] J. J. Pancrazio, F. Wang, and C. A. Kelley, "Enabling tools for tissue engineering," *Biosensors & Bioelectronics,* vol. 22, pp. 2803-2811, Jun 15 2007.

[17] L. E. Niklason, J. Gao, W. M. Abbott, K. K. Hirschi, S. Houser, R. Marini*, et al.*, "Functional arteries grown in vitro," *Science,* vol. 284, pp. 489-493, Apr 16 1999.

[18] M. S. Hahn, J. S. Miller, and J. L. West, "Three-dimensional biochemical and biomechanical patterning of hydrogels for guiding cell behavior," *Advanced Materials,* vol. 18, pp. 2679-2684, Oct 17 2006.

[19] Y. L. Cao, J. P. Vacanti, K. T. Paige, J. Upton, and C. A. Vacanti, "Transplantation of chondrocytes utilizing a polymer-cell construct to produce tissue-engineered cartilage in the shape of a human ear," *Plastic and Reconstructive Surgery,* vol. 100, pp. 297-302, Aug 1997.

[20] R. Tiruvannamalai-Annamalai, D. R. Armant, and H. W. Matthew, "A Glycosaminoglycan Based, Modular Tissue Scaffold System for Rapid Assembly of Perfusable, High Cell Density, Engineered Tissues," *PloS one,* vol. 9, p. e84287, 2014.

[21] Y. T. Matsunaga, Y. Morimoto, and S. Takeuchi, "Molding Cell Beads for Rapid Construction of Macroscopic 3D Tissue Architecture," *Advanced Materials,* vol. 23, pp. H90-H94, 2011.

[22] B. Duan, L. A. Hockaday, K. H. Kang, and J. T. Butcher, "3D

Bioprinting of heterogeneous aortic valve conduits with alginate/gelatin hydrogels," *Journal of Biomedical Materials Research Part A,* vol. 101A, pp. 1255-1264, May 2013.

[23] N. L'Heureux, S. Paquet, R. Labbe, L. Germain, and F. A. Auger, "A completely biological tissue-engineered human blood vessel," *Faseb Journal,* vol. 12, pp. 47-56, Jan 1998.

[24] J. Yeh, Y. Ling, J. M. Karp, J. Gantz, A. Chandawarkar, G. Eng*, et al.*, "Micromolding of shape-controlled, harvestable cell-laden hydrogels," *Biomaterials,* vol. 27, pp. 5391-5398, Nov 2006.

[25] T. Yue, M. Nakajima, H. Tajima, and T. Fukuda, "Fabrication of Microstructures Embedding Controllable Particles Inside Dielectrophoretic Microfluidic Devices," *International Journal of Advanced Robotic Systems,* vol. 10, 2013.

[26] T. Yue, M. Nakajima, M. Takeuchi, C. Hu, Q. Huang, and T. Fukuda, "On-chip self-assembly of cell embedded microstructures to vascular-like microtubes," *Lab on a Chip,* vol. 14, pp. 1151-1161, 2014.

[27] C. Colosi, M. Costantini, R. Latini, S. Ciccarelli, A. Stampella, A. Barbetta*, et al.*, "Rapid prototyping of chitosan-coated alginate scaffolds through the use of a 3D fiber deposition technique," *Journal of Materials Chemistry B,* vol. 2, pp. 6779-6791, 2014.

[28] N. L'Heureux, N. Dusserre, G. Konig, B. Victor, P. Keire, T. N. Wight*, et al.*, "Human tissue-engineered blood vessels for adult arterial revascularization," *Nature medicine,* vol. 12, pp. 361-365, 2006.

[29] R. Landers, U. Hubner, R. Schmelzeisen, and R. Mulhaupt, "Rapid prototyping of scaffolds derived from thermoreversible hydrogels and tailored for applications in tissue engineering," *Biomaterials,* vol. 23, pp. 4437-4447, Dec 2002.

[30] A. Pfister, R. Landers, A. Laib, U. Hubner, R. Schmelzeisen, and R. Mulhaupt, "Biofunctional rapid prototyping for tissue-engineering applications: 3D bioplotting versus 3D printing," *Journal of Polymer Science Part a-Polymer Chemistry,* vol. 42, pp. 624-638, Feb 1 2004.

[31] W. Y. Yeong, C. K. Chua, K. F. Leong, and M. Chandrasekaran, "Rapid prototyping in tissue engineering: challenges and potential," *Trends in Biotechnology,* vol. 22, pp. 643-652, Dec 2004.

[32] V. Mironov, R. P. Visconti, V. Kasyanov, G. Forgacs, C. J. Drake, and R. R. Markwald, "Organ printing: tissue spheroids as building blocks," *Biomaterials,* vol. 30, pp. 2164-2174, 2009.

[33] M. Ochsner, M. R. Dusseiller, H. M. Grandin, S. Luna-Morris, M. Textor, V. Vogel*, et al.*, "Micro-well arrays for 3D shape control and high resolution analysis of single cells," *Lab on a Chip,* vol. 7, pp. 1074-1077, 2007.

[34] C. N. Salinas and K. S. Anseth, "Mesenchymal stem cells for craniofacial tissue regeneration: designing hydrogel delivery vehicles," *Journal of dental research,* vol. 88, pp. 681-692, 2009.

[35] A. Khademhosseini, L. Ferreira, J. Blumling III, J. Yeh, J. M. Karp, J. Fukuda*, et al.*, "Co-culture of human embryonic stem cells with murine embryonic fibroblasts on microwell-patterned substrates," *Biomaterials,* vol. 27, pp. 5968-5977, 2006.

[36] J. M. Jeffrey M. KarpKarp, J. Yeh, G. Eng, J. Fukuda, J. Blumling, K.-Y. Suh*, et al.*, "Controlling size, shape and homogeneity of embryoid bodies using poly (ethylene glycol) microwells," *Lab on a Chip,* vol. 7, pp. 786-794, 2007.

[37] B. Harink, S. Le Gac, R. Truckenmueller, C. van Blitterswijk, and P. Habibovic, "Regeneration-on-a-chip? The perspectives on use of microfluidics in regenerative medicine," *Lab on a Chip,* vol. 13, pp. 3512-3528, 2013.

[38] H. Tsutsui, E. Yu, S. Marquina, B. Valamehr, I. Wong, H. Wu*, et al.*, "Efficient Dielectrophoretic Patterning of Embryonic Stem Cells in Energy Landscapes Defined by Hydrogel Geometries," *Annals of Biomedical Engineering,* vol. 38, pp. 3777-3788, Dec 2010.

[39] J. D. Roh, R. Sawh-Martinez, M. P. Brennan, S. M. Jay, L. Devine, D. A. Rao*, et al.*, "Tissue-engineered vascular grafts transform into mature blood vessels via an inflammation-mediated process of vascular remodeling," *Proceedings of the National Academy of Sciences of the United States of America,* vol. 107, pp. 4669-4674, Mar 9 2010.

[40] J. T. Krawiec and D. A. Vorp, "Adult stem cell-based tissue engineered blood vessels: A review," *Biomaterials,* vol. 33, pp. 3388-3400, Apr 2012.

[41] A. v. Bomhard, J. Veit, C. Bermueller, N. Rotter, R. Staudenmaier, K. Storck*, et al.*, "Prefabrication of 3D Cartilage Contructs: Towards a Tissue Engineered Auricle – A Model Tested in Rabbits," *Plos One,* vol. 8, p. e71667, 2013.

[42] M. S. Sakar, D. Neal, T. Boudou, M. A. Borochin, Y. Li, R. Weiss*, et al.*, "Formation and optogenetic control of engineered 3D skeletal muscle bioactuators," *Lab on a Chip,* vol. 12, pp. 4976-4985, 2012.

[43] S. E. Chung, W. Park, S. Shin, S. A. Lee, and S. Kwon, "Guided and

fluidic self-assembly of microstructures using railed microfluidic channels," *Nature Materials,* vol. 7, pp. 581-587, Jul 2008.

[44] F. Xu, T. D. Finley, M. Turkaydin, Y. Sung, U. A. Gurkan, A. S. Yavuz*, et al.*, "The assembly of cell-encapsulating microscale hydrogels using acoustic waves," *Biomaterials,* vol. 32, pp. 7847-7855, Nov 2011.

[45] T. Billiet, M. Vandenhaute, J. Schelfhout, S. Van Vlierberghe, and P. Dubruel, "A review of trends and limitations in hydrogel-rapid prototyping for tissue engineering," *Biomaterials,* vol. 33, pp. 6020-6041, Sep 2012.

[46] T. Lu, Y. Li, and T. Chen, "Techniques for fabrication and construction of three-dimensional scaffolds for tissue engineering," *International Journal of Nanomedicine,* vol. 8, pp. 337-350, 2013.

[47] M. Yamato and T. Okano, "Cell sheet engineering," *Materials Today,* vol. 7, pp. 42-47, 2004.

[48] J. Yang, M. Yamato, C. Kohno, A. Nishimoto, H. Sekine, F. Fukai*, et al.*, "Cell sheet engineering: Recreating tissues without biodegradable scaffolds," *Biomaterials,* vol. 26, pp. 6415-6422, Nov 2005.

[49] K. Ohashi, T. Yokoyama, M. Yamato, H. Kuge, H. Kanehiro, M. Tsutsumi*, et al.*, "Engineering functional two- and three-dimensional liver systems in vivo using hepatic tissue sheets," *Nature Medicine,* vol. 13, pp. 880-885, Jul 2007.

[50] K. Jakab, C. Norotte, F. Marga, K. Murphy, G. Vunjak-Novakovic, and G. Forgacs, "Tissue engineering by self-assembly and bio-printing of living cells," *Biofabrication,* vol. 2, Jun 2010.

[51] T. Shimoto, K. Nakayama, S. Matsuda, and Y. Iwamoto, "Building of HD MACs Using Cell Processing Robot for Cartilage Regeneration," *Journal of Robotics and Mechatronics,* vol. 24, pp. 347-353, 2012.

[52] G. Forgacs and W. Sun, *Biofabrication: Micro-and Nano-fabrication, Printing, Patterning and Assemblies*: Access Online via Elsevier, 2013.

[53] T. Shimoto, N. Hidaka, H. Sasaki, K. Nakayama, S. Akieda, S. Matsuda*, et al.*, "Bio Rapid Prototyping Project: Development of Spheroid Formation System for Regenerative Medicine," in *Information Technology Convergence*. vol. 253, J. J. Park, L. Barolli, F. Xhafa, and H.-Y. Jeong, Eds., ed: Springer Netherlands, 2013, pp. 855-862.

[54] Y. Du, E. Lo, S. Ali, and A. Khademhosseini, "Directed assembly of cell-laden microgels for fabrication of 3D tissue constructs," *Proceedings of the National Academy of Sciences,* vol. 105, pp. 9522-9527, July 15 2008.

[55] K. Kuribayashi-Shigetomi, H. Onoe, and S. Takeuchi, "Cell Origami: Self-Folding of Three-Dimensional Cell-Laden Microstructures Driven by Cell Traction Force," *Plos One,* vol. 7, Dec 12 2012.

[56] M. Kato-Negishi, Y. Morimoto, H. Onoe, and S. Takeuchi, "Millimeter-Sized Neural Building Blocks for 3D Heterogeneous Neural Network Assembly," *Advanced Healthcare Materials,* vol. 2, pp. 1564-70, 2013-Dec 2013.

[57] B. G. Chung, L. F. Kang, and A. Khademhosseini, "Micro- and nanoscale technologies for tissue engineering and drug discovery applications," *Expert Opinion on Drug Discovery,* vol. 2, pp. 1653-1668, Dec 2007.

[58] C. Hockin, "On the Estimation of Aperture in the Microscope," *Journal of the Royal Microscopical Society,* vol. 4, pp. 337-347, 1884.

[59] L. J. Wilson and B. P. Wheeler, "Optical Microscopy in Forensic Science," *Encyclopedia of Analytical Chemistry,* 2009.

[60] H. Thielecke, Impidjati, H. Zimmermann, and G. R. Fuhr, "Gentle cell handling with an ultra-slow instrument: creep-manipulation of cells," *Microsystem Technologies,* vol. 11, pp. 1230-1241, 2005/10/01 2005.

[61] K. A. Giuliano and D. L. Taylor, "Measurement and manipulation of cytoskeletal dynamics in living cells," *Current Opinion in Cell Biology,* vol. 7, pp. 4-12, Feb 1995.

[62] O. D. Velev and K. H. Bhatt, "On-chip micromanipulation and assembly of colloidal particles by electric fields," *Soft Matter,* vol. 2, pp. 738-750, 2006 2006.

[63] Y.-H. Lin, Y.-W. Yang, Y.-D. Chen, S.-S. Wang, Y.-H. Chang, and M.-H. Wu, "The application of an optically switched dielectrophoretic (ODEP) force for the manipulation and assembly of cell-encapsulating alginate microbeads in a microfluidic perfusion cell culture system for bottom-up tissue engineering," *Lab on a Chip,* vol. 12, pp. 1164-1173, 2012.

[64] E. Lee, H. Yim, J. Heo, H. Kim, G. Jung, and N. Hwang, "Application of magnetic nanoparticle for controlled tissue assembly and tissue engineering," *Archives of Pharmacal Research,* pp. 1-9, 2013/12/06 2013.

[65] S. Fatikow, J. Seyfried, A. Buerkle, and F. Schmoeckel, "A flexible microrobot-based microassembly station," *Journal of Intelligent and Robotic Systems,* vol. 27, pp. 135-169, 2000.

[66] S. Tasoglu, E. Diller, S. Guven, M. Sitti, and U. Demirci, "Untethered micro-robotic coding of three-dimensional material composition," *Nature communications,* vol. 5, 2014.

[67] H. Wang, Q. Shi, T. Yue, M. Nakajima, M. Takeuchi, Q. Huang*, et al.*, "Micro-assembly of a Vascular-like Micro-channel with Railed Micro-robot Team-coordinated Manipulation," *International Journal Of Advanced Robotic Systems,* vol. 11, 2014.

[68] P. Zorlutuna, N. Annabi, G. Camci-Unal, M. Nikkhah, J. M. Cha, J. W. Nichol*, et al.*, "Microfabricated biomaterials for engineering 3D tissues," *Advanced Materials,* vol. 24, pp. 1782-1804, Apr 10 2012.

[69] D. B. Weibel, W. R. DiLuzio, and G. M. Whitesides, "Microfabrication meets microbiology," *Nature Reviews Microbiology,* vol. 5, pp. 209-218, 2007.

[70] A. Ashkin, "Acceleration and trapping of particles by radiation pressure," *Physical Review Letters,* vol. 24, pp. 156-159, 1970.

[71] A. Ashkin and J. Dziedzic, "Optical levitation by radiation pressure," *Applied Physics Letters,* vol. 19, pp. 283-285, 1971.

[72] S. M. Block, D. F. Blair, and H. C. Berg, "Compliance of bacterial flagella measured with optical tweezers," 1989.

[73] S. M. Block, L. S. B. Goldstein, and B. J. Schnapp, "Bead movement by single kinesin molecules studied with optical tweezers," 1990.

[74] M. D. Wang, H. Yin, R. Landick, J. Gelles, and S. M. Block, "Stretching DNA with optical tweezers," *Biophysical Journal,* vol. 72, pp. 1335-1346, 1997.

[75] T. Yue, M. Nakajima, M. Takeuchi, and T. Fukuda, "Improved Laser Manipulation for On-chip Fabricated Microstructures Based on Solution Replacement and Its Application in Single Cell Analysis," *Int J Adv Robot Syst,* vol. 11, p. 11, 2014.

[76] I. Doh and Y. H. Cho, "A continuous cell separation chip using hydrodynamic dielectrophoresis (DEP) process," *Sensors and Actuators a-Physical,* vol. 121, pp. 59-65, May 2005.

[77] C. Iliescu, G. L. Xu, F. C. Loe, P. L. Ong, and F. E. H. Tay, "A 3-D dielectrophoretic filter chip," *Electrophoresis,* vol. 28, pp. 1107-1114, Apr 2007.

[78] M. S. Jaeger, K. Uhlig, T. Schnelle, and T. Mueller, "Contact-free single-cell cultivation by negative dielectrophoresis," *Journal of Physics D-Applied Physics,* vol. 41, Sep 2008.

[79] S. Ahadian, S. Yamada, J. Ramón-Azcón, K. Ino, H. Shiku, A. Khademhosseini*, et al.*, "Rapid and high-throughput formation of 3D embryoid bodies in hydrogels using the dielectrophoresis technique," *Lab on a Chip,* vol.

14, pp. 3690-3694, 2014.

[80] M. Azhar, J. E. J. Schultz, I. Grupp, G. W. Dorn, P. Meneton, D. G. M. Molin*, et al.*, "Transforming growth factor beta in cardiovascular development and function," *Cytokine & Growth Factor Reviews,* vol. 14, pp. 391-407, Oct 2003.

[81] P. Y. Chiou, A. T. Ohta, and M. C. Wu, "Massively parallel manipulation of single cells and microparticles using optical images," *Nature,* vol. 436, pp. 370-372, Jul 21 2005.

[82] X. W. Shi, C. Y. Tsao, X. Yang, Y. Liu, P. Dykstra, G. W. Rubloff*, et al.*, "Electroaddressing of Cell Populations by Co‐Deposition with Calcium Alginate Hydrogels," *Advanced Functional Materials,* vol. 19, pp. 2074-2080, 2009.

[83] L.-Q. Wu, A. P. Gadre, H. Yi, M. J. Kastantin, G. W. Rubloff, W. E. Bentley*, et al.*, "Voltage-dependent assembly of the polysaccharide chitosan onto an electrode surface," *Langmuir,* vol. 18, pp. 8620-8625, 2002.

[84] Y. Cheng, X. Luo, G. F. Payne, and G. W. Rubloff, "Biofabrication: programmable assembly of polysaccharide hydrogels in microfluidics as biocompatible scaffolds," *J. Mater. Chem.,* vol. 22, pp. 7659-7666, 2012.

[85] A. Montembault, C. Viton, and A. Domard, "Rheometric study of the gelation of chitosan in aqueous solution without cross-linking agent," *Biomacromolecules,* vol. 6, pp. 653-662, 2005.

[86] Y. Cheng, X. Luo, J. Betz, G. F. Payne, W. E. Bentley, and G. W. Rubloff, "Mechanism of anodic electrodeposition of calcium alginate," *Soft Matter,* vol. 7, pp. 5677-5684, 2011.

[87] F. Lv, P. Zhu, C. Wang, and L. Zheng, "Preparation, characterization, and dyeing properties of calcium alginate fibers," *Journal of Applied Polymer Science,* vol. 126, pp. E383-E388, 2012.

[88] S. Segvich, H. C. Smith, L. N. Luong, and D. H. Kohn, "Uniform deposition of protein incorporated mineral layer on three-dimensional porous polymer scaffolds," *Journal of Biomedical Materials Research Part B-Applied Biomaterials,* vol. 84B, pp. 340-349, Feb 2008.

[89] S.-H. Huang, L.-S. Wei, H.-T. Chu, and Y.-L. Jiang, "Light-Addressed Electrodeposition of Enzyme-Entrapped Chitosan Membranes for Multiplexed Enzyme-Based Bioassays Using a Digital Micromirror Device," *Sensors,* vol. 13, pp. 10711-10724, 2013.

[90] Y. Cheng, C. Y. Tsao, H. C. Wu, X. Luo, J. L. Terrell, J. Betz*, et al.*, "Electroaddressing functionalized polysaccharides as model biofilms for

interrogating cell signaling," *Advanced Functional Materials,* vol. 22, pp. 519-528, 2012.

[91] H. Ota and N. Miki, "Microfluidic experimental platform for producing size-controlled three-dimensional spheroids," *Sensors and Actuators a-Physical,* vol. 169, pp. 266-273, Oct 2011.

[92] F. Ozawa, K. Ino, Y. Takahashi, H. Shiku, and T. Matsue, "Electrodeposition of alginate gels for construction of vascular-like structures," *Journal of bioscience and bioengineering,* vol. 115, pp. 459-461, 2013.

[93] K. Ino, T. Arai, J. Ramón-Azcón, Y. Takahashi, H. Shiku, and T. Matsue, "Alginate gel microwell arrays using electrodeposition for three-dimensional cell culture," *Lab on a Chip,* vol. 13, pp. 3128-3135, 2013.

[94] R. A. Byrne, F. J. Neumann, J. Mehilli, S. Pinieck, B. Wolff, K. Tiroch*, et al.*, "Paclitaxel-eluting balloons, paclitaxel-eluting stents, and balloon angioplasty in patients with restenosis after implantation of a drug-eluting stent (ISAR-DESIRE 3): a randomised, open-label trial," *Lancet,* vol. 381, pp. 461-467, Feb 9 2013.

[95] J. Jung, M. Nakajima, T. Masaru, Q. Huang, and T. Fukuda, "A microfluidic device with multi-valves system to enable several simultaneous exposure tests on Caenorhabditis elegans," *Journal of Micromechanics and Microengineering,* vol. 24, p. 035012, 2014.

[96] A. M. Sun, "[51] Microencapsulation of pancreatic islet cells: A bioartificial endocrine pancreas," *Methods in Enzymology,* vol. 137, pp. 575-580, 1988.

[97] M. Goosen, G. King, C. McKnight, and N. Marcotte, "Animal cell culture engineering using alginate polycation microcapsules of controlled membrane molecular weight cut-off," *Journal of membrane science,* vol. 41, pp. 323-343, 1989.

[98] Z. Liu, M. Takeuchi, M. Nakajima, Y. Hasegawa, Q. Huang, and T. Fukuda, "Shape-controlled high cell-density microcapsules by electrodeposition," *Acta biomaterialia,* vol. 37, pp. 93-100, 2016.

[99] S. Sugiura, T. Oda, Y. Aoyagi, M. Satake, N. Ohkohchi, and M. Nakajima, "Tubular gel fabrication and cell encapsulation in laminar flow stream formed by microfabricated nozzle array," *Lab Chip,* vol. 8, pp. 1255-1257, 2008.

[100] N. A. Raof, M. R. Padgen, A. R. Gracias, M. Bergkvist, and Y. Xie, "One-dimensional self-assembly of mouse embryonic stem cells using an array of hydrogel microstrands," *Biomaterials,* vol. 32, pp. 4498-4505, 2011.

[101] S. R. Winn, P. A. Tresco, B. Zielinski, L. A. Greene, C. B. Jaeger, and P. Aebischer, "Behavioral recovery following intrastriatal implantation of microencapsulated PC12 cells," *Experimental neurology,* vol. 113, pp. 322-329, 1991.

[102] M. s.-p. m. f. c. o. of, Y. cellsMorimoto, W.-h. Tan, Y. Tsuda, and S. Takeuchi, "Monodisperse semi-permeable microcapsules for continuous observation of cells," *Lab Chip,* vol. 9, pp. 2217-2223, 2009.

[103] R. Sass and W. Thiemann, "Hydrolysis of poly ‐ L ‐ lysine by pronase," *Biopolymers,* vol. 12, pp. 535-539, 1973.

[104] C. Zandonella, "Tissue engineering: The beat goes on," *Nature,* vol. 421, pp. 884-886, Feb 27 2003.

[105] E. S. Place, N. D. Evans, and M. M. Stevens, "Complexity in biomaterials for tissue engineering," *Nature materials,* vol. 8, pp. 457-470, 2009.

[106] S.-H. Huang, H.-J. Hsueh, and Y.-L. Jiang, "Light-addressable electrodeposition of cell-encapsulated alginate hydrogels for a cellular microarray using a digital micromirror device," *Biomicrofluidics,* vol. 5, p. 034109, 2011.

[107] Y. A. Du, M. Ghodousi, H. Qi, N. Haas, W. Q. Xiao, and A. Khademhosseini, "Sequential assembly of cell-laden hydrogel constructs to engineer vascular-like microchannels," *Biotechnology and Bioengineering,* vol. 108, pp. 1693-1703, Jul 2011.

[108] F. Lim and A. M. Sun, "Microencapsulated islets as bioartificial endocrine pancreas," *Science,* vol. 210, pp. 908-910, 1980.

[109] M. F. A. Goosen, G. M. O'Shea, and A. M. F. Sun, "Microencapsulation of living tissue and cells," ed: Google Patents, 1989.

[110] S. Sugiura, T. Oda, Y. Aoyagi, R. Matsuo, T. Enomoto, K. Matsumoto, *et al.*, "Microfabricated airflow nozzle for microencapsulation of living cells into 150 micrometer microcapsules," *Biomedical microdevices,* vol. 9, pp. 91-99, 2007.

[111] C.-T. Ho, R.-Z. Lin, R.-J. Chen, C.-K. Chin, S.-E. Gong, H.-Y. Chang, *et al.*, "Liver-cell patterning Lab Chip: mimicking the morphology of liver lobule tissue," *Lab on a Chip,* vol. 13, pp. 3578-3587, 2013.

[112] Z. Liu, M. Takeuchi, M. Nakajima, T. Fukuda, Y. Hasegawa, and Q. Huang, "Shape-controlled production of alginate-Poly-L-lysine (PLL) microcapsules for 3D cell structures fabrication based on electrodeposition method," *19th Int. Conf. on Miniaturized Systems for Chemistry and Life Sciences (MicroTAS 2015),* pp. 385-388, 2015.

[113] Y. Cheng, J. Terrell, X. Luo, J. Betz, H.-C. Wu, G. F. Payne*, et al.*, "Immobilization and culturing of mammalian cells with biocompatible electrodeposition of calcium alginate gel in microfluidic devices," in *Proceedings of the 15th International Conference on Miniaturized Systems for Chemistry and Life Sciences (MicroTAS 2011). Seattle, WA*, 2010, pp. 121-123.

[114] R. C. Fitzgerald, M. B. Omary, and G. Triadafilopoulos, "Acid modulation of HT29 cell growth and differentiation. An in vitro model for Barrett's esophagus," *Journal of cell science,* vol. 110, pp. 663-671, 1997.

[115] H. Mizumoto, M. Hayakami, K. Nakazawa, H. Ijima, and K. Funatsu, "Formation of cylindrical multicellular aggregate (cylindroid) and expression of liver specific functions of primary rat hepatocytes," *Cytotechnology,* vol. 31, pp. 69-75, 1999.

[116] J. F. Betz, Y. Cheng, C.-Y. Tsao, A. Zargar, H.-C. Wu, X. Luo*, et al.*, "Optically clear alginate hydrogels for spatially controlled cell entrapment and culture at microfluidic electrode surfaces," *Lab Chip,* vol. 13, pp. 1854-1858, 2013.

[117] L. G. Griffith and M. A. Swartz, "Capturing complex 3D tissue physiology in vitro," *Nature reviews Molecular cell biology,* vol. 7, pp. 211-224, 2006.

[118] F. Hirschhaeuser, H. Menne, C. Dittfeld, J. West, W. Mueller-Klieser, and L. A. Kunz-Schughart, "Multicellular tumor spheroids: an underestimated tool is catching up again," *Journal of biotechnology,* vol. 148, pp. 3-15, 2010.

[119] P. Agarwal, S. Zhao, P. Bielecki, W. Rao, J. K. Choi, Y. Zhao*, et al.*, "One-step microfluidic generation of pre-hatching embryo-like core–shell microcapsules for miniaturized 3D culture of pluripotent stem cells," *Lab on a Chip,* vol. 13, pp. 4525-4533, 2013.

[120] A. Y. Hsiao, T. Okitsu, H. Onoe, M. Kiyosawa, H. Teramae, S. Iwanaga*, et al.*, "Smooth muscle-like tissue constructs with circumferentially oriented cells formed by the cell fiber technology," *PloS one,* vol. 10, p. e0119010, 2015.

[121] W. mechanically stableLee, C. Y. Bae, S. Kwon, J. Son, J. Kim, Y. Jeong*, et al.*, "Cellular hydrogel biopaper for patterned 3D cell culture and modular tissue reconstruction," *Advanced healthcare materials,* vol. 1, pp. 635-639, 2012.

[122] G. King, A. Daugulis, P. Faulkner, and M. Goosen, "Alginate‐Polylysine Microcapsules of Controlled Membrane Molecular Weight Cutoff for Mammalian Cell Culture Engineering," *Biotechnology Progress,* vol. 3, pp. 231-240, 1987.

[123] P. de Vos, C. G. Hoogmoed, and H. J. Busscher, "Chemistry and biocompatibility of alginate ‐ PLL capsules for immunoprotection of mammalian cells," *Journal of biomedical materials research,* vol. 60, pp. 252-259, 2002.

[124] V. Bocharova, O. Zavalov, K. MacVittie, M. A. Arugula, N. V. Guz, M. E. Dokukin*, et al.*, "A biochemical logic approach to biomarker-activated drug release," *Journal of Materials Chemistry,* vol. 22, pp. 19709-19717, 2012.

[125] K. Liu, H.-J. Ding, J. Liu, Y. Chen, and X.-Z. Zhao, "Shape-controlled production of biodegradable calcium alginate gel microparticles using a novel microfluidic device," *Langmuir,* vol. 22, pp. 9453-9457, 2006.

[126] Z. Liu, M. Takeuchi, M. Nakajima, T. Fukuda, Y. Hasegawa, and Q. Huang, "Batch Fabrication of Microscale Gear-Like Tissue by Alginate-Poly-L-lysine (PLL) Microcapsules System," *IEEE Robotics and Automation Letters,* vol. 1, pp. 206-212, 2016.

[127] T. Schwarz and G. Levy, "Viscosity changes of sodium alginate solutions after freezing and thawing," *Journal of the American Pharmaceutical Association,* vol. 46, pp. 562-563, 1957.

[128] X. Liu, Q. Shi, H. Wang, T. Sun, N. Yu, Q. Huang*, et al.*, "Automated bubble-based assembly of cell-laden microgels into vascular-like microtubes," in *Intelligent Robots and Systems (IROS), 2015 IEEE/RSJ International Conference on*, 2015, pp. 798-803.

[129] T. Sun, Q. Huang, Q. Shi, H. Wang, X. Liu, M. Seki*, et al.*, "Magnetic assembly of microfluidic spun alginate microfibers for fabricating three-dimensional cell-laden hydrogel constructs," *Microfluidics and Nanofluidics,* vol. 19, pp. 1169-1180, 2015.

[130] M. Yamada, R. Utoh, K. Ohashi, K. Tatsumi, M. Yamato, T. Okano*, et al.*, "Controlled formation of heterotypic hepatic micro-organoids in anisotropic hydrogel microfibers for long-term preservation of liver-specific functions," *Biomaterials,* vol. 33, pp. 8304-8315, Nov 2012.

[131] Y. Chen, L. Ke, C. Tung, C. Lu, C. C. Hu, and C. H. Liu, "Three dimensional lobule-mimetic regeneration in vitro by PEGDA-based cell sheets," in *Solid-State Sensors, Actuators and Microsystems (TRANSDUCERS & EUROSENSORS XXVII), 2013 Transducers & Eurosensors XXVII: The 17th International Conference on*, 2013, pp. 637-640.

[132] K. Nakazawa, Y. Izumi, J. Fukuda, and T. Yasuda, "Hepatocyte spheroid culture on a polydimethylsiloxane chip having microcavities," *Journal of Biomaterials Science, Polymer Edition,* vol. 17, pp. 859-873, 2006.

[133] F. Evenou, M. Hamon, T. Fujii, S. Takeuchi, and Y. Sakai, "Gas‐permeable membranes and co‐culture with fibroblasts enable high‐density hepatocyte culture as multilayered liver tissues," *Biotechnology progress,* vol. 27, pp. 1146-1153, 2011.

[134] H. Yamazaki, S. Gotou, K. Ito, S. Kohashi, Y. Goto, Y. Yoshiura*, et al.*, "Micropatterned culture of HepG2 spheroids using microwell chip with honeycomb-patterned polymer film," *Journal of bioscience and bioengineering,* 2014.

[135] C. H. Cho, F. Berthiaume, A. W. Tilles, and M. L. Yarmush, "A new technique for primary hepatocyte expansion in vitro," *Biotechnology and bioengineering,* vol. 101, pp. 345-356, 2008.

[136] A. Stampella, A. Papi, G. Rizzitelli, M. Costantini, C. Colosi, A. Barbetta*, et al.*, "Synthesis and characterization of a novel poly (vinyl alcohol) 3D platform for the evaluation of hepatocytes' response to drug administration," *Journal of Materials Chemistry B,* vol. 1, pp. 3083-3098, 2013.

[137] A. Stampella, G. Rizzitelli, F. Donati, M. Mazzarino, X. de la Torre, F. Botrè*, et al.*, "Human hepatoma cell lines on gas foaming templated alginate scaffolds for in vitro drug-drug interaction and metabolism studies," *Toxicology in Vitro,* vol. 30, pp. 331-340, 2015.

[138] Y. Du, M. Ghodousi, H. Qi, N. Haas, W. Xiao, and A. Khademhosseini, "Sequential assembly of cell‐laden hydrogel constructs to engineer vascular‐like microchannels," *Biotechnology and bioengineering,* vol. 108, pp. 1693-1703, 2011.

[139] C. YunáBae, "User-friendly 3D bioassays with cell-containing hydrogel modules: narrowing the gap between microfluidic bioassays and clinical end-users' needs," *Lab on a Chip,* vol. 15, pp. 2379-2387, 2015.

[140] V. Chan, P. Zorlutuna, J. H. Jeong, H. Kong, and R. Bashir, "Three-dimensional photopatterning of hydrogels using stereolithography for long-term cell encapsulation," *Lab on a Chip,* vol. 10, pp. 2062-2070, 2010.

[141] X.-H. Ge, J.-P. Huang, J.-H. Xu, and G.-S. Luo, "Controlled stimulation-burst targeted release by smart decentered core–shell microcapsules in gravity and magnetic field," *Lab Chip,* vol. 14, pp. 4451-4454, 2014.

[142] M. Takeuchi, M. Nakajima, M. Kojima, and T. Fukuda, "Handling of micro objects using phase transition of thermoresponsive polymer," *Journal of Micro-Bio Robotics,* vol. 8, pp. 53-64, 2013.

[143] H. Wang, Q. Huang, Q. Shi, T. Yue, S. Chen, M. Nakajima*, et al.*, "Automated assembly of vascular-like microtube with repetitive single-step

contact manipulation," *Biomedical Engineering, IEEE Transactions on* vol. VOL. 62, NO. 11, 2015.

[144] K. Dubbin, Y. Hori, K. K. Lewis, and S. C. Heilshorn, "Dual‐Stage Crosslinking of a Gel‐Phase Bioink Improves Cell Viability and Homogeneity for 3D Bioprinting," *Advanced healthcare materials,* vol. 5, pp. 2488-2492, 2016.

[145] Z. Liu, M. Takeuchi, M. Nakajima, Y. Hasegawa, Q. Huang, and T. Fukuda, "Shape-controlled High Cell-density Microcapsules by Electrodeposition," *Acta Biomaterialia,* 2016.

[146] H. Onoe, T. Okitsu, A. Itou, M. Kato-Negishi, R. Gojo, D. Kiriya*, et al.*, "Metre-long cell-laden microfibres exhibit tissue morphologies and functions," *Nature Materials,* vol. 12, pp. 584-590, Jun 2013.

[147] H. Hirama, T. Kambe, K. Aketagawa, T. Ota, H. Moriguchi, and T. Torii, "Hyper alginate gel microbead formation by molecular diffusion at the hydrogel/droplet interface," *Langmuir,* vol. 29, pp. 519-524, 2013.

[148] S. Zhao, P. Agarwal, W. Rao, H. Huang, R. Zhang, Z. Liu*, et al.*, "Coaxial electrospray of liquid core–hydrogel shell microcapsules for encapsulation and miniaturized 3D culture of pluripotent stem cells," *Integrative Biology,* vol. 6, pp. 874-884, 2014.

[149] C. Kim, S. Chung, Y. E. Kim, K. S. Lee, S. H. Lee, K. W. Oh*, et al.*, "Generation of core-shell microcapsules with three-dimensional focusing device for efficient formation of cell spheroid," *Lab on a Chip,* vol. 11, pp. 246-252, 2011.

[150] Y. Sequential assembly of cellZuo, X. He, Y. Yang, D. Wei, J. Sun, M. Zhong*, et al.*, "Microfluidic-based generation of functional microfibers for biomimetic complex tissue construction," *Acta biomaterialia,* vol. 38, pp. 153-162, 2016.

[151] F. Yang, C. G. Williams, D.-a. Wang, H. Lee, P. N. Manson, and J. Elisseeff, "The effect of incorporating RGD adhesive peptide in polyethylene glycol diacrylate hydrogel on osteogenesis of bone marrow stromal cells," *Biomaterials,* vol. 26, pp. 5991-5998, 2005.

[152] S.-Y. Teh, R. Lin, L.-H. Hung, and A. P. Lee, "Droplet microfluidics," *Lab on a Chip,* vol. 8, pp. 198-220, 2008.

[153] Y. Cheng, X. L. Luo, J. Betz, G. F. Payne, W. E. Bentley, and G. W. Rubloff, "Mechanism of anodic electrodeposition of calcium alginate," *Soft Matter,* vol. 7, pp. 5677-5684, 2011.

[154] Z. Liu, M. Takeuchi, M. Nakajima, C. Hu, Y. Hasegawa, Q. Huang,

et al., "Three-dimensional Hepatic Lobule-like Tissue Constructs Using Cell-microcapsule Technology," *Acta Biomaterialia,* 2016.

[155] W. Shang, Y. Liu, W. Wan, C. Hu, Z. Liu, C. T. Wong*, et al.*, "Hybrid 3D printing and electrodeposition approach for controllable 3D alginate hydrogel formation," *Biofabrication,* 2017.

[156] S. J. Bidarra, C. C. Barrias, M. A. Barbosa, R. Soares, and P. L. Granja, "Immobilization of human mesenchymal stem cells within RGD-grafted alginate microspheres and assessment of their angiogenic potential," *Biomacromolecules,* vol. 11, pp. 1956-1964, 2010.

Publications

Journal Articles (First author):

1. **Z. Liu**, M. Takeuchi, M. Nakajima, C. Hu, Y. Hasegawa, Q. Huang, T. Fukuda, Three-dimensional Hepatic Lobule-like Tissue Constructs Using Cell-microcapsule Technology, Acta Biomaterialia, Vol. 50, pp. 178-187, 2017.

2. **Z. Liu**, M. Takeuchi, M. Nakajima, T. Fukuda, Y. Hasegawa and Q. Huang. "Batch Fabrication of Microscale Gear-Like Tissue by Alginate-Poly-L-lysine (PLL) Microcapsules System.", IEEE Robotics and Automation Letters, (IEEE), 2377-3766, vol. 01, pp 206 – 212, 2016.

3. **Z. Liu**, M. Takeuchi, M. Nakajima, Y. Hasegawa, Q. Huang, and T. Fukuda, "Shape-controlled high cell-density microcapsules by electrodeposition," Acta Biomaterialia, vol. 37, pp. 93-100, 2016.

4. **Z. Liu**, M. Lu, M. Takeuchi, T. Yue, Y. Hasegawa, Q. Huang and T. Fukuda, "In vitro mimicking the morphology of hepatic lobule tissue based on Ca-alginate cell sheets," Biomedical Materials, https://doi.org/10.1088/1748-605X/aaa4c4, 2017.

Conference Articles:

1. **Zeyang Liu**, Minmin Lu, Masaru Takeuchi, Tao Yue, Yasuhisa Hasegawa, Qiang Huang and Toshio Fukuda. "In Vitro Mimic of Hepatic Lobule Tissue Using Ca-alginate Cell-containing Hydrogel Modules", 2017 Int. Symp. on Micro-NanoMechatronics and Human Science (MHS 2017).

2. **Zeyang Liu**, Masaru Takeuchi, Yasuhisa Hasegawa, Toshio Fukuda and Qiang Huang. "Bio-fabrication of Ca-alginate cell sheets with the electrodeposition method for hepatic lobule tissue reconstructs", 21th Int. Conf. on Miniaturized Systems for Chemistry and Life Sciences (MicroTAS 2017), pp. 1017-1018.

3. **Zeyang Liu**, Minmin Lu, Masahiro Nakajima, Masaru Takeuchi, Toshio Fukuda, Yasuhisa Hasegawa and Qiang Huang. "Fabrication of Multilayered Hepatic Lobule Tissues Using Ca-Alginate Hydrogel Platforms", The 17th IEEE International Conference on Nanotechnology (IEEE NANO 2017), pp. 561-564.

4. **Zeyang Liu**, Masaru Takeuchi, Masahiro Nakajima, Toshio Fukuda, Yasuhisa Hasegawa and Qiang Huang. “microencapsulation of culture of hepatic lobule model using shape-controlled alginate-poly-l-lysine (PLL) microcapsules with the electrodeposition method”, 20th Int. Conf. on Miniaturized Systems for Chemistry and Life Sciences (MicroTAS 2016).

5. **Zeyang Liu**, Masaru Takeuchi, Masahiro Nakajima. Toshio Fukuda, Yasuhisa Hasegawa and Qiang Huang. “Assembly of Hepatic Lobule-like Microtissue with Repetitive Single-Step Contact Manipulation”, 2016 Int. Symp. on Micro-NanoMechatronics and Human Science (MHS 2016).

6. **Zeyang Liu**, Masaru Takeuchi, Masahiro Nakajima, Toshio Fukuda, Yasuhisa Hasegawa and Qiang Huang. (2015, September). “Electrodeposition of cell-laden alginate-PLL hydrogel structures for spatially selective entrapment”. In Intelligent Robots and Systems (IROS), 2015 IEEE/RSJ International Conference on (pp. 1379-1384). IEEE.

7. **Zeyang Liu**, Masaru Takeuchi, Masahiro Nakajima, Toshio Fukuda, Yasuhisa Hasegawa and Qiang Huang. “Shape-controlled production of alginate-Poly-L-lysine (PLL) microcapsules for 3D cell structures fabrication based on electrodeposition method”, 19th Int. Conf. on Miniaturized Systems for Chemistry and Life Sciences (MicroTAS 2015), 1556-5904, pp 385-388, 2015.

8. **Zeyang Liu**, Masaru Takeuchi, Masahiro Nakajima, Toshio Fukuda, Yasuhisa Hasegawa and Qiang Huang. “Shape-controlled production of alginate hydrogel-poly-L-lysine microcapsules based on electrodeposition method”. 41st Annual Conf. of the IEEE Industrial Electronics Society (IECON 2015), pp 244-249, 2015.

9. **Zeyang Liu**, Masaru Takeuchi, Masahiro Nakajima. Toshio Fukuda, Yasuhisa Hasegawa and Qiang Huang. “Fabrication of Hepatic Lobule Model based on Electrodeposition”, 2015 Int. Symp. on Micro-NanoMechatronics and Human Science (MHS 2015), 181-182, 2015.

10. **Zeyang Liu**, Masaru Takeuchi, Masahiro Nakajima, Toshio Fukuda, Yasuhisa Hasegawa and Qiang Huang. “Electrodeposition of Alginate Hydrogel for Spatially Selective Entrapment of Biological Cells”, 2014 Int. Symp. on Micro-NanoMechatronics and Human Science (MHS 2014), 278-279, 2014.

11. **Zeyang Liu**, Kosuke Sekiyama, and Toshio Fukuda. “Architectural Design of an Autonomous Decentralized System for Controlling Heterogeneous Function Multi-robots”, 2013 Int. Symp. on Micro-NanoMechatronics and Human Science (MHS 2013), 42-47, 2013.

Supplementary

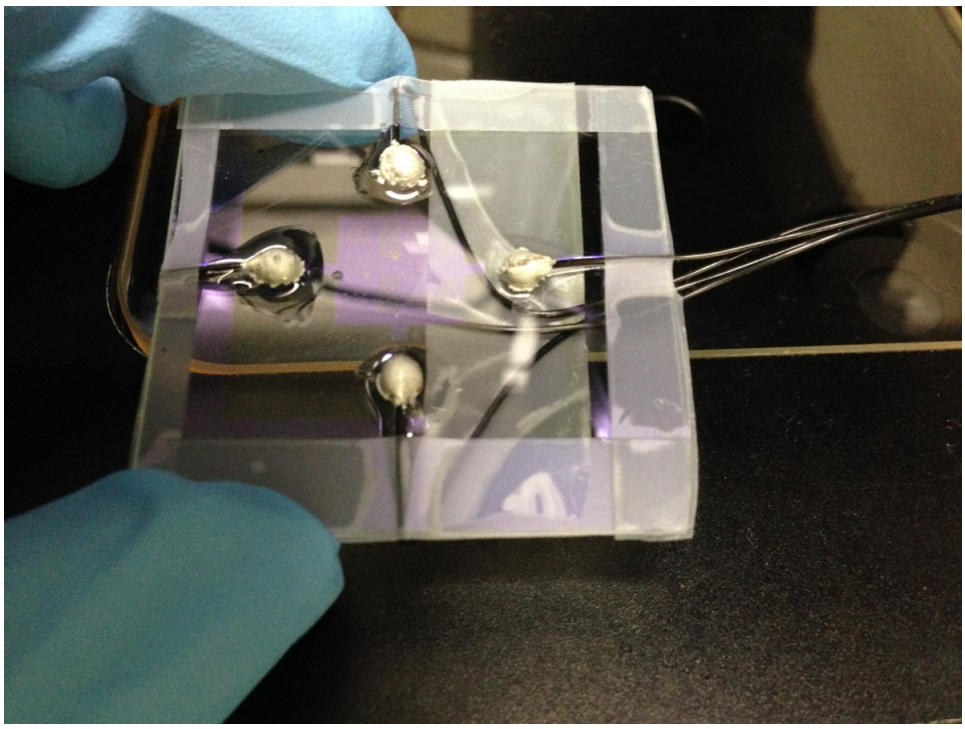

Figure S1. The 1st version of electrode device for electrodeposition of Ca-alginate hydrogel structures.

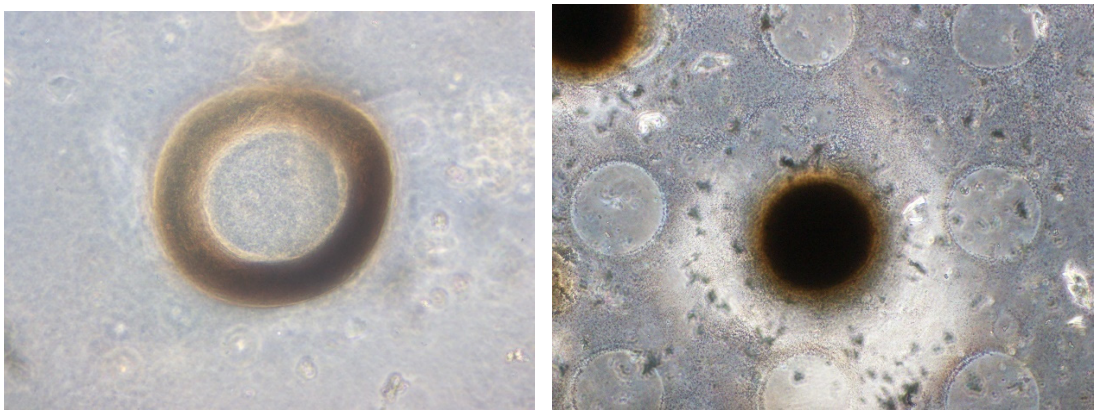

Figure S2. The fabricated micro well gel structures for 3D cell culture in deferent geometry.

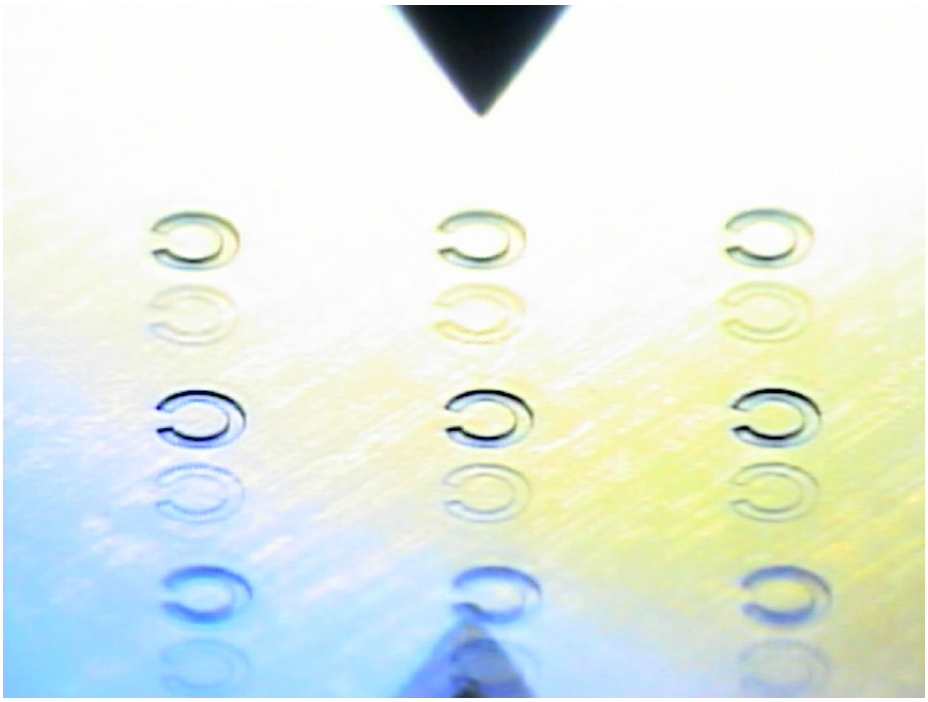

Figure S3. The fabrication of micro-patterns made of SU-8 based on the photolithography technique.

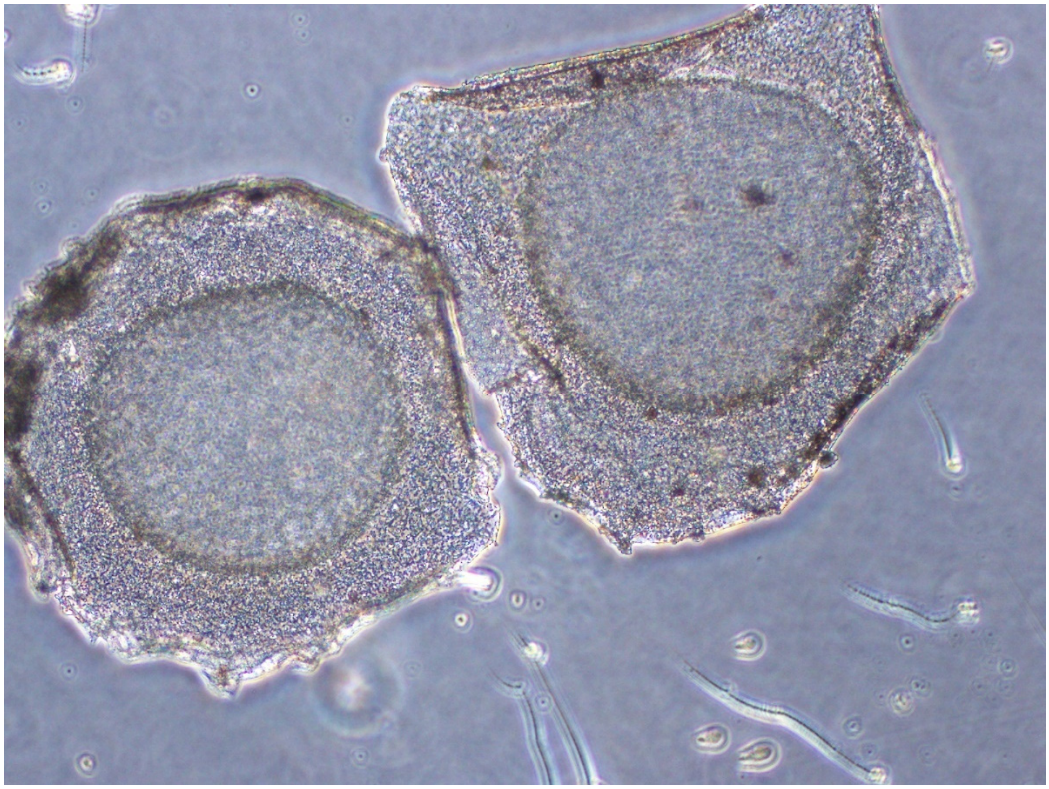

Figure S4. The failure case of APA microcapsules without sufficient time for dissolving process using sodium citrate.

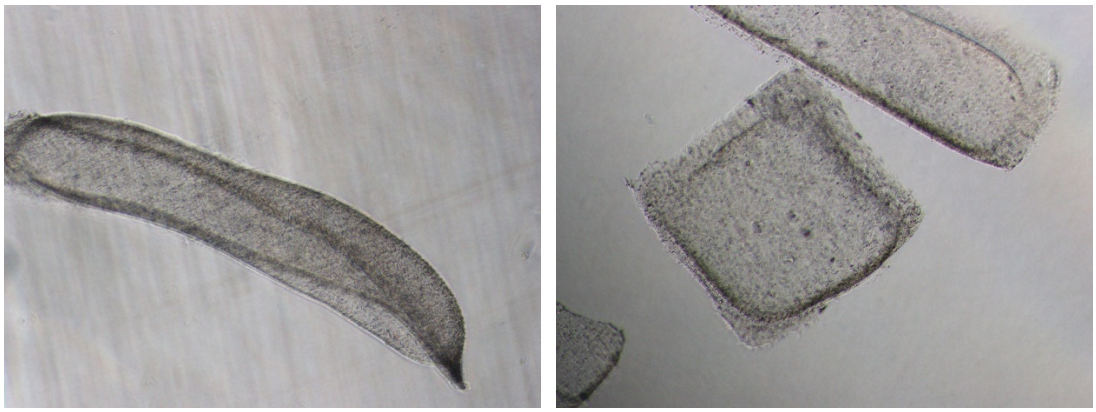

Figure S5. The results of fabricated APA microcapsules based on electrodeposition method.

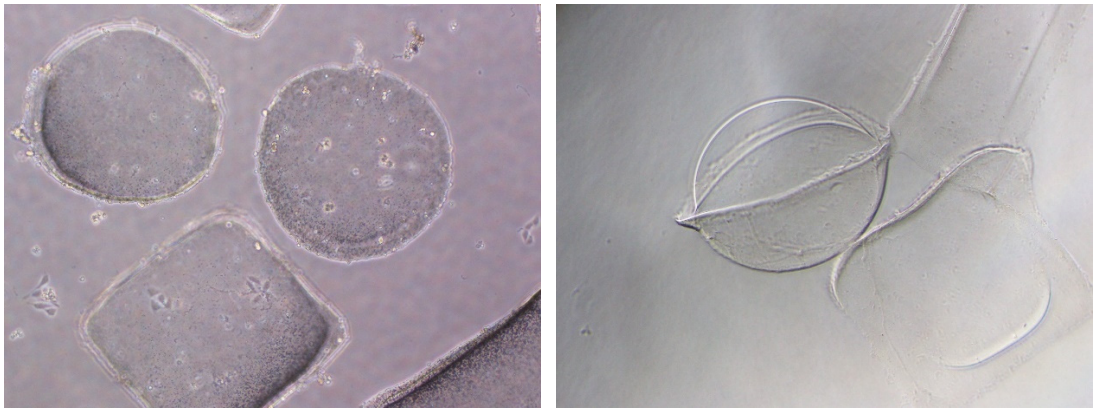

Figure S6. The fabricated APA microcapsules become transparent due to the loss of $CaCl_3$ particles.

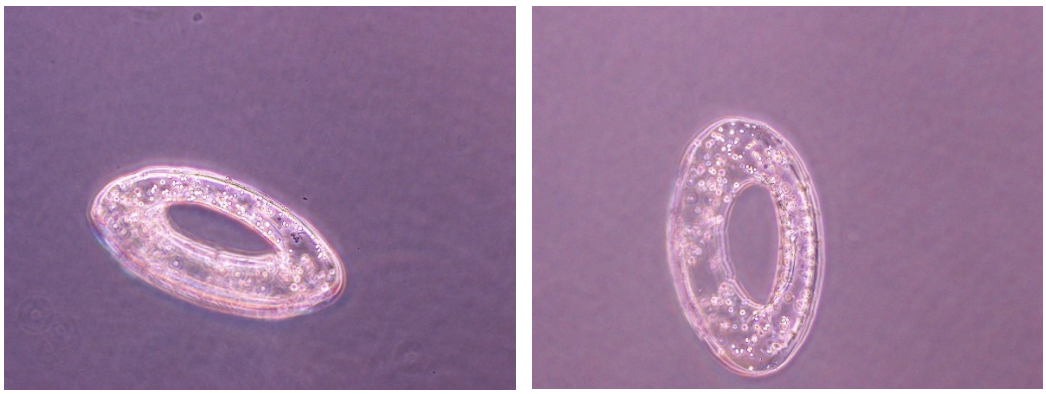

Figure S7. The fabrication results of APA microcapsules in donuts shape.

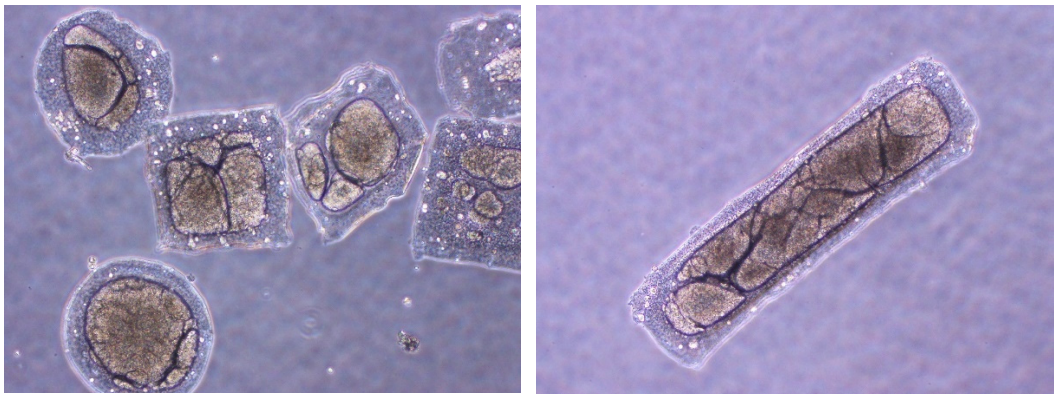

Fugure S8. The culture results of APA microcapsules encapsulated liver cells in two weeks.

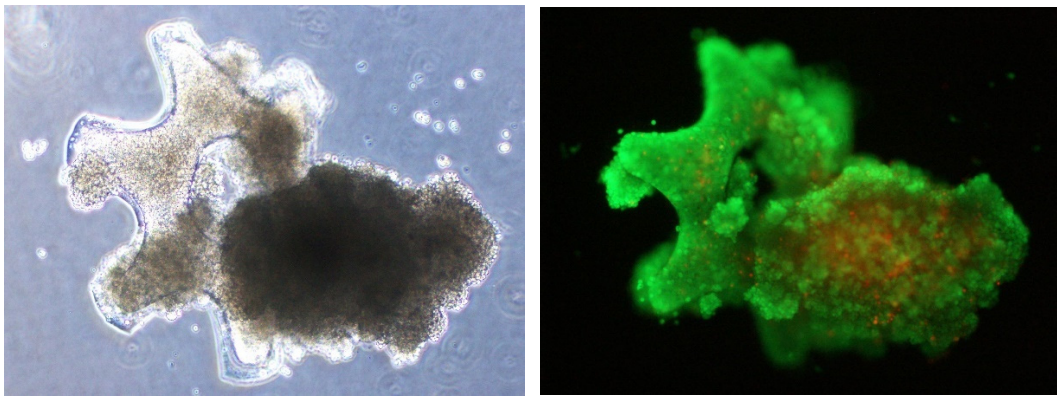

Figure S9. The optical and fluorescent images of gear-shape micro-tissue. The cells broke through the alginate-PLL complex semi-membrane to form a cluster with central necroes.

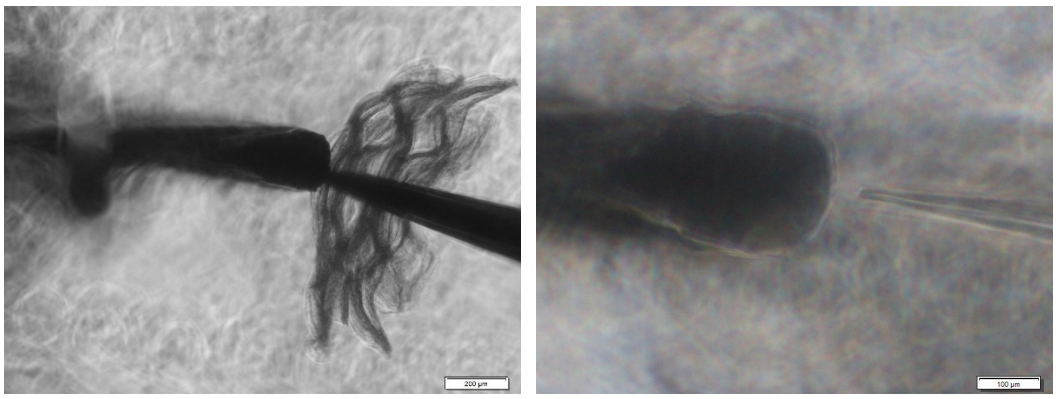

Figure S10. The tentative experiment for assembly of multilayered APA microcapsules onto a pillar.

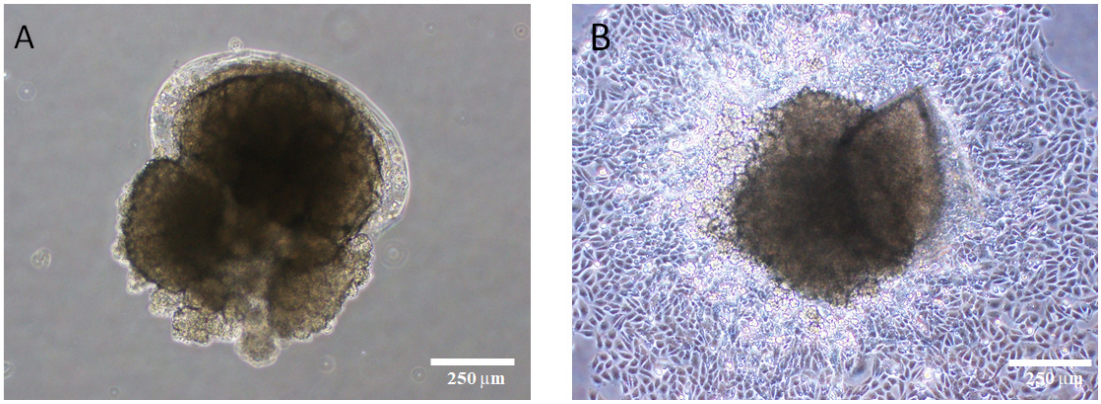

Figure. S11. The culture results of APA microcapsules in spheroid shape containing RLC-18 cells at the day of 18 (A) and 20 (B). The encapsulated cells broke through the alginate-PLL complex membrane and attached to the bottom surface of the culture dish.

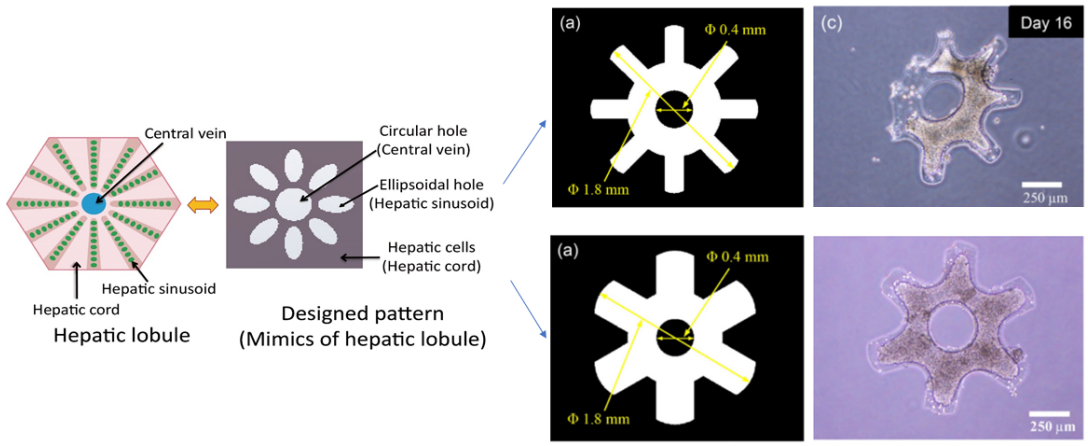

Figure S12. We design the hepatic lobule model based on the modified version of the gear-like microtissue. Originally, we have two types of designs (8-tooths gear and 6-tooths gear) for mimicking the morphology of the hepatic lobule structure. However, 8-tooth gear microcapsules are not stable and easily to be damaged during fabrication process. Therefore, we chose the 6-tooths gear design as the current utilized shape.

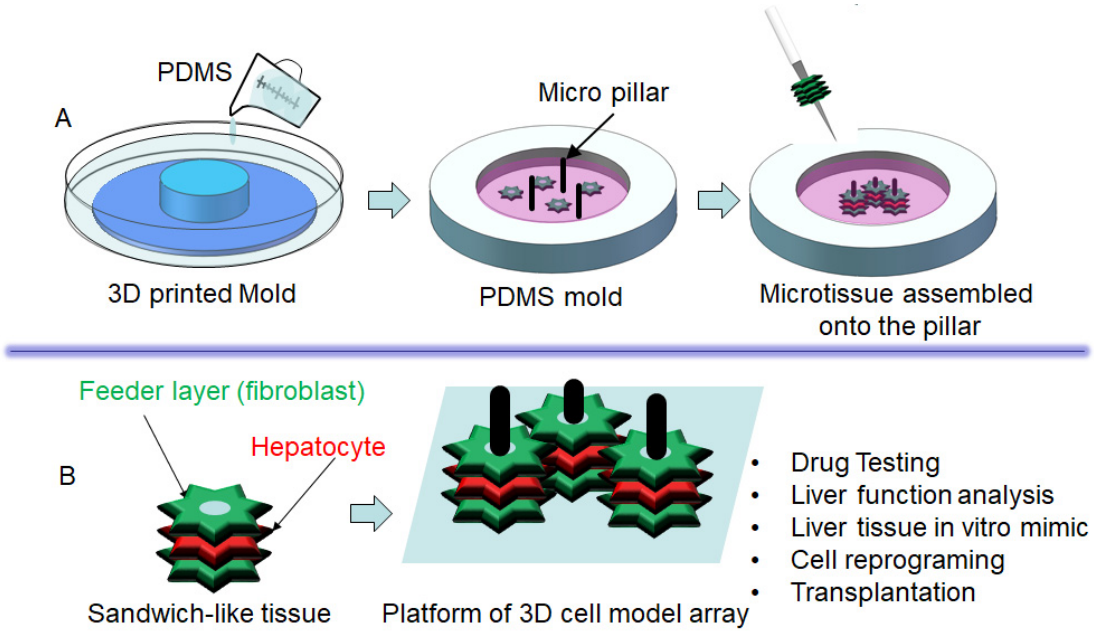

Figure S13. we plan to build polydimethylsiloxane (PDMS) with pillars to better investigate the functional and histological characteristics of the assembled 3D multilayered tissue. We intend to load the HLSM onto the pillar that is made of a titanium wire, using a one-step micromanipulator. By means of such pillar as a substrate, ‘‘sandwich” hepatic cord-like tissue co-cultured with 3T3 feeder cells for long-term preservation of liver-specific functions will be assembled and evaluated, comparing them with monocultures of hepatocytes in 3-dimension.

albumin								
Gear	4	6	8	10	12	14	16	18
C7	0.18628	0.17578	0.30156	0.44308	0.62311	0.69813	0.7539	
	0.11475	0.15128	0.232	0.33612	0.42733	0.62857	0.6788	
C12	0.19853	0.23069	0.35209	0.42996	0.56798	0.6697	0.72285	
	0.17819	0.22981	0.2915	0.30374	0.40218	0.55005	0.59139	
S13	0.30156	0.42777	0.50324	0.66926	0.77251	0.95669	0.94203	0.8541
S13	0.26765	0.41946	0.47611	0.51942	0.5927	0.65985	0.76551	0.82435
S13-2	0.35996	0.41858	0.47874	0.75238	0.76507	0.7981	0.85475	0.89391
	0.32146	0.36565	0.51527	0.61633	0.5413	0.55727	0.57564	0.6312
C7/7	0.026611	0.025111	0.04308	0.063297	0.089016	0.099733	0.1077	
C7/7	0.016393	0.021611	0.033143	0.048017	0.061047	0.089796	0.096971	
C12/12	0.022059	0.028836	0.044011	0.061423	0.08114	0.095671	0.090356	
C12/12	0.019799	0.028726	0.036438	0.043391	0.057454	0.078579	0.073924	
S13/13	0.023197	0.032905	0.038711	0.051482	0.059424	0.073592	0.072464	0.0657
	0.020588	0.032266	0.036624	0.039955	0.045592	0.050758	0.058885	0.063412
s13-2/13	0.027689	0.032198	0.036826	0.057875	0.058852	0.061392	0.06575	0.068762
	0.024728	0.028127	0.039636	0.04741	0.041638	0.042867	0.04428	0.048554
Gear								
SD	0.004285	0.00344	0.005245	0.00983	0.015324	0.009198	0.014147	#DIV/0!
maen	0.021216	0.026071	0.039168	0.054032	0.072164	0.090945	0.092238	
N	4	4	4	4	4	4	4	
Spherods								
SD	0.002967	0.002188	0.001466	0.007509	0.009109	0.013332	0.01206	0.008974
Mean	0.024051	0.031374	0.037949	0.049181	0.051377	0.057152	0.060345	0.061607
N	4	4	4	4	4	4	4	4
times	0.882121	0.830979	1.032113	1.098648	1.404616	1.591273	1.528514	

第一次						
		end	start		hight	
	Gear	2137.42	2440.42		303	
		2145.42	2463.42		318	
		2164.92	2470.92		306	
		2115.42	2427.42		312	
		2181.92	2487.92		306	
		2124.42	2448.42		324	
		2138.92	2351.92		213	
		2011.92	2344.92		333	
				SD	37.33033	
				mean	301.875	
				N	8	
第二组		P1	P2	P3	P4	P5
		8815	5006	1979	1147	665
		8875	5010	1976	1150	667
		8863	4992	1973	1156	667
		9451	4800	2020	1124	638
		9488	4785	2012	1127	636
	SD	339.7614	115.4288	22.19234	14.37707	16.10279
	mean	9098.4	4918.6	1992	1140.8	654.6
	N	5	5	5	5	5
	*E3	1000	200	40	8	1.6
	mean	9098.4	4918.6	1992	1140.8	654.6
		1.00E+05	2.00E+04	4.00E+03	8.00E+02	1.60E+02
400ul 里的细胞数量		400000	80000	16000	3200	640
	mean	9098.4	4918.6	1992	1140.8	654.6
第一组		P1	P2	P3	P4	P5
		3118	1161	659	610	590
		3167	1163	673	610	589
		3029	1129	678	606	572
		3039	1129	680	623	575
	SD	65.88563	19.07005	9.469248	7.410578	9.327379
	mean	3088.25	1145.5	672.5	612.25	581.5
	N	4	4	4	4	4
		1E5	2E4	4E3	8E2	1.6E2
	mean	3088.25	1145.5	672.5	612.25	581.5

Figure S14. The rough data for the quantitative analysis of albumin secretion and cell proliferation for the HLSM and spheroids group.

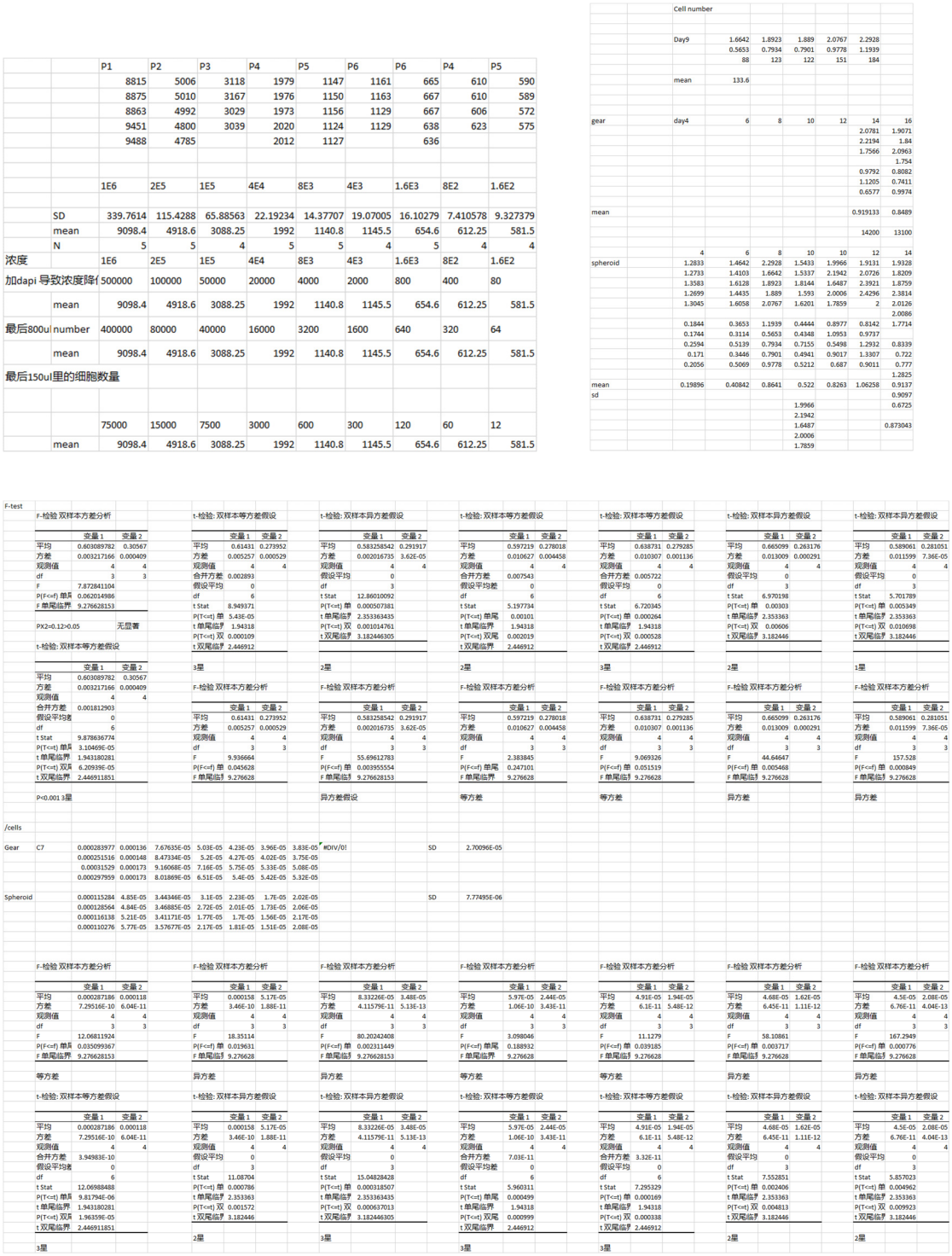

Figure S15. The two-tailed student's t test was used to determine statistical differences between groups. A $p < 0.05$ was considered statistically significant.

Standard Albumin curve																
									3D							
	2	1	0.5	0.25	0.125					0.1012	0.2928	0.3236	0.3374	0.3128	0.3095
	0.7263	0.367	0.2202	0.1355	0.0975					0.08	0.3004	0.3389	0.3389	0.3335	0.3219
	0.6819	0.3275	0.3363	0.1215	0.0978					0.0771	0.3059	0.2449	0.2642	0.2769	0.2488
	0.8317	0.3952	0.2261	0.1334	0.0891					0.0788	0.3179	0.2677	0.2878	0.2632	0.2649
	0.7125	0.365	0.345	0.1252	0.0886										
								平均		0.084275	0.30425	0.293775	0.307075	0.2966	0.286275
								sd		0.011346	0.010567	0.044701	0.037158	0.032289	0.034975
	0.7381	0.363675	0.2819	0.1289	0.09325			减去对照组		0.028775	0.24875	0.238275	0.251575	0.2411	0.230775
	0.125	0.25	0.5	1	2		0.0661			0.069055	0.724523	0.69331	0.732941	0.701728	0.670962
	0.0975	0.1355	0.2202	0.367	0.7263		0.0537								
	0.0978	0.1215	0.3363	0.3275	0.6819		0.0514	一半，因为2张		0.034528	0.362262	0.346655	0.366471	0.350864	0.335481
	0.0891	0.1334	0.2261	0.3952	0.8317		0.0509	X1000		34.52771	362.2616	346.6552	366.4705	350.8641	335.4812
	0.0886	0.1252	0.345	0.365	0.7125			/cell			6.138675	4.61936	4.439537	2.68814	1.36329
								SD			0.089529	0.29783	0.225074	0.12369	0.071064
	0.09325	0.1289	0.2819	0.363675	0.7381		0.055525								
	0.037725	0.073375	0.226375	0.30815	0.682575										
							2d			0.0698	0.0849	0.1221	0.1754	0.2497	0.3219
										0.0693	0.0731	0.1214	0.1381	0.1797	0.2255
										0.0535	0.075	0.1262	0.1752	0.2508	0.3346
										0.0511	0.0741	0.1214	0.1488	0.1871	0.2464

	3D			0.1012	0.2928	0.3236	0.3374	0.3128	0.3095
				0.08	0.3004	0.3389	0.3389	0.3335	0.3219
				0.0771	0.3059	0.2449	0.2642	0.2769	0.2488
				0.0788	0.3179	0.2677	0.2878	0.2632	0.2649
				0.0457	0.2373	0.2681	0.2819	0.2573	0.254
				0.0245	0.2449	0.2834	0.2834	0.278	0.2664
				0.0216	0.2504	0.1894	0.2087	0.2214	0.1933
				0.0233	0.2624	0.2122	0.2323	0.2077	0.2094
				0.028775	0.24875	0.238275	0.251575	0.2411	0.230775
			SD	0.011346	0.010567	0.044701	0.037158	0.032289	0.034975
		求浓度		0.119487	0.690405	0.782181	0.823302	0.75	0.740167
				0.056317	0.713051	0.827771	0.827771	0.811681	0.777116
				0.047676	0.72944	0.547676	0.605185	0.643027	0.559297
				0.052741	0.765197	0.615614	0.675507	0.602205	0.607271
	X1000 变pg 除以2 再除细胞数			#DIV/0!	5.849603	5.211484	4.986865	2.873057	1.503903
				#DIV/0!	6.041476	5.515239	5.013938	3.109339	1.578977
				#DIV/0!	6.180332	3.649031	3.665698	2.463272	1.136403
				#DIV/0!	6.483289	4.101686	4.091648	2.306892	1.233878
	平均			#DIV/0!	6.138675	4.61936	4.439537	2.68814	1.36329
	SD			#DIV/0!	0.266774	0.887456	0.670661	0.368564	0.211753
	X1000 除以2，不除细胞			59.74374	345.2026	391.0906	411.6508	375	370.0834
				28.15852	356.5256	413.8856	413.8856	405.8403	388.5578
				23.8379	364.7199	273.8379	302.5924	321.5137	279.6484
				26.37068	382.5983	307.8069	337.7533	301.1025	303.6353
			SD	16.90389	15.7431	66.59824	55.36106	48.10608	52.10856
		平均		34.52771	362.2616	346.6552	366.4705	350.8641	335.4812
2D				0.0698	0.0849	0.1221	0.1754	0.2497	0.3219
				0.0693	0.0731	0.1214	0.1381	0.1797	0.2255
				0.0535	0.075	0.1262	0.1752	0.2508	0.3346
				0.0511	0.0741	0.1214	0.1488	0.1871	0.2464
				0.0143	0.0294	0.0666	0.1199	0.1942	0.2664
				0.0138	0.0176	0.0659	0.0826	0.1242	0.17
				-0.002	0.0195	0.0707	0.1197	0.1953	0.2791
				-0.0044	0.0186	0.0659	0.0933	0.1316	0.1909
	浓度			0.025924	0.070918	0.181764	0.340584	0.561979	0.777116
				0.024434	0.035757	0.179678	0.22944	0.353397	0.489869
				-0.02265	0.041418	0.193981	0.339988	0.565256	0.814958
				-0.0298	0.038737	0.179678	0.261323	0.375447	0.552145
	乘以1000			25.92372	70.91776	181.764	340.584	561.9785	777.1156
				24.43385	35.75685	179.6782	229.4398	353.3969	489.8689
				-22.646	41.41836	193.9809	339.9881	565.2563	814.9583
				-29.7974	38.73659	179.6782	261.323	375.447	552.1454
	平均			0.52	46.70739	183.7753	292.8337	464.0197	658.5221
	SD			0	16.30505	6.874417	56.31855	115.3651	161.5514
SD	/CELL			0	0.326101	0.068744	0.201138	0.128183	0.121467
平均	/cell			0.0104	0.467074	0.65634	0.325371	0.348887	
乘以16.5	/cell			0.104	4.670739	6.563405	3.253708	3.48887	0
乘以16.5	整体			5.2	467.0739	1837.753	2928.337	4640.197	
乘以16.5	/cell SD			0	5.217615	1.099907	3.218203	2.050935	
乘以16.5	整体SD			0	163.0505	68.74417	563.1855	1153.651	

累积的平均值		362.2616	708.9169	1075.387366	1426.251	1761.733	335.4812	
	重新计算一次3D的累计浓度							
				0.690405244	0.782181	0.823302	0.75	0.740167
				0.713051251	0.827771	0.827771	0.811681	0.777116
				0.729439809	0.547676	0.605185	0.643027	0.559297
				0.765196663	0.615614	0.675507	0.602205	0.607271
	X1000 除以2，不除细胞			345.2026222	391.0906	411.6508	375	370.0834
				356.5256257	413.8856	413.8856	405.8403	388.5578
				364.7199046	273.8379	302.5924	321.5137	279.6484
				382.5983313	307.8069	337.7533	301.1025	303.6353
	累计值计算			345.2026222	736.2932	1147.944	1522.944	1893.027
				356.5256257	770.4112	1184.297	1590.137	1978.695
				364.7199046	638.5578	941.1502	1262.664	1542.312
				382.5983313	690.4052	1028.159	1329.261	1632.896
	平均			362.261621	708.9169	1075.387	1426.251	1761.733
	SD			15.74310462	57.22498	111.6183	155.3233	207.4086
	平均	/cell		6.138674885	9.446683	13.02758	10.9272	7.159129
	SD	/cell		0.266773501	0.762552	1.352178	1.190007	0.842844
左边第一	这个0.52是自己写的，因为原本是个负值，-0.52							
	SD不可以直接除以细胞数来求得							
	除以细胞数			5.849603006	9.811487	13.90655	11.66801	7.692669
				6.041476043	10.26613	14.34694	12.18281	8.040795
				6.180331531	8.509112	11.40139	9.67388	6.267473
				6.483288959	9.200006	12.45543	10.18411	6.635578
平均值是一样的		平均	/cell	6.138674885	9.446683	13.02758	10.9272	7.159129
SD完全不同		SD		0.266773501	0.762552	1.352178	1.190007	0.842844

Figure S16. The rough data for the quantitative analysis of the albumin secretion and cell number of the fabricated cell sheets.

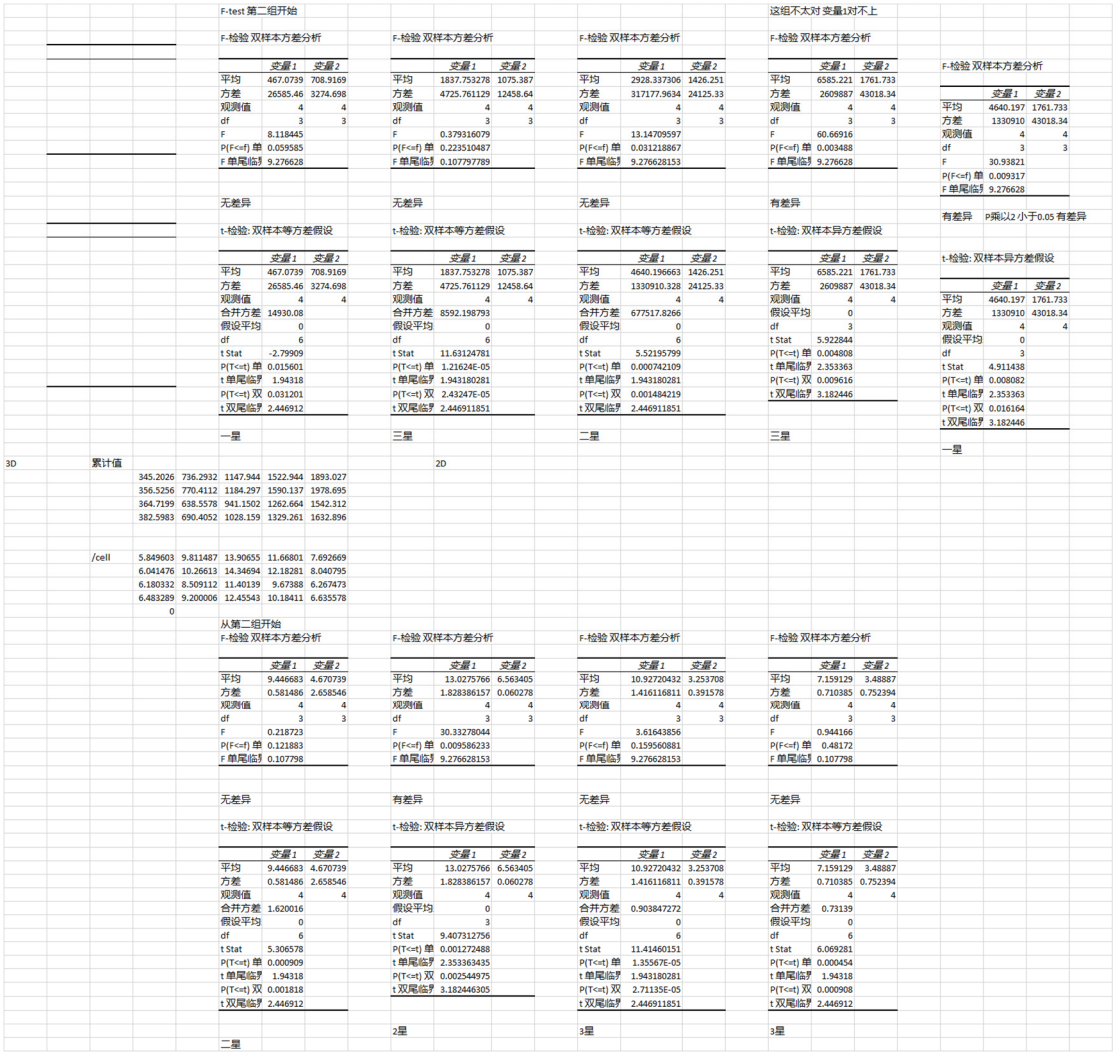

Figure S17. The two-tailed student's t test was used to determine statistical differences between groups. A $p < 0.05$ was considered statistically significant for Chapter 5.